秋田県立大学大学院博士学位論文

Fabrication and Performance Evaluation of Carbon/Polymer Functional Nanocomposites by Surface Treatment

表面処理によるカーボン/高分子機能性ナノ複合材料の創製と性能評価

Division of Material and Structure Engineering

Integrated Course of Systems Science and Technology

Graduate School of Systems Science and Technology, Akita Prefectural University

武　学麗

2014 年 3 月

Abstract

Carbon materials touch every aspect of our daily lives. Activated carbons are used for water and air purification, carbon black is used to reinforce tires, carbon fiber composites are used to manufacture ultra-light graphite sporting goods and aircraft brakes, and carbon foams are used to make fire retardant insulation. Carbon nanotubes can be used for numerous applications ranging from sensors and actuators to composites. Graphene has been used as field effect transistors, sensors and electromechanical resonators. However, carbon materials are all aggregate easily, and the poor interfacial adhesion between carbon materials and other matrix limits their widely use. In the present study, the composites of several kinds of carbon materials are investigated. Different types of surface treatment of carbon materials are available to improve the interfacial adhesion between carbon materials and polymer matrix and the influences on the composite properties are well studied. The significantly improved electrical conductivity, mechanical properties and other properties of composites are attributed to the interfacial adhesion improvement by carbon materials surface treatment was investigated by properties test.

In chapter 1, the research backgrounds, research significance, summary of the research and the construction of this thesis are described. The objectives of the research are to study the influence of different treatments on the properties of carbon materials composites.

In chapter 2, the properties of polymer matrix and carbon materials are presented. The experimental methods and characteristics are also presented in this chapter.

In chapter 3, carbon black/polystyrene (CB/PS) nanocomposites were successfully prepared through a facile strategy. Some of the styrene molecules were grafted and polymerized onto the surface of the CB via the in situ free radical addition process in ionic liquid, and others self-polymerized and coated on the polystyrene grafted CB. The ionic liquid improves the grafting percentage because of its high viscosity. The electrical

properties of polymer composites before and after the grafting were measured. It was found that the electrical conductivity of the CB/PS composites decreased with increasing amounts of monomer styrene and initiator 2, 2'-azobis (isobutyronitrile) (AIBN). The microstructure, morphology and thermal properties of the composites were characterized by Fourier transform infrared spectroscopy (FT-IR), thermal gravimetric analysis (TGA), scanning electron microscopy (SEM), transmission electron microscopy (TEM) and Raman spectroscopy. The results proved that the polystyrene had been successfully grafted onto the CB surface.

In chapter 4, Multi-walled carbon nanotube/polystyrene (MWCNT/PS), carbon black/polystyrene (CB/PS) and multi-walled carbon nanotube-carbon black/polystyrene (M-C/PS) nanocomposites with different contents of carbon materials were prepared by bulk radical polymerization. The products were pressed into slices to prepare specimens for electrical conductivity testing. All of the nanocomposites demonstrated good electrical conductivity. Compared to MWCNT/PS and CB/PS composites, the M-C/PS composites showed a good synergistic effect between the MWCNTs and CB, and the electrical conductivity of M-C/PS was higher than that of CB/PS. To investigate the structure and morphology of the grafted carbon nano-materials, samples were submitted to Fourier transform infrared spectroscopy (FT-IR), thermal gravimetric analysis (TGA) and transmission electron microscopy (TEM) after being extracted with toluene. The results show that some polystyrene was grafted onto the surfaces of the MWCNTs, CB and M-C, which is likely responsible for the increase in the electrical conductivity of the composites. Furthermore, the mechanical properties of the M-C/PS nanocomposites increased with the M/C ratio.

In chapter 5, multi-walled carbon nanotube/poly (methyl methacrylate) (MWCNT/PMMA) composites were synthesized by Pickering emulsions polymerization in the presence of MWCNTs as a colloidal surfactant. MWCNTs behaved like a functional surfactant in a Pickering emulsions. The effect of monomer concentration on the electrical properties of MWCNT/PMMA composites was

investigated. It was found that the MWCNT/PMMA composites have excellent electrical conductivity. The microsphere morphology and MWCNTs as a colloidal surfactant for MWCNT/PMMA composites were examined by scanning electron microscopy (SEM) and transmission electron microscopy (TEM). The thermal gravimetric analysis (TGA) of the prepared composites confirmed that MWCNTs as a thermal stabilizer for PMMA, which could have a wide range of potential applications, such as in catalysts, sensors, environmental remediation, and energy storages. The Poly (lactic acid) (PLA) based composite with MWCNT/PMMA composites was prepared with twin-screw extruding and injection molding. The lower mechanical properties of PLA based composites suggested the brittle MWCNTs stabilized PMMA spherical particles were formed during the Pickering emulsions polymerization.

In chapter 6, in order to improve the affinity with polymers graphite powder (GP) were modified by a proposed chemical method to improve their affinity with polyamide 6 (PA6). The GP was first oxidized with hydrogen peroxide (GP-OH) and then modified with hexamethylene diisocryanate (GP-NH_2). The X-ray photoelectron spectroscopy (XPS), elemental analysis, thermal gravimetric analysis (TGA) and X-ray diffraction (XRD) results proved the successful modification of GP by the proposed method. The composites of GP and PA6 (GP/PA), GP-OH and PA6 (GP-OH/PA) and GP-NH_2 and PA6 (GP-NH_2/PA) were prepared via the twin-screw extruding and injection molding processes. The scanning electron microscopy (SEM) images and the optical microscopy images of composites showed good compatibility between modified GP and PA6. The test results of tensile strength and bending strength suggested that the modified GP can enhance the mechanical properties of PA6, which will increase its application in various fields.

In chapter 7, general conclusions of the study are made.

Contents

Chapter 1 Introduction

1.1 Background

Penn State has a rich 62-year history in carbon materials research. The EMS Energy Institute's Carbon Materials Program focuses its research on materials such as graphite, petroleum and metallurgical coke, activated carbon, anthracite, and pitch. Carbon can be said the earliest element that human touched, is also one of the earliest element which human used and studied, is widely distributed in nature. There are three carbon allotropes in initial studies: sp2 hybridized graphite, sp3 hybridized diamond and C_{60}. Since Kroto discovered fullerenes in 1985 and Iijima discovered carbon nanotubes in 1991 [1, 2], the carbon allotrope scope was enlarged, and the carbon studies had more profound understanding correspondingly. The discovery of these two kinds of carbon nano-materials has led contribution on people and the community in the field of science and technology. Furthermore, Novoselov successfully prepared another allotrope of carbon-graphene in 2004 [3], it has an ideal two-dimensional structure and peculiar electronic properties, because of this, the studies of carbon materials entered a new round of high tide [4].

Carbon materials include carbon nanotube, graphene, fullerene, carbon black, carbon fiber and graphite. Carbon nanotubes can be considered to graphite layers around the central axis by a certain degree of curl spiral made of tube-like. Carbon atoms in the main carbon sp2 hybrid orbitals, there is a small part of a certain sp3 hybridized bond, each carbon atom and its adjacent three carbon atoms connected to form a hexagonal mesh structure [5]. According to the structure of carbon nanotubes, they can be divided into single-walled carbon nanotube and multi-walled carbon nanotube. The length of SWCNTs is about several hundred nanometers to several tens of microns, its diameter is generally between 1-6 nm. And multi-walled carbon nanotube micron in length or more, even up to millimeter level, the diameter is from several nanometers to several tens of

nanometers, the distance between the layers of the wall is about 0.34 nm, layers up to tens of layer even to the hundreds of layers [6]. Graphene is a single atom thick sheet of carbon atoms, the two-dimensional sheet of honeycomb structure, which can be expanded as a carbon nanotube structure, its carbon nanotube structure is very similar. The average chip thickness is 0.60-1.38 nm, with outstanding physical, chemical and electrical properties, and is the world's greatest strength nano-materials, with a large range of applications. Fullerene was found in 1985 [7], its molecules entirely composed of carbon atoms, a hollow sphere or ellipsoid. Typical fullerene C_{60} is 12 five-membered rings with 20 six-membered rings combination polyhedral cluster compounds of carbon atoms, each carbon atom is sp2 hybridized into construction, this hybrid is not standard. Each carbon atom is surrounded by three adjacent carbon atoms in the outer and the inner wall of C_{60} to form spherical ball bond, is a kind of special aromatic system [8]. Carbon black (CB) was first manufactured in the US from natural gas on soap-stone plates in 1872 [9], and it refers to a group of industrial products including acetylene black, furnace black, channel black, thermal black and lamp black. In 1958, Roger Bacon created high performance carbon fibers at the Union Carbide Parma Technical Center [10]. The basic structure of graphite consists of a hexagonal arrangement of carbon atoms which form stable planar lattices with only weak inter-layer bonding (Van der Waals forces) [11].

1.2 Carbon nanotube

1.2.1 The structure of carbon nanotube

Carbon nanotube exists as a macro-molecule of carbon, analagous to a sheet of graphite (the pure, brittle form of carbon in pencil lead) rolled into a cylinder. Carbon nanotube is built from sp2 carbon units, with each atom joining to three neighbours in graphite [12]. They consist of honeycomb lattices and are a seamless structure. The tubes can therefore be considered as rolled-up graphene sheets (graphene is an

individual graphite layer). Diameters usually range between 2 and 25 nm, and the distance between sheets is about 0.34 nm [13, 14]. They are tubular having a diameter of a few nanometers, but their lengths are many microns. In fact, nanotube has been known to be up to one hundred times as strong as steel and almost two millimeters long. These nanotubes have a hemispherical "cap" at each end of the cylinder. They are light, flexible, thermally stabile, and chemically inert. They have the ability to be either metallic or semi-conducting depending on the "twist" of the tube.

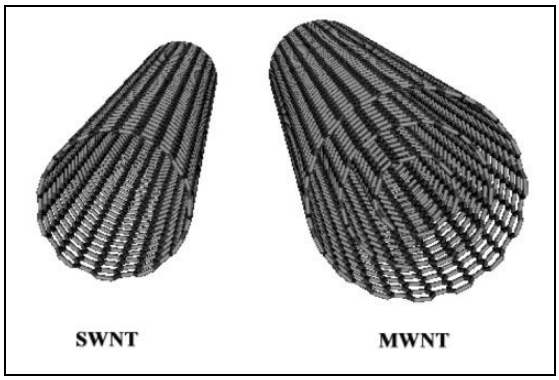

Fig. 1-1 The structure of SWCNT and MWCNT [15]

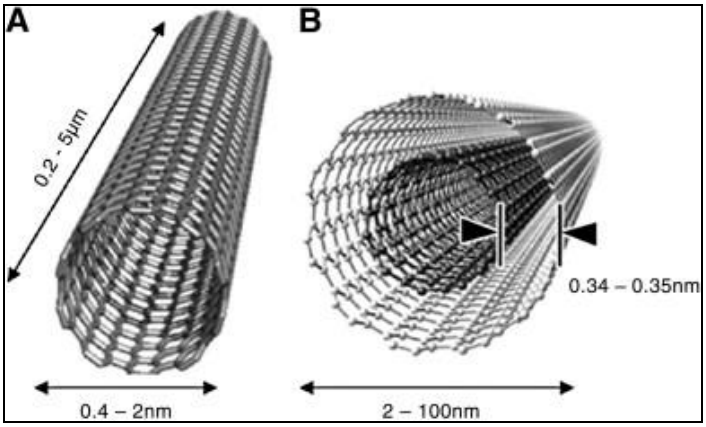

Fig. 1-2 The size of SWCNT and MWCNT [15]

Carbon nanotube divided in two large classes: Multi-walled carbon nanotube (MWCNT) and Single-walled carbon nanotube (SWCNT). This classification depends on the number of graphite walls: several in the case of MWCNT and only one for SWCNT. As shown in Fig. 1-1. MWCNTs are closed graphite tubules rolled like a

graphite sheet. Diameters usually range between 2 and 25 nm, and the distance between sheets is about 0.34-0.35 nm. SWCNTs are made of a single seamlessly rolled graphite sheet with a typical diameter of about 1.4 nm as shown in Fig. 1-2 [15, 16].

1.2.2 Properties

There are many useful and unique properties of carbon nanotubes as follows [17]:

(1) High electrical conductivity;

(2) Very high tensile strength;

(3) Highly flexible, which can be bent considerably without damage;

(4) Very elastic, about 18% elongation to failure;

(5) High thermal conductivity;

(6) Low thermal expansion coefficient;

(7) Good field emission of electrons;

(8) Highly absorbent;

(9) High aspect ratio (length = ~1000 x diameter).

1.2.2.1 Mechanical properties

Carbon nanotube is one of the strongest materials in nature. Carbon nanotube (CNT) is basically long hollow cylinders of graphite sheets. Although a graphite sheet has a 2-D symmetry, carbon nanotubes by geometry have different properties in axial and radial directions. It has been shown that CNTs are very strong in the axial direction, with the Young's modulus on the order of 270-950 GPa and tensile strength of 11-63 GPa [18]. Carbon nanotube demonstrates very high stiffness to an axial load or a bending of small amplitude, which translates to the record-high efficient linear-elastic modulus [19].

Salvetat et al. reported that the Young's modulus for MWCNTs is dependent upon the degree of order within the tube walls [20]. Fig. 1-3 shows a schematic representation of these findings, where the Young's modulus decreases as the disorder increases. Pan et al.

have directly measured the Young's modulus and tensile strength of MWCNT by pulling very long (~2 mm) aligned nanotube ropes with a specially designed stress-strain puller. The average Young's modulus and tensile strength obtained were 0.45±0.23 TPa and 1.72±0.64 GPa, respectively [21]. Young's modulus for a SWCNT has been estimated by Yu et al. [22] in a range of 0.32-1.47 TPa and its strengths are between 10 and 52 GPa with a toughness of ~770 Jg-1.

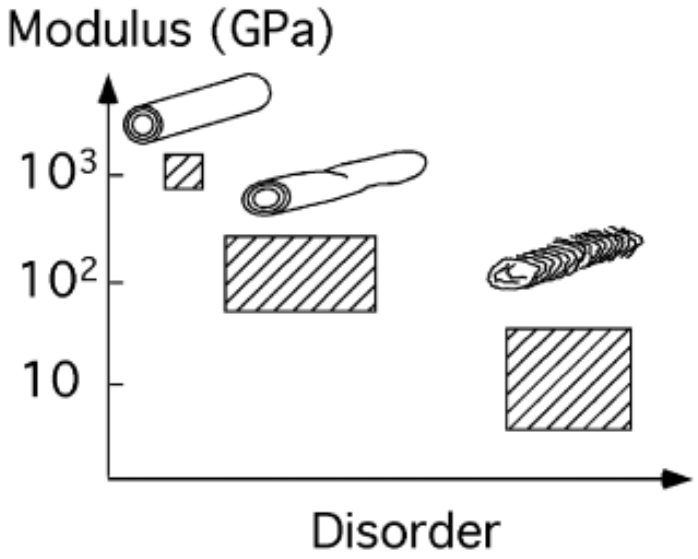

Fig. 1-3 Modulus vs. disorder in MWCNT [20]

1.2.2.2 Electrical properties

The electrical properties of both SWCNT and MWCNT have been relatively well explored. Carbon nanotube is predicted to be metallic or semiconducting depending on their diameter and the helicity of the arrangement of graphitic rings in their walls [23, 24]. A nanotube consists of either one cylindrical graphene sheet [25, 26] or a set of coaxially stacked cylinders [27]. Most of the groups have investigated the transport in SWCNT, because measurements were expected to be interpreted easier than in MWCNT. Electronic properties of SWCNT have been studied in a number of theoretical works [28]. Their electronic properties vary in a periodic way from metallic to semiconducting as a function of both the diameter and the helicity.

Carbon nanotube can exhibit a variety of structural defects, from bends, twisting, and

collapse [29] to pentagon-heptagon (p-h) pairs in the hexagonal network [30]. SWCNTs intramolecular junctions can be formed by interposing one or more p-h pairs between two nanotube sections with different indices (*n, m*). Theoretical models have predicted that metal-semi-conductor (M-S), metal-metal (M-M), or semi-conductor-semi-conductor (S-S) junctions are possible in SWCNTs [31]. The Fermi liquid theory which is used to describe electronic excitations, in the non-interacting electron limit, is found to be inadequate to describe the electrical properties in SWCNTs, in the one-dimensional limit [32]. Raman spectroscopy, widely used for determining the metallic/semiconducting characteristics of nanotubes [33], offers one possible way to determine the charge transfer characteristics through spectroscopic line shifts [34]. Charged defects are also known to modify electronic properties through local modification of the electronic structure [35]. Another extension of scanning tunneling microscope (STM) studies of SWCNTs is to introduce magnetic perturbations to the nanotube system. Odom et al. decorated SWCNTs with magnetic Co clusters or created magnetic nanostructures consisting of a Co cluster in a SWCNT quantum box to get spectroscopic data [36].

MWCNTs are composed of coaxial nanotube cylinders, of different helicities. These adjacent layers are generally non-commensurate (different chiralities) with a negligible inter-layer electronic coupling and could alternate randomly between metallic and semiconducting varieties [37]. The layers, constituting the individual cylinders, are found to close in pairs at the very tip of a MWCNT, and the detailed structure of the tips plays an important role, say in the electronic and field emission properties of nanotube [38]. The mutual interaction between the adjacent coaxial cylinders of MWCNTs might be very small, it cannot be completely neglected, and which makes for a richer band structure in contrast to SWCNTs [39]. Quantized conductance, corresponding to multiples of G_o ($2\ e^2/h$) and ballistic transport, was measured at room temperature, in a single MWCNT mounted on a scanning probe microscope (SPM) tip and dipped into liquid mercury metal by replacing the tip of a scanning probe microscope with a

nanotube fiber [40]. In doped MWCNTs, the Fermi energy (EF) is shifted by changing the total number of participating conduction channels [41]. A typical magnet-resistance measurement of MWCNTs in a perpendicular magnetic field was reported by Schonenberger et al. [42]. MWCNTs display characteristics ranging from localization to metallic behavior at low temperature resulting in either a small or large phase coherence length. The non-local interactions manifest in a disordered sample can cause difficulties in the interpretation of even four-terminal measurements [41].

SWCNTs can be described as quantum wires due to the ballistic nature of electron transport [43], the transport in MWCNTs is found to be diffusive/quasi-ballistic [44]. Quantum dots can also be formed in both SWCNTs and MWCNTs and the Coulomb blockade and the quantization of the electron states can be used to fabricate single-electron transistors [45]. Branched nanotube with T-, Y-, L- and more complex junctions, was initially observed in arc-discharge produced nanotube [46]. The current theoretical explanations of the observed electrical behavior in Y-junctions are based on SWCNT Y-junctions, the experimental demonstrations were made on MWCNTs, which are easier to experimentally manipulate compared to SWCNTs [47].

1.2.2.3 Thermal properties

Carbon-based materials to diamond and in-plane graphite display the highest measured thermal conductivity of any known materials at moderate temperatures [48]. Thermal properties of CNTs, including specific heat, thermal conductivity and thermopower, display a wide range of behaviors which stem from both their relation to a 2D graphene layer and their unique structure and tiny size. The specific heat of individual nanotube should be similar to that of 2D graphene at high temperatures, with the effects of phonon quantization becoming apparent at lower temperatures for SWCNTs of small diameter (less than 2 nm) [16]. The thermal conductivity, along with the specific heat, provides a sensitive tool for probing the interesting low energy phonon structure of nanotube, and also has the potential for practical applications that exploits

the high thermal conductivity of these nanostructures [49]. Since the thermal conductivity along the tube axis is at least two orders of magnitude larger than that normal to the tube axis, the magnitude and temperature dependence of the thermal conductivity of a SWCNT bundle or of an isolated MWCNT should be close to those of their constituent tubes, though some inter-tube thermal conduction could occur. The thermal conductivity of 'mat' samples, however, is expected to be dominated by inter-tube thermal conduction processes [50].

Measurements have been reported on the thermal conductivity of an individual SWCNT bundle [51] and an individual MWCNT [52]. In both cases, the nanotube sample is made by using the SWCNTs bundles or the MWCNTs to bridge the two heating pads/thermal contacts. Hone et al. have measured the temperature-dependent thermal conductivity κ(T) of crystalline ropes of SWCNTs from 350 K to 8 K. κ(T) decreases smoothly with decreasing temperature, and displays linear temperature dependence below 30 K [53]. The thermal expansion of SWCNTs bundles has been measured using X-ray diffraction techniques [54], and the results are consistent with expectations based on graphite, which has an exceedingly small in-plane thermal expansion coefficient, but a large inter-planar expansion coefficient. Thermal power or seebeck coefficient of SWCNTs bundles to be very sensitive to exposure to oxygen and other gaseous species [55], because oxygen adsorption causes SWCNTs to become p-type, and to yield quite high thermal power values. Specific heat of SWCNTs was measured closely matches calculations based on the phonon band-structure of isolated nanotube, and shows direct evidence of 1-D quantization of the phonon band structure [56].

1.2.3 Carbon nanotube's applications

1.2.3.1 Filled composites

The most important application of nanotubes based on their mechanical properties will be as reinforcements in composite materials. The main problem is creating a good

interface between nanotube and the polymer matrix and attaining good load transfer from the matrix to the nanotube during loading. First, nanotube is atomically smooth and has nearly the same diameters and aspect ratios (length/diameter) as polymer chains. Second, nanotubes are almost always organized into aggregates which behave differently in response to a load, as compared to individual nanotube. There have been conflicting reports on the interface strength in nanotube-polymer composites [57]. To maximize the advantage of nanotube as reinforcing structures in high strength composites, the aggregates needs to be broken up and dispersed or cross-linked to prevent slippage [58]. There are certain advantages that have been realized in using carbon nanotube for structural polymer composites. Nanotube reinforcements will increase the toughness of the composites by absorbing energy during their highly flexible elastic behavior. This will be especially important for nanotube-based ceramic matrix composites [59]. Use of the non-linear optical and optical limiting properties of nanotube has been reported for designing nanotube-polymer systems for optical applications, including photo-voltaic applications [60]. CNTs filled polymers could be useful in electrical magnetic induction (EMI) shielding applications where carbon fibers have been used extensively [61].

Large aspect ratios of carbon nanotube can enhance the electrical conductivity of polymer composite [62]. Coleman et al. in 1998 first mixed lab-produced CNTs with a conjugated polymer, and observed that the composite conductivity improved for several orders of magnitude with around 10 wt% CNTs in the composites [63]. Due to their high aspect ratio, only small amount of CNTs can already introduce good levels of conductivity in the composites. In the case of SWCNTs, the properties, especially the electrical properties, are highly related to the structure of the CNTs. The electron transport property of the MWCNTs is more complicated than SWCNTs. The network formation process in conductive polymer composites is very complicated. An ideal percolated network can be described by the percolation theory. However, in reality, the conductivity of most conductive polymer composites is controlled by the tunnelling

resistance, which can vary across many orders of magnitudes. This is defined as a continuum percolation network [64].

1.2.3.2 Field emitters

Field emission characteristics of CNTs have been intensively studied using various methods [65]. The reliability of CNTs emitters in terms of current decay is of interest, and could be due to tip blunting, caused by bombardment from surrounding ions and/or carbon evaporation. The use of CNTs in cold cathode devices allows for [41] (i) instantaneous turn-on; (ii) high power; (iii) low control voltage operation, along with long life-times and miniaturization.

Compared to thermionic emission, field emission induced from nanotube also offers the additional advantages of lower power consumption and room temperature operation. When employed as electron emitters, there is a large enhancement factor (β) in the field emission. In CNTs, however, β (the field enhancement factor which is the ratio of the electric field at the CNTs tip and the macroscopic electric field and a function of tip geometry) can be as high as 3000 [66], with orders of magnitude lower turn on voltages (<10 V/m) [67], and larger currents (up to 1 A from a single MWCNT) [68] and current densities.

1.2.3.3 Bio-chemical sensors

The small size and high sensitivity of carbon nanotube make them excellent sensors for biological and chemical systems. A number of mechanisms have been proposed to explain the response in different situations, including direct charge transfer between the analyte and the nanotube, local capacitive gating of the nanotube by a charged analyte, and more subtle interactions of the analyte with things other than the nanotube, such as the metal electrical contacts. The first nanotube sensing experiment was performed by Kong et al. in Hongjie Dai's Stanford Laboratory [69].

The gas that is sensed by the CNTs devise depends not only upon the selection of

CNTs and the measurement method but also on the substrate and functionalizations that are used. One of the earliest gases detected was hydrogen and the CNT FET was activated with a Pd metal layer [70]. The detection of liquids can be performed at CNTs since they are basically fullerenes and stable in electrolytes over a wide range of pH values. However, the electrodes are often fabricated as CNTs powder electrodes, as has been applied to the detection of cysteine, or as composites, has been applied to the detection of glucose [71]. SWCNTs embedded in polymer can be used as mechanical sensors because the position of the D* Raman band of SWCNTs is strongly dependent on the strain transferred from the matrix to the nanotube [72].

1.2.3.4 Energy and hydrogen storage

Nanotube is special because they have small dimensions, a smooth surface topology, and perfect surface specificity, since only the basal graphite planes are exposed in their structure. Electrochemical intercalation of MWCNTs [73] and SWCNTs [74] has been investigated by several groups. A reversible capacity (Crev) of 100-640 mAh/g has been reported, depending on the sample processing and annealing conditions. The SWCNTs are also found to perform well under high current rates. 60% of the full capacity can be retained when the charge-discharge rate is increased from 50 mA/h to 500 mA/h.

The area of hydrogen storage in CNTs remains active and controversial. Extraordinarily high and reversible hydrogen adsorption in SWCNTs-containing materials has been reported and has attracted considerable interest in both academia and industry [75, 76]. An even higher hydrogen uptake, up to 14-20 wt%, at 20-400 ^{o}C under ambient pressure was reported [77] in alkali-metal intercalated CNTs. An electrochemical absorption and desorption of hydrogen experiment performed on SWCNTs-containing materials reported a capacity of 110 mAh/g at low discharge currents [78].

1.3 Graphite

1.3.1 Structure

Carbon has two natural crystalline allotropic forms: graphite and diamond. Each has its own distinct crystal structure and properties. Graphite consists of several layers of honeycomb lattices of carbon atoms, characterized by two non-equivalent sites, A and B, in the Bernal (ABABAB...) stacking configuration [79]. The ideal graphite structure is shown in Fig. 1-4. In this stable hexagonal lattice, the interatomic distance within a layer plane is 1.42 Å, and with a layer spacing of 3.35 Å. Crystal density is 2.266 g/cm^3 [80, 81]. Graphite looks like a sheet of chicken wire, a tessellation of hexagonal rings of carbon. Sheets of graphite in your pencil lay stacked on top on one another, but they slide past each other and can be separated easily, which is how it is used for writing. However, when coiled, the carbon arrangement becomes very strong.

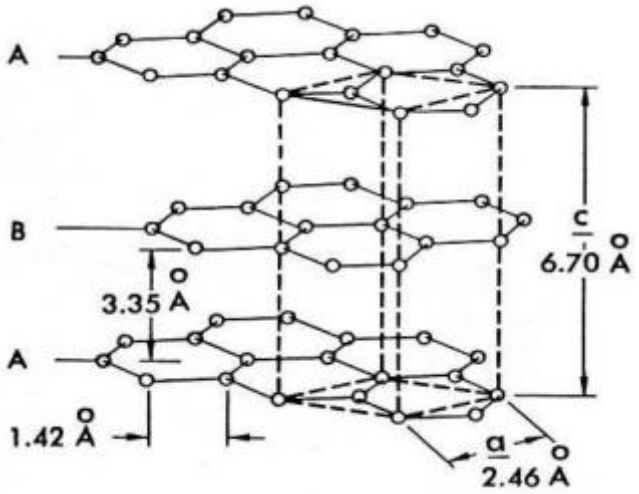

Fig. 1-4 The crystal structure of graphite

The structure of graphite has been determined through such methods as X-ray diffraction [82], transmission electron microscopy, neutron diffraction [83] and convergent beam electron diffraction.

1.3.2 Properties and applications

Table 1-1 shows the main properties of graphite [84].

Table 1-1 The properties of graphite

Graphite	property	Unit
Density	2.26	g/cm^{-3}
Elastic modulus	1 (In plane)	TPa
Strength	130	GPa
Resistivity	50 (In plane)	μΩ • cm
Thermal conductivity	3000 (In plane)	$Wm^{-1}K^{-1}$
Thermal expansion	$\sim 1\times10^{-6}$ (In plane), 29×10^{-6} (z-axis)	K^{-1}
Thermal stability	450-650 (In air)	^{o}C

1.3.2.1 Hardness

The hardness of minerals is compared using the Mohs Hardness Scale, a relative scale numbered 1 (softest) to 10 (hardest). Graphite is very soft and has a hardness of 1 to 2 on this scale. Brown had measured the hardness of irradiated graphite after annealing at successively higher temperatures [85]. The crystal structure of graphite yields physical properties that permit the use of graphite as a lubricant and as pencil lead. Most pencil cores are made of graphite mixed with a clay binder, leaving grey or black marks that can be easily erased. A set of pencils ranging from a very hard, light-marking pencil to a very soft, black-marking pencil usually ranges from hardest to softest as Fig. 1-5.

Fig. 1-5 Twenty grades graphic pencils from 9H to 9B

1.3.2.2 Electrical conductivity

Natural graphite flakes provide good electrical conductivity (106 S/m at ambient temperature) and layered structure with a *c*-axis lattice constant, which indicates interplanar spacing, of 0.66 nm [86]. The expanded graphite, however, contains abundant multi-pores ranging from 2 nm to 10 mm. Average size of the pores is about 2 mm. The graphite maintains a layered structure similar to natural flake graphite but with larger layer spacing [87]. Graphite has been widely used as a conducting filler in fabricating conductive polymer composites. The corresponding percolation threshold of graphite nanoplatelet (GNP) polymer nanocomposites is very low-often below 2 wt%. This unique property is attributed to the extremely large surface area and aspect ratio of the GNPs, allowing the formation of an uninterrupted conducting network for electrons within the polymer [88].

Recently, plenty of works have been done to study the electronic application of graphite. Li et al. investigated the effects of ultrasonication and UV/ozone treatment of graphite on electrical conductivity of epoxy-based nanocomposites containing graphite nanoplatelets [89]. A four probe method was used to measure the electrical conductivities of poly (styrene-co-acrylonitrile)/expanded graphite composites. The composites showed excellent electrical conductivities in both *a*- axis and *c*-axis [90]. Hishiyama obtained large and highly crystallized kish graphite flakes and measured the temperature dependence of the in-plane electrical resistivity for the specimens at temperatures between 1.28 and 300 K [91]. The resistivity is proportional to T^2, the dependence in the temperature range from 5 to 15 K is due to the scattering of carriers by the out-of-plane phonons. The T^2 dependence at temperatures below about 5 K is attributed to the electronhole scattering as described by Morelli and Uher. Zheng et al.

prepared PMMA/expanded graphite composites and measured its electrical conductivity by a four-point probe resistivity determiner [92]. They found that only 1 wt% filler content was required to reach the percolation threshold of transition in electrical conductivity from an insulator to a semiconductor. The improvement of electrical conductivity was attributed to the difference in filler geometry (aspect ratio and surface area) and the formation of conductive networks in the composites.

1.3.2.3 Thermal properties

Graphite has good thermal and mass transfer characteristics that have led to its being used as a matrix for heat and mass transfer intensification. Graphite is also believed to be a promising material for thermal transfer enhancement in the storage of hydrogen by adsorption. For a pure graphite pellet with a porosity of 79.1%, the effective thermal conductivity of pure graphite pellets is about 8 W/(m·K) while the density of graphite is 1250 kg/m^3 [93]. In gas separation, graphite had been utilized as an additive for the granular adsorbents of activated carbon, in which the thermal conductivity of activated carbon is improved by over than 20 times. Graphite has also been utilized for heat transfer intensification of phase change materials, such as paraffin, in which the thermal conductivity was improved from 0.22 to over than 0.8 W/(m·K). The main problem in research on compacted adsorbents with graphite as a matrix is the large variation in the values of thermal conductivities that are reported by different researchers. Mostly the value is lower than 6 W/(m·K), but for the compacted adsorbents that react with water and utilizes graphite as matrix, the thermal conductivity was reported to be as high as 9-10 W/(m·K) while the samples are tested under the ambient conditions by unsteady conductivity test methods. The reason for this anomaly is analyzed, and it is suggested to be caused by the reaction heat between hydrophilic adsorbents and the water in the air. In such conditions, the temperature difference between measuring point and heating point will be less than the condition without reaction heat, and then the calculated thermal conductivity will be much larger than the normal values [94].

Recently, expanded graphite (EG) has been employed to enhance the heat transfer in phase-change materials (PCMs), due to its desirable properties of high thermal conductivity, high stability, good compatibility with organic PCMs, and lower density and weight as compared with metal promoters. It has been shown that EG can improve the thermal conductivity of a PCM without much reduction in energy storage capacity and liquid exudation during its phase change. Zhang et al. produced EG by microwave irradiation performed at room temperature. And then the paraffin/EG composite PCM was prepared by absorbing liquid paraffin into EG, in which paraffin was chosen as the PCM. It was found that the EG prepared at 800 W irradiation power for 10 s exhibited the maximum sorption capacity of 92 wt% for paraffin [95].

1.4 Carbon black

1.4.1 Structure and manufacture

Carbon black, a kind of amorphous carbon, is light, loose and very fine black powder as shown in Fig. 1-6. The surface area of carbon black is in the range of 10 to 3000 m^2/g. Carbon black is a commercial product manufactured by thermal decomposition, including detonation, or by incomplete combustion of carbon hydrogen compounds and has a well-defined morphology with a minimum content of tars or other extraneous materials. The structure of carbon black can be described in terms of the graphite structure shown by Fig. 1-7. Carbon blacks vary greatly in their structure. The structural characterization of these materials is difficult because of the very small particle size in the materials. In general, the structures are described as being either a “high” structure or a “low” structure. A high structure carbon black usually consists of many primary particles of carbon black fused together in an aciniform (“grape-like”) aggregate structure. A low structure carbon black consists of a small number of carbon black particles fused together in an aggregate, generally with a larger primary particle size [96].

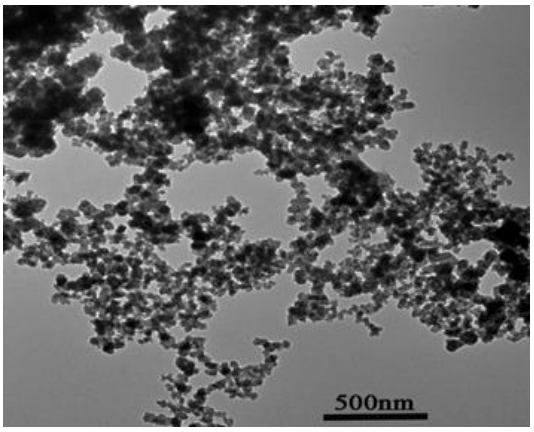

Fig. 1-6 The appearance of carbon black

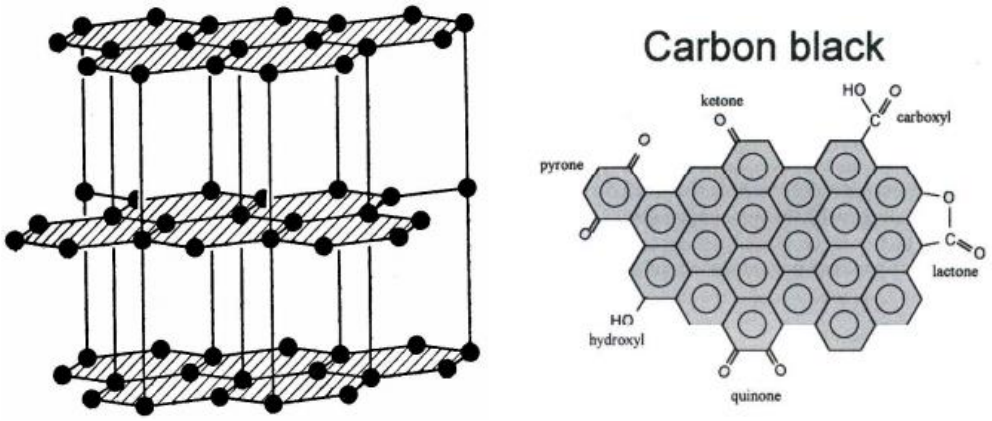

Fig. 1-7 The structure of carbon black [96]

1.4.2 Properties and applications

One of the more innovative uses for carbon black pigments in the plastics industry is in the electronics field. Products in this industry are called electrically conductive compounds. Since few plastic resins are inherently conductive, it is necessary to add special fillers to the plastic matrix to give them the desired conductive characteristics.

An increasingly important use for carbon black is as filler in polymers in order to enhance the electrical conductivity of the polymer. It was discovered that when mixed into rubber it improves its mechanical properties [97]. The increase in strength of the rubber containing carbon black led to many practical application of the rubber throughout the world. Carbon black is known to significantly change the flow and viscosity of an uncured rubber compound. The hydrodynamic effect from the carbon

black present reduces the volume fraction of the flow medium causing shear strain amplification when the compound is forced to flow thus increasing the viscosity. Higher surface area of carbon black impacts higher levels of reinforcement with resulting higher hysteresis. Higher structure generally gives improving extrusion behavior, higher compounds modulus and higher compound viscosity. Some rubber properties like tensile strength, abrasion resistance, are increased with the increasing loading of carbon black to an optimum and then they decrease. There are many reviews of filler reinforcement by authors such as Kraus [98] and Leblanc [99]. The principal factors that determine the reinforcement capability are,

(1) The Van der Waal forces between the carbon black and the polymer;

(2) The chemical crosslinks or chemical absorptions of the polymer on to the filler surface due to free radical reaction between carbon atoms in the filler and in the rubber;

(3) The mechanical interlocking of the polymer on to the filler surface.

1.5 Purpose of this research

The application of carbon materials has been limited because of their easy aggregating and poor affiliation with polymers. Therefore, the present study aimed on developing carbon materials based composites with good electrical and mechanical properties. This study focused on polymer modified carbon nanotube, graphite and carbon black prepared by proposed approaches.

In chapter 1, the research backgrounds, research significance, and the construction of this thesis were described. The objectives of the research were to prepare carbon materials/polymer composites and characterize their properties.

In chapter 2, the properties of experiment materials and reagents were presented. The experimental methods and characteristics are also presented in this chapter.

In chapter 3, carbon black/polystyrene nanocomposites (CB/PS) were successfully prepared through a facile strategy. The ionic liquid improves the percentage grafting because of its high viscosity. The electrical properties of polymer composites before and

after the grafting were measured. The microstructure, morphology and thermal properties of the composites were characterized by Fourier transform infrared spectroscopy (FT-IR), thermal gravimetric analysis, (TGA), scanning electron microscopy (SEM), transmission electron microscopy (TEM) and Raman spectroscopy. The results proved that the polystyrene had been successfully grafted onto the CB surface.

In chapter 4, the multi-walled carbon nanotube/polystyrene (MWCNT/PS), carbon black/polystyrene (CB/PS) and the multi-walled carbon nanotube-carbon black/Polystyrene (M-C/PS) nanocomposites with different contents of carbon materials were prepared by bulk radical polymerization. The electrical resisitivity of all nanocomposites were measured and compared. The Fourier transform infrared spectroscopy (FT-IR), thermal gravimetric analysis (TGA), and transmission electron microscope (TEM) of samples which were extracted with Soxhlet extraction in toluene from polymerides were tested. The mechanical properties of nanocomposites were also investigated.

In chapter 5, the MWCNT/PMMA composites were synthesized by Pickering emulsions polymerization in the presence of MWCNT as a colloidal surfactant. The effect of monomer concentration on the electrical properties of MWCNT/PMMA composites was investigated. It was found that the composites have excellent electrical conductivity. The morphology of MWCNT/PMMA composites was also examined by SEM. The thermal gravimetric analysis of the prepared composites confirmed that they were MWCNT/PMMA composite particles, which could have a wide range of potential applications, such as in catalysts, sensors, environmental remediation, and energy storage. The poly (lactic acid) based composite with the MWCNT/PMMA was also prepared with twin-screw extruding and injection molding. The mechanical properties suggested the greatly damage for MWCNTs and their stability during the Pickering emulsions polymerization.

In chapter 6, graphite powder (GP) was modified by a proposed chemical method to

improve their affinity with polyamide 6 (PA6). The X-ray photoelectron spectroscopy (XPS), elemental analysis, thermal gravimetric analysis (TGA) and X-ray diffraction (XRD) results proved the successful modification of GP by the proposed method. The composites of GP and PA6 (GP/PA), GP-OH and PA6 (GP-OH/PA) and GP-NH_2 and PA6 (GP-NH_2/PA) were prepared via the twin-screw extruding and injection molding processes. The scanning electron microscopy (SEM), optical microscopy, tensile strength and bending strength have been done to investigate their morphology and mechanical properties.

In chapter 7, general conclusions of the study are made. The future works are also prospected.

The overall structure of the present study is presented in Fig. 1-8.

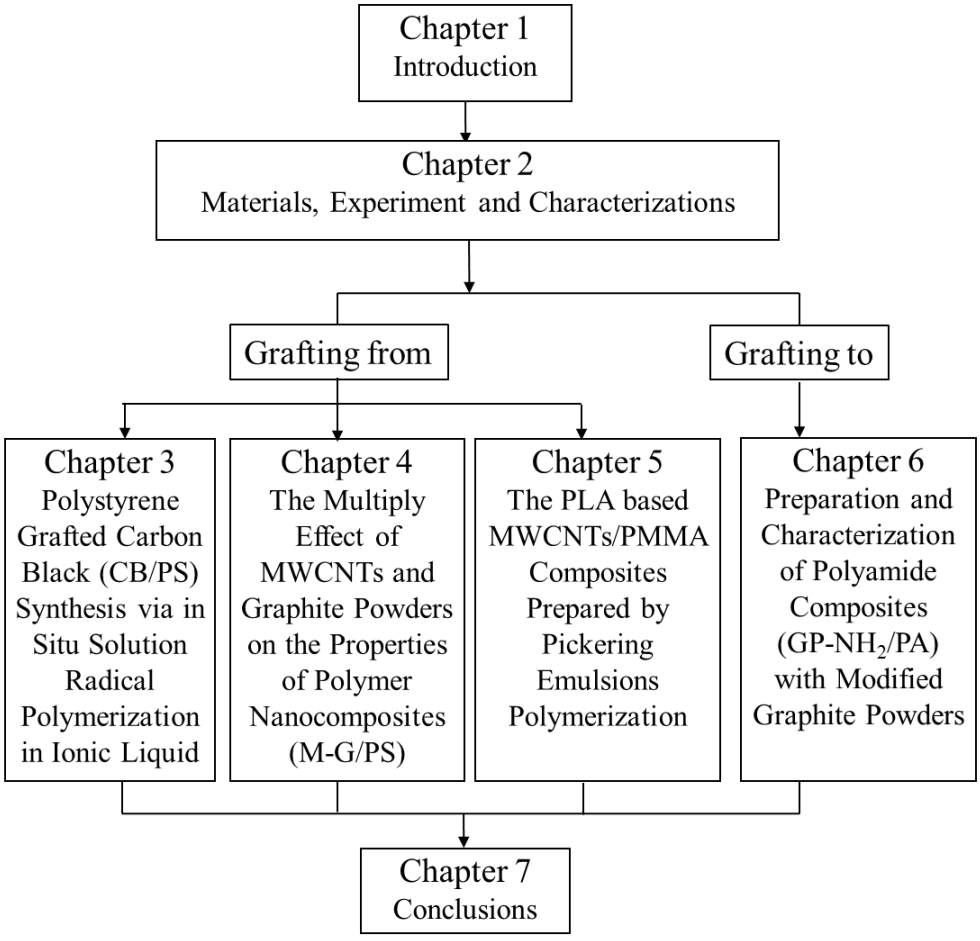

Fig. 1-8 The overall structure of the present study

References

[1] [http://www.camelclimatechange.org/articles/view/153658/?topic=66027; accessed in September 2011].

[2] Japanese Plastic Waste Management Institute, [http://www.pwmi.or.jp/flow/flame04.htm; accessed in September 2011].

[3] Intergovernmental Panel on Climate Change, Climate change 2007: the physical science basis, IPCC WGI Fourth Assessment Report, Paris, February 5 (2007).

[4] A.K. Geim, Graphene: Status and Prospects, Science, 324 (2009) 1530-1534.

[5] P.M. Ajayan, O.Z. Zhou, Applications of Carbon Nanotubes, Topics in Applied Physics, 80 (2001) 391-425.

[6] http://en.wikipedia.org/wiki/Carbon_nanotube.

[7] H.W. Kroto, J.R. Heath, S.C. O' Brien, R.F. Curl, R.E. Smalley, C_{60}: Buckminster Fullerence, Nature, 318 (1985) 162-163.

[8] http://en.wikipedia.org/wiki/Fullerene.

[9] Federal Trade Commission Carbon Black Export I, et al. Investigations and Recommendations under the Export Trade Act, (1948)1245-1345.

[10] High Performance Carbon Fibers. National Historic Chemical Landmarks. American Chemical Society, 2013.

[11] T.D. Burchell, 2.10-Graphite: Properties and Characteristics, Comprehensive Nuclear Materials, 2 (2012) 285-305.

[12] P.J.F. Harris, Carbon Nanotubes and Related Structures, London: Cambridge University Press, 1999.

[13] L.C. Qin, X.L. Zhao, K. Hirahara, Y. Miyamoto, Y. Ando, S. Lijima, Materials Science: The Smallest Carbon Nanotube, Nature, 408 (2000) 50.

[14] D.C. Huang, D.H. Huang, Carbon Nanotubes and Their Applications, Progress in Physics, 23 (2004) 274-288.

[15] Z.W. Pan, S.S. Xie, B.H. Chang, C.Y. Wang, L. Lu, W. Liu, W.Y. Zhou, W. Z. Li,

L.X. Qian, Very Long Carbon Nanotube, Nature, 394 (1998) 631-632.

[16] M. Bockrath, D. Cobden, P. McEuen, N. Chopra, A. Zettl, A. Thess, R. Smalley, Single-Electron Transport in Ropes of Carbon Nanotubes, Science, 275 (1997) 1922-1925.

[17] M.S. Dresselhaus, G. Dresselhaus, J.C. Charlier, E. Hernández, Electronic, Thermal and Mechanical Properties of Carbon Nanotubes, Philosophical Transactions of Royal Society of London A, 362 (2004) 2065-2098.

[18] M.-F. Yu, O. Lourie, M.J. Dyer, K. Moloni, T.F. Kelly, R.S. Ruoff, Strength and Breaking Mechanism of Multiwalled Carbon Nanotubes Under Tensile Load, Science, 287 (2000) 637-640.

[19] B.Yakobson1, P. Avouris. Mechanical Properties of Carbon Nanotubes, Topics in Applied Physics, 80, 287-327 (2001).

[20] J.-P. Salvetat, J.-M. Bonard, N.H.Thomson, A.J. Kulik, L. Forr´o, W. Benoit, L. Zuppiroli, Mechanical Properties of Carbon Nanotubes, Applied Physics A Materials Science & Processing, 69 (1999) 255-260.

[21] Z.W. Pan, S.S. Xie, L. Lu, B.H. Chang, L.F. Sun, W.Y. Zhou, G. Wang, D.L. Zhang, Tensile Tests of Ropes of Very Long Aligned Multiwall Carbon Nanotubes, Applied Physics Letters, 74 (1999) 3152-3154.

[22] M.-F. Yu, B.S. Files, S. Arepalli, R.S. Ruoff, Tensile Loading of Ropes of Single Wall Carbon Nanotubes and Their Mechanical Properties, Physical Review Letters, 84 (2000) 5552-5555.

[23] J.W. Mintmire, B.I. Dunlap, C.T. White, Are Fullerene Tubesmetallic? Physical Review Letters, 68 (1992) 631-634.

[24] R. Saito, M. Fujita, G. Dresselhaus, M.S. Dresselhaus, Electronic Structure of Chiral GrapheneTubules, Applied Physics Letters, 60 (1992) 2204-2206.

[25] D.S. Bethune, C.H. Kiang, M.S. Vries, G. Gorman, R. Savoy, J. Vasquez, R. Beyers, Cobalt-Catalysed Growth of Carbon Nanotubes with Single-Atomic-Layer Walls, Nature, 363 (1993) 605-607.

[26] M.S. Dresselhaus, G. Dresselhaus, P.C. Eklund, Scienceof Fullerenes and Carbon Nanotubes, Academic, San Diego, 1986.

[27] I. Sumino, Helical Microtubules of Graphitic Carbon, Nature, 354 (1991) 56-58.

[28] T.W. Odom, J.-L. Huang, P. Kim, C.M. Lieber, Atomic Structure and Electronic Properties of Single-Walled Carbon Nanotubes, Nature, 391 (1998) 62-64.

[29] T. Hertel, R.E. Walkup, Deformation of carbon nanotubes by surface van der Waals forces, Physical Review B, 58 (1998) 13870-13873.

[30] V. Meunier, L. Henrard, Ph. Lambin, Energetics of Bent Carbon Nanotubes, Physical Review B, 57 (1998) 2596-2606.

[31] L. Chico, V.H. Crespi, L.X. Benedict, S.G. Louie, M.L. Cohen, Pure Carbon Nanoscale Devices: Nanotube Heterojunctions, Physical Review Letters, 76 (1996) 971-974.

[32] J. Voit, One-Dimensional Fermi Liquids, Reports of Progress in Physics, 58 (1995) 977-1116.

[33] M.A. imenta, A. arucci, S.D.M. rown, M.J. atthews, A.M. ao, P.C. klund, R.E. malley, G. Delhaus, M.S. Dresselhaus, Resonant Raman Effect in Single-Wall Carbon Nanotubes, Journal of Materials Research, 13 (1998) 2396-2404.

[34] M.S. Dresselhaus, G.D. resselhaus, A. Jorio, Unusual Properties and Structure of Carbon Nanotubes, Annual Review of Materials Research, 34 (2004) 247-278.

[35] M. Freitag, M. Radosavljevic, Y. Zhou, A.T. Johnson, Controlled Creation of a Carbon Nanotube Diode by a Scanned Gate, Applied Physics Letters, 79 (2001) 3326-3328.

[36] T.W. Odom, J.L. Huang, C.L. Cheung, and C.M. Lieber, Magnetic Clusters on Single-Walled Carbon Nanotubes: The Kondo Effect in a One-Dimensional Host, Science, 290 (2000) 1549-1552.

[37] R. Saito, G. Dresselhaus, M.S. Dresselhaus, Electronic Structure of Double-Layer Graphene Tubules, Journal of Applied Physics, 73 (1993) 494-500.

[38] P.G. Collins, M.S. Arnold, P. Avouris, Engineering Carbon Nanotubes and

Nanotube Circuit Using Electrical Breakdown, Science, 292 (2001) 706-709.

[39] R. Saito, G. Dresselhaus, M.S. Dresselhaus, Electronic Structure of Chiral Graphene Tubules, Journal of Applied Physics, 60 (1992) 2204-2206.

[40] S. Frank, P. Poncharal, Z.L.Wang, W.A. Heer, Carbon Nanotube Quantum Resistors, Science, 280 (1998) 1744-1746.

[41] P. Bandaru, Electrical Properties and Applications of Carbon Nanotube Structures, Journal of Nanoscience and Nanotechnology, 7 (2007) 1-29.

[42] C. Schonenberger, A. Bachtold, C. Strunk, J.-P. Salvetat, L. Forro, Interference and Interaction in multi-wall carbon nanotubes, Applied Physics A, 69 (1999) 283-295.

[43] S.J. Tans, M.H. Devoret, H. Dai, A. Thess, R.E. Smalley, L.J. Geerligs, C. Dekker, Individual Single-Wall Carbon Nanotubes as Quantum Wires, Nature, 386 (1997) 474-477.

[44] M. Buitelaar, T.N.A. Bachtold, M. Iqbal, C. Schönenberger, Multiwall Carbon Nanotubes as Quantum Dots, Physical Review Letters, 88 (2002) 156801-156804.

[45] S.J. Tans, A.R.M. Verschueren, C. Dekker, Room-Temperature Transistor Based on a Single Carbon Nanotube, Nature, 393 (1998) 49-52.

[46] D. Zhou, S. Seraphin, Complex Branching Phenomena in the Growth of Carbon Nanotubes, Chemical Physics Letters, 238 (1995) 286-289.

[47] C. Papadapoulos, A. Rakitin, J. Li, A.S. Vedeneev, J.M. Xu, Electronic Transport in Y-Junction Carbon Nanotubes, Physical Review Letters, 85 (2000) 3476-3479.

[48] G.W.C. Kaye, T.H. Laby, Tables of Physical and Chemical Constants, 16th Ed. Longman, London, 1995.

[49] R.S. Ruoff, D.C. Lorents, Mechanical and Thermal Properties of Carbon Nanotubes. Carbon, 33 (1995) 925-930.

[50] J. Hone, Phonons and Thermal Properties of Carbon Nanotubes, Topics in Applied Physics, 80 (2001) 273-286.

[51] D. Li, Thermal Transport in Individual Nanowires and Nanotubes. Phd Thesis, Department of Mechanical Engineering, University of California, Berkeley, CA, USA,

2002.

[52] J.P. Small, L. Shi, P. Kim, Mesoscopic Thermal and Thermoelectric Measurements of Individual Carbon Nanotubes, Solid State Commun, 127 (2003) 181-186.

[53] J. Hone, M. Whitney, C. Piskoti, A. Zettl, Thermal Conductivity of Single-Walled Carbon Nanotubes, Physics Review B, 59 (1999) R2514-R2516.

[54] Y. Maniwa, R. Fujiwara, H. Kira, H. Kataura, S. Suzuki, Y. Achiba, E. Nishibori, M. Takata, M. Sakata, A. Fujiwara H. Suematsu, Thermal Expansion of SWNT Bundles: X-Ray Diffraction Studies, Physical Review B, 64 (2001) 241402-1-241402-3.

[55] G.G. Samsonidze, G.G. Samsonidze, B.I. Yakobson, Kinetic Theory of Symmetry-Dependent Strength in Carbon Nanotubes, Physical Review Letters, 88 (2002) 065501-1-065501-4.

[56] J. Hone, Carbon Nanotubes: Thermal Properties, Dekker Encyclopedia of Nanoscience and Nanotechnology, Columbia University, New York, U.S.A., 2004.

[57] L. Jin, C. Bower, O. Zhou, Alignment of Carbon Nanotubes in a Polymer Matrix by Mechanical Stretching, Applied Physics Letters, 73 (1998) 1197-1120.

[58] P.M. Ajayan, L.S. Schadler, C. Giannaris, A. Rubio, Single-Walled Carbon Nanotube-Polymer Composites: Strength and Weakness, Advanced Materials, 12 (2000) 750-753.

[59] S. Chang, R.H. Doremus, P.M. Ajayan, R.W. Siegel, Processing and Mechanical Properties of C-Nanotube Reinforced Alumina Composites, Ceramic Engineering and Science Proceedings, 21 (2000) 653-658.

[60] H. Ago, K. Petritsch, M.S.P. Shaffer, A.H. Windle, R.H. Friend, Composites of Carbon Nanotubes and Conjugated Polymers for Photovoltaic Devices, Advanced Materials, 11 (1999) 1281-1285.

[61] M.S. Dresselhaus, G. Dresselhaus, K. Sugihara, I.L. Spain, H.A. Goldberg, Graphite Fibers And Filaments, Springer, Berlin, Heidelberg, 1988.

[62] P.C. Ramanmurthy, W.R. Harrell, R.V. Gregory, B. Sadanadan, A.M. Rao, Electronic Properties of Polyaniline/Carbon Nanotube Composites, Synthetic Metals,

137 (2003) 1497-1498.

[63] J.N. Coleman, S. Curran, A.B. Dalton, A.P. Davey, B. Mccarthy, W. Blau, R.C. Barklie, Percolation-Dominated Conductivity in a Conjugated Polymer-Carbon-Nanotube Composite, Physical Review B, 58 (1998) R7492-R7495.

[64] R Zhang, Conductive TPU/CNT Composites for Strain Sensing, University of London, London, 2009.

[65] Y.C. Choi, Y.M. Shin, Y.H. Lee, B.S. Lee, G.S. Park, W.B. Choi, N.S Lee, J.M. Kim, Controlling the Diameter, Growth Rate, and Density of Vertically Aligned Carbon Nanotubes Synthesized by Microwave Plasma-Enhanced Chemical Vapor Deposition, Applied Physics Letters, 76 (2000) 2367-2369.

[66] Y. Cheng, O. Zhou, Electron Field Emission from Carbon Nanotubes, Comptes Rendus Physique, 4 (2003) 1021-1033.

[67] S.H. Jo, Y. Tu, Z.P. Huang, D.L. Carnahan, D.Z. Wang, Z.F. Ren, Effect of Length and Spacing of Vertically Aligned Carbon Nanotubes on Field Emission Properties, Applied Physics Letters, 82 (2003) 3520-3522.

[68] A.G. Rinzler, J.H.Hafner, P. Nikolaev, L. Lou, S.G. Kim, D. Tomanek, P. Nordlander, D.T. Colbert, R.E. Smalley, Unraveling Nanotubes: Field Emission from an Atomic Wire, Science, 269 (1995) 1550-1553.

[69] J. Kong, N.R. Franklin, C. Zhou, M.G. Chapline, S. Peng, K. Cho, H. Dai. Nanotube Molecular Wires as Chemical Sensors, Science, 287 (2000) 622-625.

[70] J. Kong, M.G. Chapline, H. Dai, Functionalized Carbon Nanotubes for Molecular Hydrogen Sensors, Advanced Materials, 13 (2001) 1384-1386.

[71] C.Q. Wu, Y. Cao, X. Sun, D.B. Zhu, Glucose Sensors Based on Glucose-Oxidase-Containing Polypyrrole/Aligned Carbon Nanotube Coaxial Nanowire Electrodes, Synthetic Metals, 137 (2003) 1393-1394.

[72] Q. Zhao, M. Frogley, H. Wagner, Direction-Sensitive Stress Measurements with Carbon Nanotube Sensors, Polymers for Advanced Technologies, 13 (2002) 759-764.

[73] E. Frackowiak, S. Gautier, H. Gaucher, S. Bonnamy, F. Beguin, Electrochemical

Storage of Lithium in Multi-Walled Carbon Nanotubes, Carbon, 37 (1999) 61-69.

[74] B. Gao, A. Kelinhammes, X.P. Tang, C. Bower, Y. Wu, O. Zhou, Electrochemical Intercalation of Single-Walled Carbon Nanotubes with Lithium, Chemical Physics Letters, 307 (1999) 153-157.

[75] A.C. Dillon, K.M. Jones, T.A. Bekkedahl, C.H. Kiang, D.S. Bethune, M.J. Heben, Storage of Hydrogen in Single-Walled Carbon Nanotubes, Nature, 386 (1997) 377-379.

[76] C. Liu, Y.Y. Fan, M. Liu, H.T. Cong, H.M. Cheng, M.S. Dresselhaus, Hydrogen Storage in Single-Walled Carbon Nanotubes at Room Temperature, Science, 286 (1999) 1127-1129.

[77] P. Chen, X. Wu, J. Lin, K. Tan, High H_2 Uptake by Alkali-Doped Carbon Nanotubes Under Ambient Pressure and Moderate Temperatures, Science, 285 (1999) 91-93.

[78] C. Nutenadel, A. Zuttel, D. Chartouni, L. Schlapbach, Electrochemical Storage of Hydrogen in Nanotube Materials, Solid State Letters, 2 (1999) 30-32.

[79] B.T. Kelly, Physics of Graphite, Applied Science, London, 1981.

[80] Properties and Characteristics of Graphite, for the Semicondeuctor Industry, 2013.

[81] W.H. Brixius, Mercury Porosimetry Analysis of Fine-Grained Graphite, 16th Biennial Conference on Carbon, 1983, 465-466.

[82] Z.Q. Li, C.J. Lu, Z.P. Xia, Y. Zhou, Z. Luo, X-Ray Diffraction Patterns of Graphite and Turbostratic Carbon, Carbon, 45 (2007) 1686-1695.

[83] P. Trucano, R. Chen, Structure of Graphite by Neutron Diffraction, Nature, 258 (1975) 136-137.

[84] R. Sengupta, M. Bhattacharya, S. Bandyopadhyay, A. Bhowmick, A Review on the Mechanical and Electrical Properties of Graphite Andmodified Graphite Reinforced Polymer Composites, Progress in Polymer Science, 36 (2011) 638-670.

[85] R.G. Brown, The Hardness of Irradiated Graphite, Carbon, 6 (1968) 27-30.

[86] N.Z. Cao, W.C. Shen, S.Z. Wen, Y.J. Liu, Z.D. Wang, M. Inagaki, The Factors Influencing the Porous Structure of Expanded Graphite. Materials Science and

Engineering (Chinese), 14 (1996) 22-26.

[87] X.Y. Chuan, Electrical Properties of Expanded Graphite Intercalation Compoumds, Journal of Materials Science & Technology, 17 (2001) 371-374.

[88] Y.X. Pan, Z.Z. Yu, Y.C. Ou, G.H. Hu, A New Process of Fabricating Electrically Conducting Nylon 6/Graphite Nanocomposites via Intercalation Polymerization, Journal of Polymer Science Part B: Polymer Physics, 38 (2000) 1626-1633.

[89] J. Li, J.-K. Kim, M.L. Sham, Conductive Graphite Nanoplatelet/Epoxy Nanocomposites: Effects of Exfoliation and UV/Ozone Treatment of Graphite, Scripta Materialia, 53 (2005) 235-240.

[90] W.P. Wang, C.Y. Pan, J.S. Wu, Electrical Properties of Expanded Graphite/Poly (Styrene-Co-Acrylonitrile) Composites, Journal of Physics and Chemistry of Solids, 66 (2005) 1695-1700.

[91] Y. Hishiyama, Y. Kaburagi, Electrical Resistivity of Highly Crystallized Kish Graphite, Carbon, 30 (1992) 483-486.

[92] W.G. Zheng, S.C. Wong, Electrical Conductivity and Dielectric Properties of PMMA/Expanded Graphite Composites, Composites Science and Technology, 63 (2003) 225-235.

[93] H.P. Klein, M. Groll, Heat Transfer Characteristics of Expanded Graphite Matrices in Metal Hydride Beds. International Journal of Hydrogen Energy, 29 (2004) 1503-1511.

[94] L.W. Wang, Z. Tamainot-Telto, S.J. Metcalf, R.E. Critoph, R.Z. Wang, Anisotropic Thermal Conductivity and Permeability of Compacted Expanded Natural Graphite, Applied Thermal Engineering, 30 (2010) 1805-1811.

[95] Z.G. Zhang, N. Zhang, J. Peng, X.M. Fang, X.N. Gao, Y.T. Fang, Preparation and Thermal Energy Storage Properties of Paraffin/Expanded Graphite Composite Phase Change Material, Applied Energy, 91 (2012) 426-431.

[96] P.J. Mather, K.M. Thomas, Carbon Black/High Density Polyethylene Conducting Composite Materials, Journal of Materials Science, 32 (1997) 401-407.

[97] K. Baranwal, H. Stephens, “Basic Elastomer Technology”, First Edition, Rubber Division, American Chemical Society, The University of Akron, Akron, OH, 2001.

[98] G. Kraus, Reinforcement of Elastomers by Carbon Black. Rubber Chemistry and Technology, 51 (1978) 297-321.

[99] J.L. Leblanc, Rubber-Filler Interactions and Rheological Properties in Filled Compounds, Progress in Polymer Science, 27 (2002) 627-687.

Chapter 2 Materials, Experiment and Characterizations

2.1 Materials

2.1.1 Multi-walled carbon nanotube (MWCNT)

MWCNTs were obtained from Showa Denko Company, Tokyo, Japan, and they are special carbon nanotubes for resin composites. MWCNTs, the Vapor Grown Carbon Fiber (VGCF®-X), are synthesized by catalytic chemical vapor deposition method. The average diameter of MWCNTs is approximate 10-15 nm. The parameters of MWCNTs are shown in Table 2-1, and the structure is shown in Fig. 2-1. MWCNTs can give electrical conductivity to insulate resin and rubber with quite a small amount, less than 3 wt% of MWCNTs were added to them. MWCNTs are used for electrical-conductive, electrostatic-dissipative, or antistatic polymer composites as raw material of molded packages and parts, which should be electrically conductive, in electric, electronic and automotive application fields.

Table 2-1 The parameters of MWCNTs

Parameters	Unit	Value
Average diameter	nm	10-15
Average length	μm	3
Bulk density	g/cm^3	0.08

Because of unique structure, mechanical and electrical properties of MWCNTs, they have attracted more and more interest for wide applications [1], such as in the field of electrical conductivity, mechanical strength and thermal conductivity as shown in Fig. 2-2.

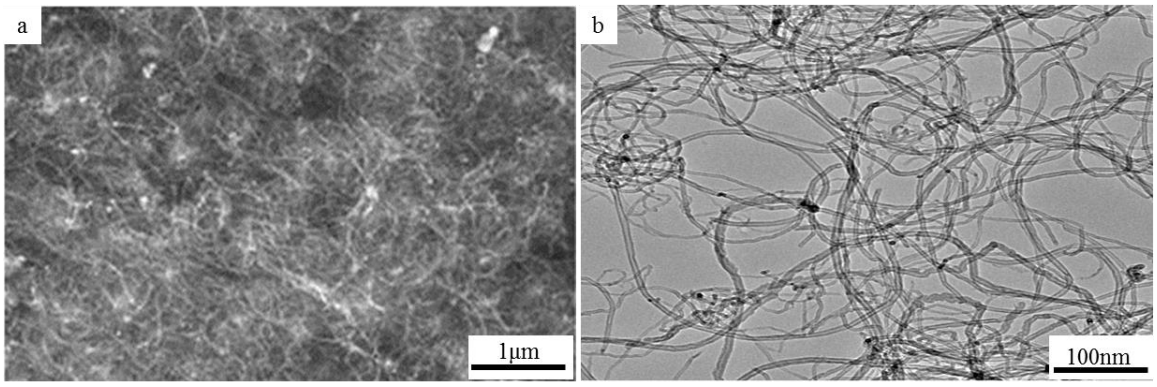

Fig. 2-1 SEM (a) and TEM (b) images of MWCNTs

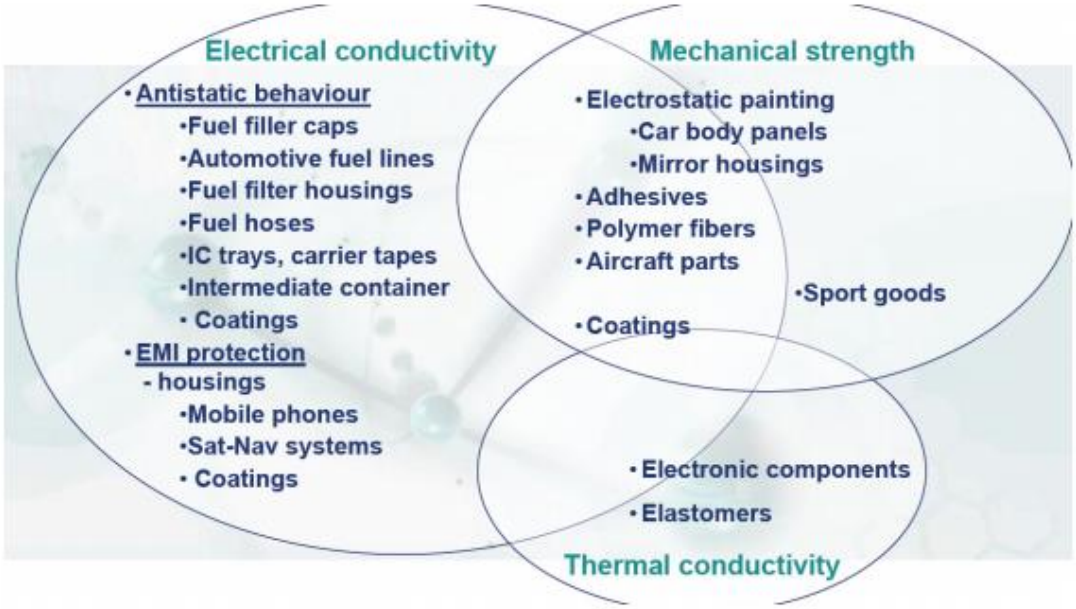

Fig. 2-2 Key properties of MWCNTs give rise to a number of potential application fields

2.1.2 Graphite

Natural graphite is generally found or obtained in the form of small, soft flakes or powders. There are three principal types of natural graphite: 1. Crystalline flake graphite (or flake graphite for short); 2. Amorphous graphite; 3. Lump graphite (also called vein graphite). Natural graphite is mostly consumed for refractories, batteries, steelmaking, expanded graphite, brake linings, foundry facings and lubricants.

Graphite has the advantage of being readily and cheaply available in a variety of

shapes and sizes [2, 3]. Graphite has a high thermal conductivity due to the vast electron delocalization within the carbon layers (a phenomenon called aromaticity). Because these valence electrons are free to move, they are able to conduct electricity. However, the electricity is mainly conducted within the plane of the layers. Powdered graphite can be used as a semiconductor substitute in early carbon microphones because the well conductive properties [4].

In this work, the graphite was bought from Nippon Graphite Industries, Japan. It is the highly purified soil-type graphite with an excellent dispersion suited to plastics and rubber materials. It has even higher lubricating and conductive qualities than carbon black, which making it a great choice for conductive compounds.

2.1.3 Carbon black (CB)

Carbon black, named as DENKA BLACK (DB), was obtained from Showa Denko Company, Tokyo, Japan. CB is acetylene black, a type of carbon black, obtained from thermal decomposition of acetylene. It is highly purified and extremely conductive. These characteristics make it an ideal material in the production of dry cells, electric power cables, as well as in such sectors as silicon products, IC packaging materials and so on. Carbon black has been used in dry cells, rubber reinforcements, cables, tires, belts, hoses, flooring, shoes, surface heating element, black pigment, electronic components, etc.

2.1.4 2, 2'-Azoisobutyronitrile (AIBN)

2, 2'-Azoisobutyronitrile (AIBN) is the most common kind of azo initiators. Its decomposition reaction is relatively stable, produce only one kind of radical, without induced decomposition, and thus commonly used in radical polymerization kinetics. Because of its stability, it can be easily storaged and used. The decomposition temperature of AIBN is from 50 to 70 ^{o}C, decomposition activation energy is 129 kJ/mol, is a low-active initiator. The decomposition mechanism is shown in Fig. 2-3.

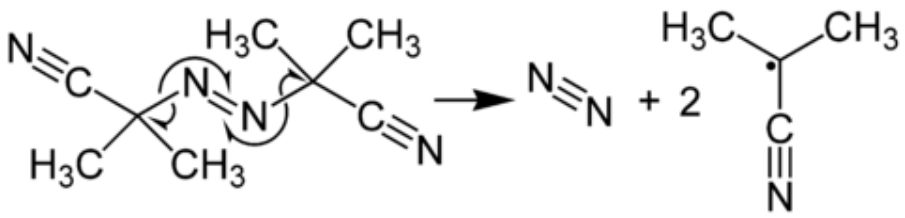

Fig. 2-3 The reaction mechanism of AIBN

2.1.5 Poly (lactic acid) (PLA)

Poly (lactic acid) or polylactide (PLA) is aliphatic biodegradable polyester made up of lactic acid (2-hydroxy propionic acid). PLA is a thermoplastic aliphatic polyester derived from renewable resources, such as corn starch (in the United States), tapioca roots, chips or starch (mostly in Asia), or sugarcane (in the rest of the world). Owing to PLA can biodegrade under certain conditions, such as the presence of oxygen, it has been considered as one of the solutions to alleviate white waste disposal problems and to lessen the dependence on petroleum-based plastics for packaging materials.

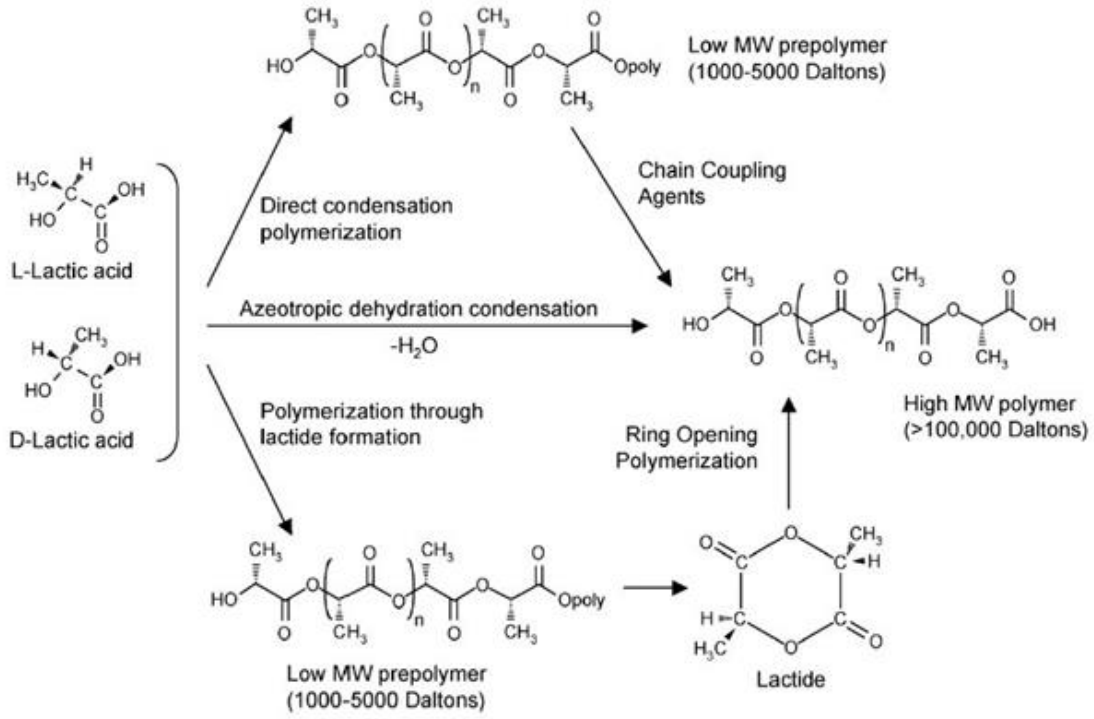

Fig. 2-4 Synthesis methods for obtaining PLA.

PLA can be produced using several techniques, including azeotropic dehydrative condensation, direct condensation polymerization and polymerization through lactic acid formation which is pressed in Fig. 2-4.

In this work, PLA (Ingeo 3001D) in pellet form was supplied by NatureWorks LLC, the biopolymer, is designed for injection molding applications. It is designed for clear applications with heat deflection temperatures lower than 120 ºF (49 ºC). The properties of PLA are given in Table 2-2.

Table 2-2 Properties of PLA

Properties	Unit	Value
Specific gravity	g/cm^3	1.24
MFR	g/10 min (210 ºC, 2.16 kg)	22
Clarity	Transparent	
Tensile yield strength	MPa	62
Tensile elongation	%	3.5
Notched izod impact	J/m	16
Flexural strength	MPa	108
Flexural modulus	MPa	3600
Heat distortion temperature	ºC	55

2.2 Experiment method

2.2.1 Bulk polymerization

Bulk polymerization or mass polymerization is carried out by adding a soluble initiator to pure monomer in liquid state. The initiator should dissolve in the monomer. The reaction is initiated by heating or exposing to radiation. As the reaction proceeds the mixture becomes more viscous. The reaction is exothermic and a wide range of molecular masses are produced.

Bulk polymerization is carried out in the absence of any solvent or dispersant and is thus the simplest in terms of formulation. It is used for most step-growth polymers and many types of chain-growth polymers. In the case of chain-growth reactions, which are generally exothermic, the heat evolved may cause the reaction to become too vigorous and difficult to control unless efficient cooling. The overall kinetic scheme for the free radical polymerization of styrene as follows [5],

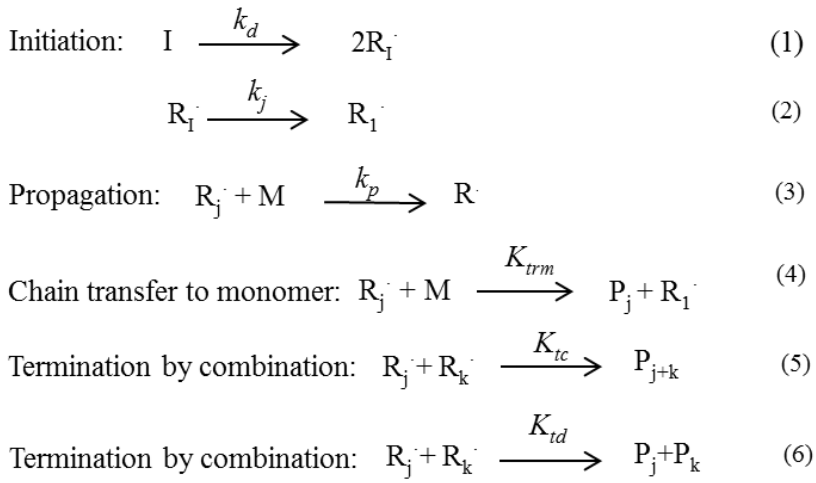

Bulk polymerization has several advantages over other methods, these advantages are:

(1) The system is simple and requires thermal insulation;

(2) The polymer is obtained pure;

(3) Large castings may be prepared directly;

(4) Molecular weight distribution can be easily changed with the use of a chain transfer agent;

(5) The product obtained has high optical clarity.

Disadvantages:

(1) Heat transfer and mixing become difficult as the viscosity of reaction mass increases;

(2) The problem of heat transfer is compounded by the highly exothermic nature of free radical addition polymerization;

(3) The polymerization is obtained with a broad molecular weight distribution due to

the high viscosity and lack of good heat transfer;

(4) Very low molecular weights are obtained.

2.2.2 Pickering emulsions polymerization

Recently, self-assembly of colloidal particles at the liquid-liquid interface has been well documented and offers a straightforward pathway for the production of organized nanostructures [6]. Typically, a so-called Pickering emulsion is stabilized and novel microcapsules known as colloidosomes whose shells consist of colloidal particles have been developed by this method [7, 8]. The solid particles first self-assemble at the liquid-liquid interface and act as the effective stabilizers during the polymerization process without the need for any conventional stabilizers. After completion of polymerization, the particles are captured on the surface of the resultant polymer beads, where they can be most effective for subsequent applications [9]. Such surfactant-free emulsion polymerization is more attractive for the preparation of hybrid beads than conventional emulsion polymerization. Chen et al. reported ZnO/polystyrene composite particles were synthesized by Pickering emulsion polymerization [10]. ZnO nanoparticles were first prepared by reaction of zinc acetate and sodium hydroxide in ethanol medium. Then different amount of styrene monomer was emulsified in water under the presence of ZnO nanoparticles either by mechanical stirring or by sonication, followed by polymerization of styrene.

Two kinds of initiators were used to start the polymerization, 2, 2'-Azoisobutyronitrile (AIBN) and potassium persulfate (KPS). Different morphologies were observed for the composite particles when using different initiators. AIBN-initiated system produced mainly core-shell composite particles with PS as core and ZnO as shell, while KPS-initiated system showed both composite particles and pure PS particles. Fig. 2-5 shows the mechanism of Pickering emulsion polymerization of ZnO and polystyrene initiated by AIBN. Two schemes of reaction mechanism were proposed to explain the morphologies accordingly. Both systems of composite particles

showed good pH adjusting ability.

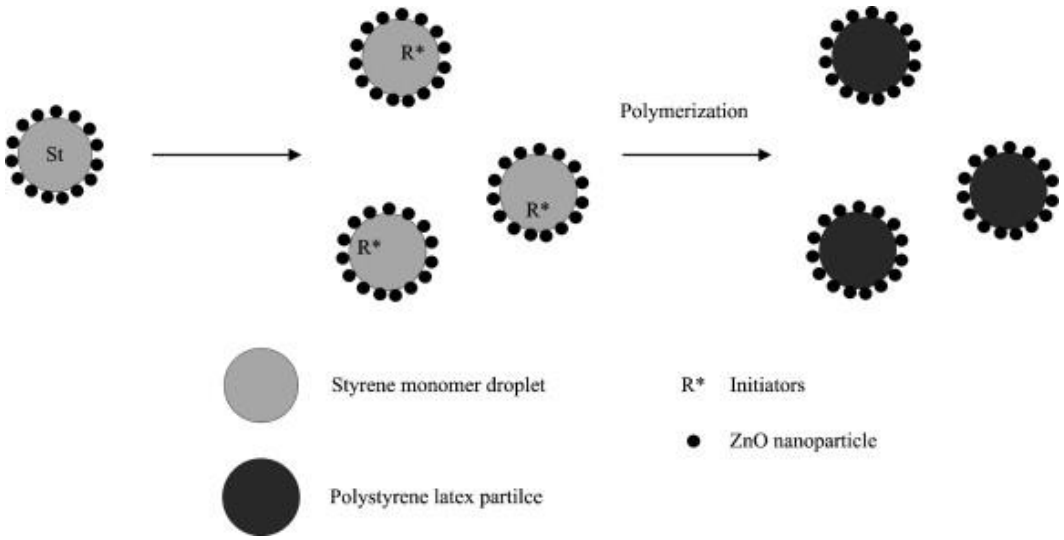

Fig. 2-5 Mechanism of Pickering emulsion polymerization of ZnO and polystyrene initiated by AIBN [11]

2.3 Instruments and Characteristics

2.3.1 Twin-screw extruder

Fig. 2-6 The image of twin-screw extruder

The treated or untreated carbon materials and polymer matrix with the desired filler weight contents were mixed. The mixtures were dried at 80 ºC for 24 h before extruding.

The mixtures were extruded using a twin-screw extruder (KZW15TW-30MG-NH (-700)-AKTP, Technovel Corporation, Japan) as shown in Fig. 2-6.

2.3.2 Injection molding machine

The extruding plates are formed into specimens using an injection molding machine (NP7-1F, Nissei Plastic Industrial Co., Ltd., Nagano, Japan) as shown in Fig. 2-7.

Fig. 2-7 Injection molding machine

The shape and measurement of tensile and bending test specimens are presented in Fig. 2-8 and Fig. 2-9 respectively.

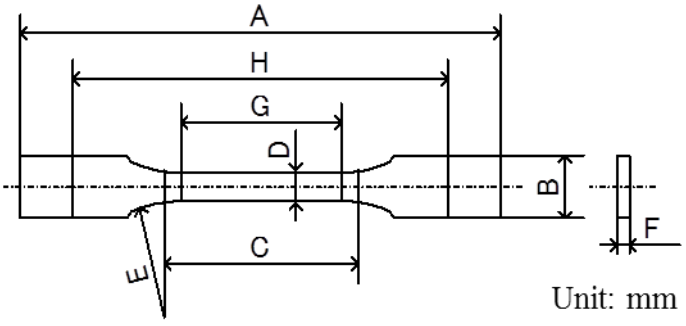

A: Whole length 75 B: Width 10 C: Length of parrallel 30
D: Width of parrallel 5 E: Radius 30 F: Thickness 2
G: Fulcrum 25 H: Grips distance 58±2

Fig. 2-8 Shape and measurement of tensile test specimens (JIS K 7113)

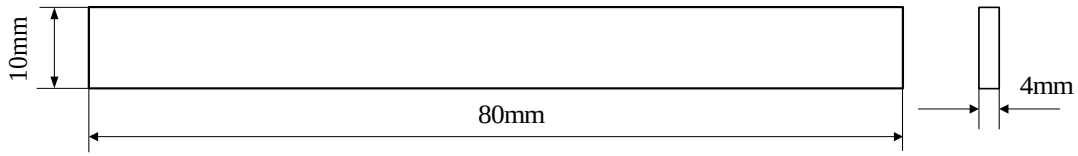

Fig. 2-9 Shape and measurement of bending test specimens

2.3.3 Electrical conductivity

A high resistance meter (MCP-HT450, Mitsubishi Chemical Analytical, Japan) was employed to test volume conductivity of the composites with low conductivity (10^{-14}<conductance<10^{-4} S/cm). In contrast, for moderate conductivity of the samples (conductance>10^{-4} S/cm), a four-probe device (SDY-4 Resistivity Measuring Instrument, Guangzhou Semiconductor Material Academy, Guangzhou, China) was operated to determine volume conductivity according to "Four Point Probes (FPP) technique" [11]. Sample preparation preceded the measurements of conductivity. The samples were shaped into the circular pellets with the assistance of a hot-press machine with ~1 mm and ~1.5 mm thickness for low and moderate conductivity testing, respectively. As shown in Fig. 2-10 and Fig. 2-11, different measurement methods lead to different sizes of sample. Samples after polymerization were all powders or plates, in the case of four-probe device, samples were shaped into the circular pellets. The diameter of pellets is 4.322 mm. The *I* in Fig. 2-10 was calculated according to the formula 2-1. The samples for high resistance test were pressed into slice with the thickness of about 0.5 mm with a hot press (ImotoMachin-ery Co., Ltd., Kyoto, Japan). The pressing conditions were: pressure, 200 kgf/cm^{-2}, as shown on the pressure gage; temperature, 170 °C±10 °C; and time, 5 min.

$$I = F(D/S) \times F(W/S) \times W \times Fsp \times 10^{n} \qquad (2\text{-}1)$$

In the formula 2-1, D is diameter, S is the distance between probes, W is the thickness of sample, F(D/S) and F(W/S) are the values obtained from attached tables respectively, Fsp is confirmed as 1.01.

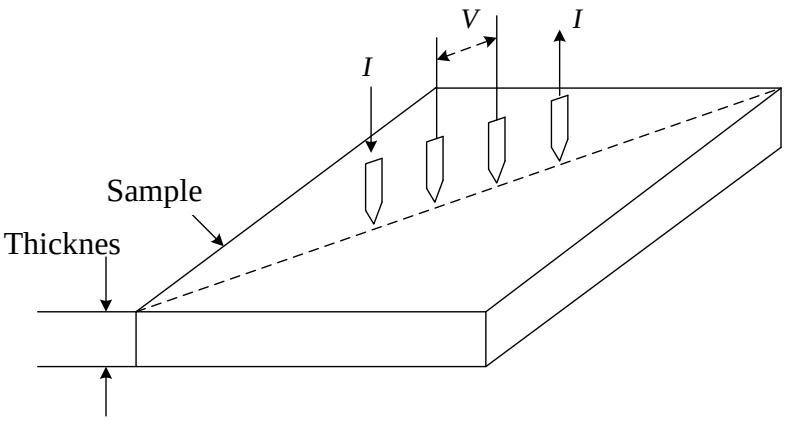

Fig. 2-10 The principle of measurement for four-probe device

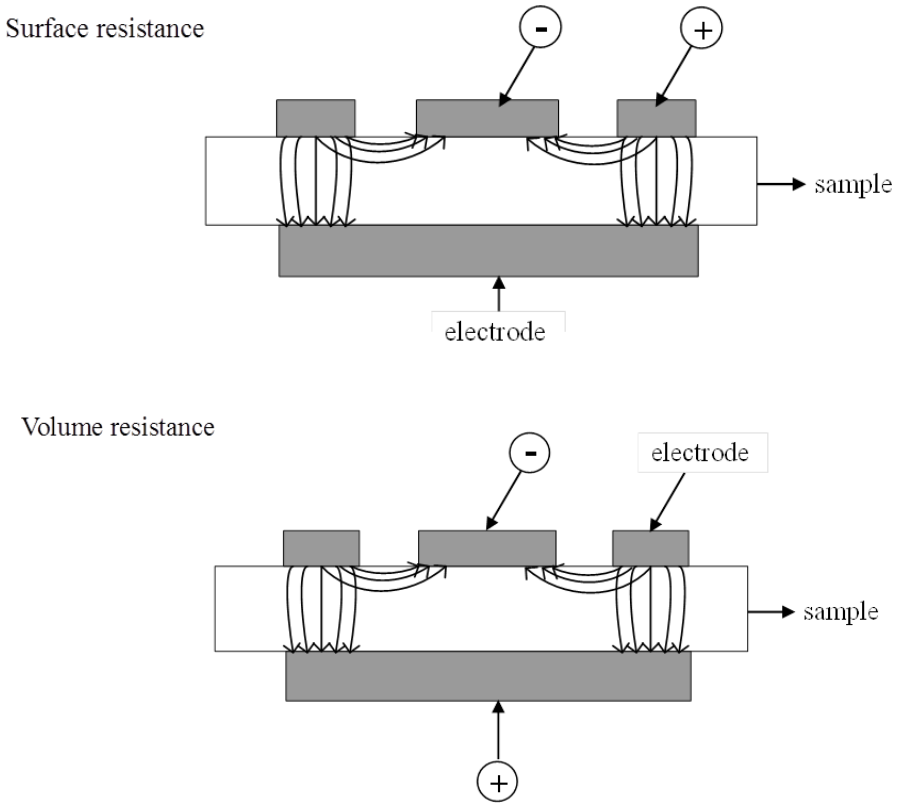

Fig. 2-11 The principle of measurement for high resistance meter

2.3.4 Fourier transforms infrared spectroscopy (FT-IR)

The infrared spectra were measured using a micro sampling FT-IR spectrometer (MFT-2000, Jasco Co., Ltd., Tokyo, Japan) with the KBr pellet method. The wavelength range was between 4000 and 600 cm^{-1}, and the resolution was 4 cm^{-1}. Fifty scans were averaged for each sample.

2.3.5 X-ray diffraction (XRD)

X-ray diffraction (XRD) patterns were recorded in the range of 2θ=5-90° by step scanning with a diffractometer (XRD-6000, Shimadzu Co., Ltd., Kyoto, Japan). Nickel-filter Cu Kα radiation (λ=0.15417 nm) was used with a generator voltage of 40 kV and a current of 30 mA.

2.3.6 Tensile test

The tensile strength and fracture strain were measured according to JIS K7113 using a universal testing machine (Series 3360, Instron Co., Ltd., Canton, America) with a tensile speed of 10 mm/min. The specimen of tensile test is presented in Fig. 2-8 and the schematic of tensile test is presented in Fig. 2-12. The samples were placed for 48 h at room temperature (23±2 ^{o}C) and atmospheric conditions (relative humidity of 50±5%) before test.

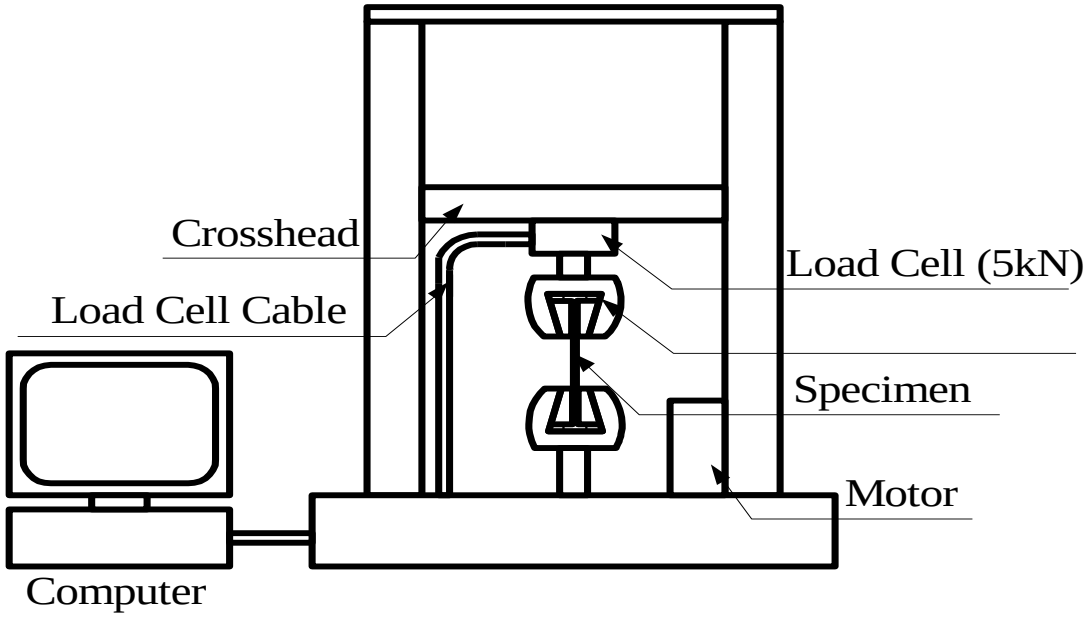

Fig. 2-12 Schematic of tensile test

2.3.7 Bending test

The bending strength and fracture strain were measured according to JIS K7171 using a universal testing machine (Series 3360, Instron Co., Ltd., Canton, America) with

a bend speed of 2 mm/min. The specimen of bending test is present in Fig. 2-9 and the schematic of bending test is presented in Fig. 2-13. The samples were placed for 48 h at room temperature (23±2 ºC) and atmospheric conditions (relative humidity of ~50±5%) before test.

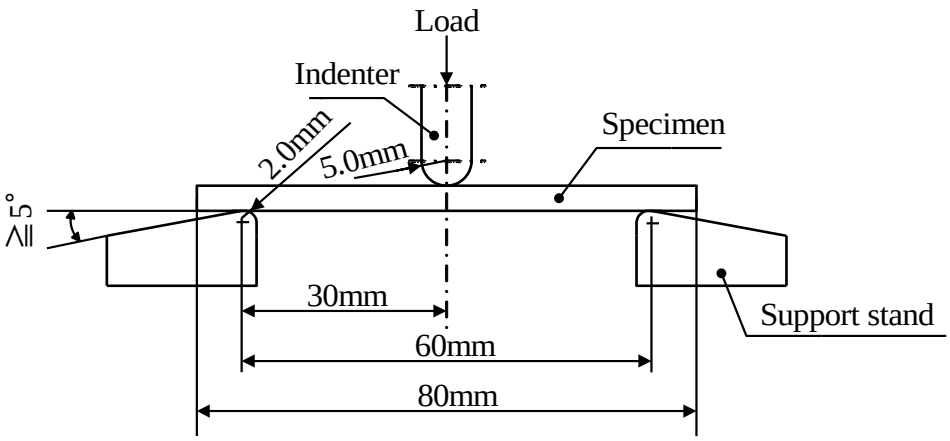

Fig. 2-13 Schematic of bending test

The bending strength obtain from formula 2-2, Bending fracture strain at break was obtained from formula 2-3. *F* is the bending stress, *L* is the fulcrum distance, *h* is the thickness of specimen (mm), *b* is the width of specimen (mm). *S* is the bending strain (mm).

$$\sigma = \frac{3FL}{2bh^2} \qquad (2\text{-}2)$$

$$\varepsilon = \frac{6hS}{L^2} \qquad (2\text{-}3)$$

2.3.8 Scanning electron microscope (SEM)

Morphology of the fractured specimens after tensile testing or bending testing was observed. Dispersion of carbon materials and interfacial adhesion between carbon materials and polymer matrix were examined using a scanning electron microscope (S-4300, Hitachi Co., Ltd., Tokyo, Japan). The fracture surface was sputter-coated by gold with Ion sputter (E-1030, Hitachi Co., Ltd., Tokyo, Japan) for 2 min to provide enhanced conductivity. The test voltage was 15 kV, and electric current was 10 μA.

2.3.9 Thermal analysis (TA)

An automatic thermal analyzer (DTA-60/60H, Shimadzu DTG-60) was used for the thermal gravimetric analysis (TGA). TGA conditions were: heating rate was 10 ^{o}C/min from room temperature to 800 ^{o}C in nitrogen atmosphere.

2.3.10 Transmission electron microscopy (TEM)

The microstructure of the composites was determined by transmission electron microscopy (TEM) (Model H-8100, Hitachi Ltd.). To prepare TEM specimens, composite powders were dispersed in toluene or ethanol in an ultrasonic bath for 30 min, and then deposited on a copper grid covered with a perforated carbon film.

2.3.11 Raman spectra

Raman spectra were carried out with a FT-Raman spectrometer (NRS-1000/RFT-600, Jasco, Japan). The wavelength range was between 2000 and 800 cm^{-1}, and the resolution was 2 cm^{-1}. Fifteenth scans were averaged for each sample.

2.3.12 X-ray photoelectron spectroscopy (XPS)

X-ray photoelectron spectroscopy (Perkin-Elmer Corp.) measurements were done by sticking the powders or plate on an electrically conductive adhesive.

2.3.13 Ultrasonic waving

Ultrasonic cleaning (KQ-300DE, Numerical Control Ultrasonic Cleaner, Shanghai, China) was used to disperse the filler in solvent. The size：300×240×150 mm, ultrasonic frequency: 40 Hz, ultrasonic power: 300 W, temperature range: 10-80 ^{o}C.

2.4 Conclusions

The experimental procedure was displayed as Fig. 2-14.

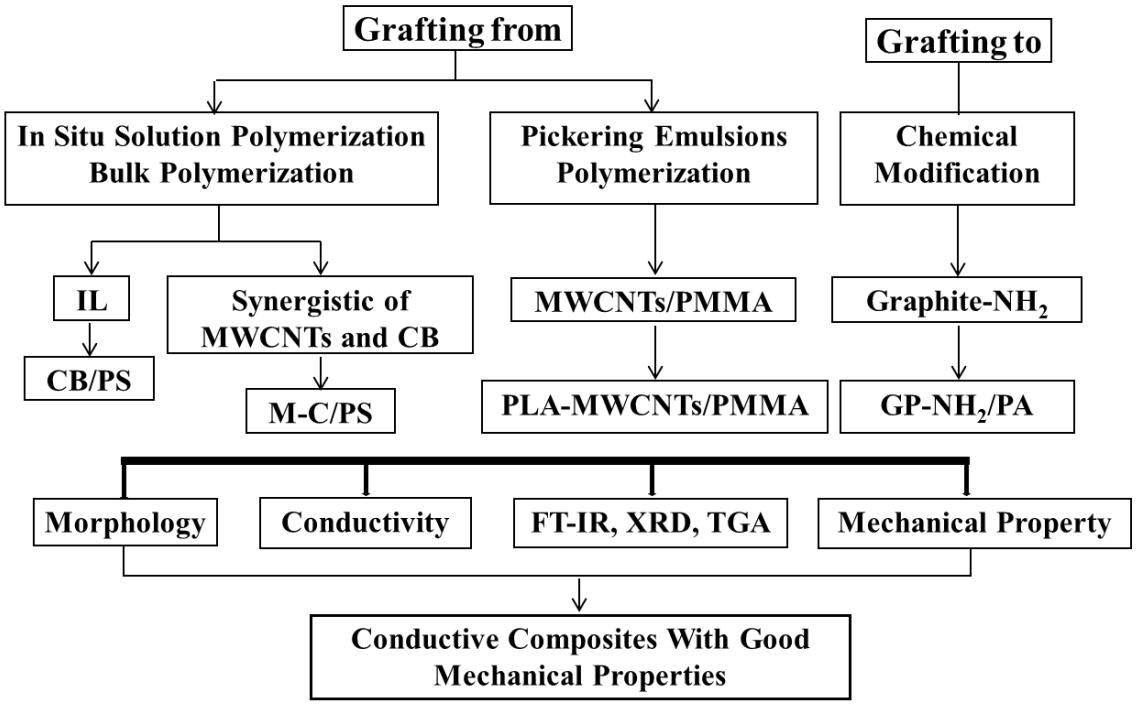

Fig. 2-14 The experimental procedure

References

[1] D. Tasis, N. Tagmatarchis, A. Bianco, M. Prato, Chemistry of Carbon Nanotubes, Chemical Reviews, 106 (2006) 1105-1136.

[2] Q. Wang, X.H. Han, A. Sommers , Y. Parkc, C.T. Joen, A. Jacobi, A Review on Application of Carbonaceous Materials and Carbon Matrix Composites for Heat Exchangers and Heat Sinks, International Journal of Refrigeration, 35 (2012) 7-26.

[3] M. Wissler, Graphite and Carbon Powders for Electrochemical Applications, Journal of Power Sources, 156 (2006) 142-150.

[4] N. Deprez, D.S. Mclachan, The Analysis of the Electrical Conductivity of Graphite Conductivity of Graphite Powders During Compaction, Journal of Physics D: Applied Physics, 21 (1988) 101.

[5] N. Tefera, Free Radical Suspension Polymerization Kinetics of Styrene up to High Conversion, Macromolecular Chemistry and Physics, 195 (1994) 3067-3085.

[6] R. Aveyard, B.P. Binks, J.H. Clint, Emulsions Stabilised Solely by Colloidal Particles, Advances in Colloid and Interface Science, 100-102 (2003) 503-546.

[7] B.P. Binks, R. Murakami, S.P. Armes, S. Fujii, Temperature-Induced Inversion of Nanoparticle-Stabilized Emulsions, Angewandte Chemie International Edition, 44 (2005) 4795-4798.

[8] T. Hasell, J.X. Yang, W.X. Wang, J. Li, P.D. Brown, M. Poliakoff, Preparation of Polymer-Nanoparticle Composite Beads by a Nanoparticle-Stabilised Suspension Polymerization, Journal of Materials Chemistry, 17 (2007) 4382-438.

[9] H. Liu, C. Wang, Q. Gao, X. Liu, Z. Tong, Magnetic Hydrogels with Supracolloidal Structures Prepared by Suspension Polymerization Stabilized by Fe_2O_3 Nanoparticles, Acta Biomaterialia, 6 (2010) 275-281.

[10] J.H. Chen, C.Y. Cheng, W.Y. Chiu, C.F. Lee, N.Y. Liang, Synthesis of Zno/Polystyrene Composites Particles by Pickering Emulsion Polymerization, European Polymer Journal, 44 (2008) 3271-3279.

[11] F.M. Smits, Measurement of Sheet Resistivities with the Four-Point Probe, Bell System Technical Journal, (1958) 711-718.

Chapter 3 Polystyrene Grafted Carbon Black Synthesis via in Situ Solution Radical Polymerization Ionic Liquid

3.1 Introduction

Carbon black (CB) was first manufactured in the US from natural gas on soap-stone plates in 1872 [1], and it was widely used since when mixed with rubber, the mechanical properties of rubber were significantly improved [2]. CB refers to a group of industrial products including acetylene black, furnace black, channel black, thermal black and lampblacks. They are composed essentially of elemental carbon in the form of near-spherical particles of colloidal sizes, combined mainly into particle aggregates obtained by partial ignition or thermal decomposition of hydrocarbons [2]. CB is considered to have high prospects for use as filler materials for future polymer composites due to its high aspect ratio and superior electrical and thermal conductivities. Also, CB can be spread in a layer of nanometer scale thickness. Recently, there has been increased interest in composites of CB and polymers [3-5]. However, processing of CB has been limited by its poor solubility or dispersibility in most common solvents due to the strong Van der Waals attraction [6].

Many methods have been used to modify the CB properties, such as physical coating, chemical covalent bonding and non-covalent bonding. Among these methods, functionalization of CB with polymers is gaining wide interest, because the polymer chains not only improve the solubility of the CB but also enhance the thermodynamic stability, electrical conductivity and mechanical properties [7-10]. Moreover, this functionalization can lead to formation of CB/Polymer composites which are useful materials. Celzard et al. [11] were the first to investigate the conductive behavior of 100 μm thick composite films composed of epoxy resin and expanded graphite flakes with the aspect ratio of about 100 nm and the filler volume fraction of around 1%.

Bouazzaoui's group reported microwave measurements on a large series of epoxy samples based on the CB-filled diglycidylic ether of bisphenol A (DGEBA) [12, 13]. They concluded that fitting the experimental data with mixing law and effective medium equation predictions had limited applicability because the mean field model of the predictions assumed a given microstructure for the composite material. Another important property of CB is its good anti-friction characteristic. Many researches study on the friction and wear behavior have been reported focused on the CB-reinforced metals and plastics [14-17].

Moreover, ionic liquids (ILs) have applications in electrochemical, synthetic, catalytic, and separations technologies because they are high in viscosity, have a large temperature range in which they can be used, and they are environmentally friendly [18]. ILs are composed solely of ionized species and have been proven to be useful solvents in polymer chemistry and engineering [19, 20].

In this work, carbon black (CB, a trade name for acetylene black) was chosen as a type of CB to prepare CB/PS nanocomposites via an in situ free radical addition process using IL as solvent because of its nonvolatile, nonflammable, and thermally stable characteristics [20]. Styrene (St) was grafted and polymerized onto the CB surface. The polystyrene-grafted CB agglomerated and separated from the IL because the polystyrene cannot be suspended in the IL. The results of FT-IR, TGA, TEM and Raman spectrum measurements proved that the polystyrene was successfully grafted onto the CB surface. Electrical resistance measurements showed that the electrical conductivity of CB/PS nanocomposites was much higher than that of pure polystyrene (10^{-16} S/cm). The effects of initiator addition and the amount of styrene on the grafting of CB were evaluated by changing several experimental parameters.

3.2 Experimental

3.2.1 Materials

The IL (1-hexyl-3-methylimidazolium tetrafluroborate) was bought from Flute Cypress Chemistry Technology Company, Shanghai, China.

3.2.2 In situ solution polymerization

A certain amount of CB and IL (10 mL) were mixed in a 100 mL round bottom flask and subjected to ultrasonic scattering for about 4 h. Then a certain amount of St was added and the mixture was subjected to ultrasonic for another 2 h. The flask was heated to a certain temperature in an oil bath and then a certain amount of initiator AIBN was added. The mixture was reacted for 12 h until the polystyrene grafted onto the surface of CB and separated from the IL. The IL solution was filtered to obtain the solid product. Then, the solid product was soaked in toluene for about a day and precipitated with ethanol, and air dried.

3.3 Results and discussion

In the present work, the polystyrene was grafted onto the CB surface via in situ solution polymerization in IL. In the polymerization process, the polymer chain radicals that reacted with the C=C bonds of the CB were produced by three approaches: (1) the in situ radical polymerization of the monomer in the presence of the CB after initiation with initiator; (2) a controlled/‘living’ radical polymerization; and (3) the polymer chain transfer reaction [21]. Then the Soxhlet extraction was carried out for some of the CB/PS nanocomposites to remove the polystyrene which was just coated on the polystyrene grafted CB. Table 3-1 shows the reaction conditions, percentage grafting (PG%) and surface resistance of CB/PS nanocomposites.

Table 3-1 Percentage grafting (PG) and surface resistance of CB/PS at different conditions

No.	CB(g)	St(ml)	AIBN(g)	T(°C)	PG(%)	ρ(S/cm)
CB/PS1	0.2	10	0.0500	90	49.46	0.87×10^{-10}
CB/PS2	0.2	10	0.0250	90	5.89	0.32×10^{-8}
CB/PS3	0.2	10	0.0125	90	3.77	0.18×10^{-10}
CB/PS4	0.2	10	0.0063	90	3.05	0.22×10^{-11}
CB/PS5	0.2	10	1.0000	90	32.4	0.91×10^{-11}
CB/PS6	0.2	5	0.0150	90	20.47	0.40×10^{-5}
CB/PS7	0.2	2.5	0.0125	90	17.86	0.26×10^{-4}
CB/PS8	0.2	1.25	0.0063	90	9.46	0.07×10^{-3}
CB/PS9	0.2	10	0.0500	80	10.73	0.70×10^{-10}
CB/PS10	0.2	10	0.0500	70	8.42	0.12×10^{-6}
CB/PS11*	0.2	10	0.0500	90	3.55	0.03×10^{-11}

CB/PS11*: With no ionic liquid

3.3.1 FT-IR spectroscopy measurements

FT-IR spectroscopy measurements are important in the detection of the structure of CB/PS nanocomposites. Fig. 3-1 shows the asymmetrical and symmetrical stretching vibrations of $–CH_2$ at 2916 and 2854 cm^{-1}, the flexural vibrations of $–CH_2$ at 1446 cm^{-1}, the characteristic C–C ring stretching vibration at 1600 cm^{-1} and the benzene ring plane stretching vibration of –CH at 756 and 706 cm^{-1} for the CB/PS1 specimen nanocomposites. All of these vibrations did not appear in the FT-IR spectrum of pure CB. This indicates that the polystyrene chains had been grafted onto the CB surface via the free radical addition polymerization.

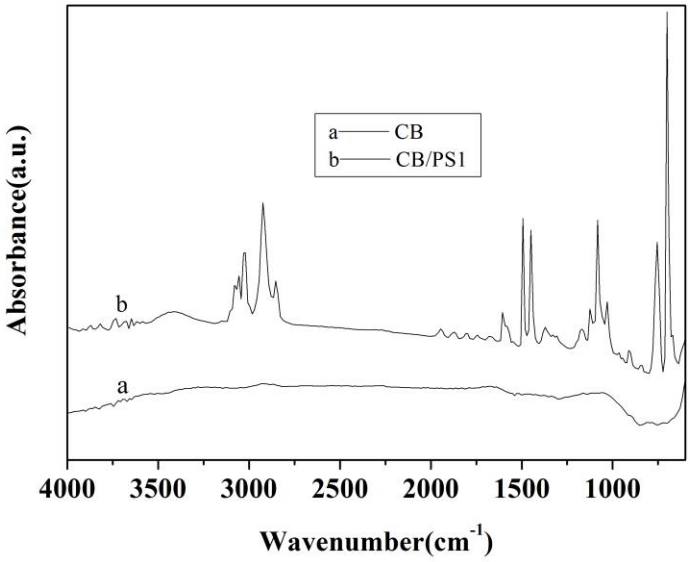

Fig. 3-1 FT-IR spectra of (a) pure CB and (b) CB/PS1

3.3.2 Advantage of IL use

In order to prove that the IL can raise the grafting percentage of PS on the CB surface, CB/PS11 specimen was prepared without IL and other conditions the same as for CB/PS1. TGA was used to determine the grafting percentage of PS onto the CB surface. Before the TGA analysis, the CB/PS nanocomoposite specimens were extracted with the Soxhlet extractor. As shown in Fig. 3-2, the PG of CB/PS1 was much more than that of CB/PS11. This might be due to the fact that the lifetime of the surface radicals formed was prolonged because of the high viscosity of IL.

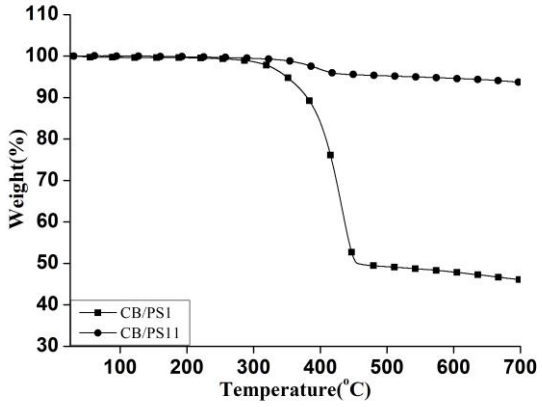

Fig. 3-2 The effect of IL on the percentage grafting of nanocomposites

3.3.3 Effect of the monomer amount

Fig. 3-3 shows the thermal gravimetric weight of CB and the four composites with different amounts of styrene. The obviously weight loss can be found in the temperature range of 300-420 ^{o}C for the CB/PS nanocomposites, which were attributed to the decomposition of the polystyrene grafted onto the CB surface. The weight loss of CB/PS nanocomposites decreased with decreasing amount of styrene, which is consistent with the change in electrical resistance.

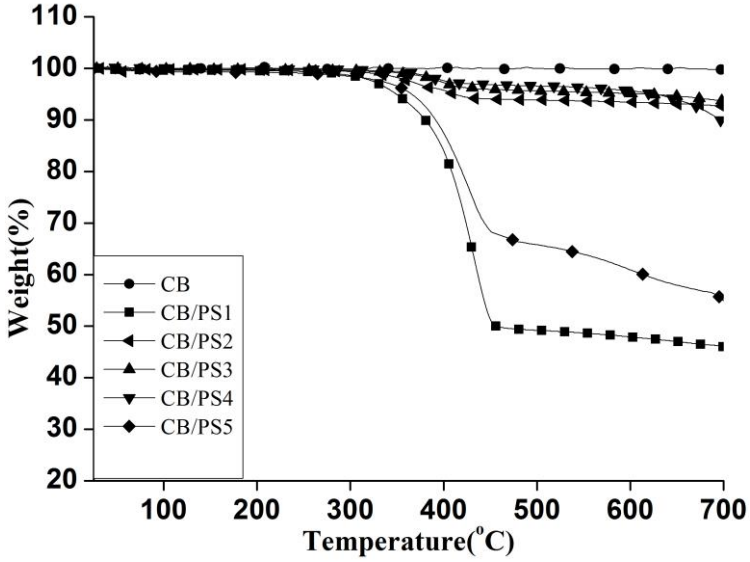

Fig. 3-3 The TGA curves of CB and CB/PS nanocomposites prepared with different amounts of initiator

3.3.4 Effects of the amount of initiator and temperature on PG

Fig. 3-4 plots the TGA curves of the CB/PS nanocomposites with different amounts of initiators. The weight loss of CB/PS1 was the biggest. It was concluded that the optimal amount of initiator for optimal PG was 0.5 wt% of the monomer.

Fig. 3-5 shows the weight loss of nanocomposites prepared at different temperatures. As described in table 3-1, higher polymerizing temperature was favorable to form higher percentage grafting polymer. However, when the temperature was too high, the

AIBN would be decomposed. Because of this, 90 ºC was determined as the optical polymerization temperature.

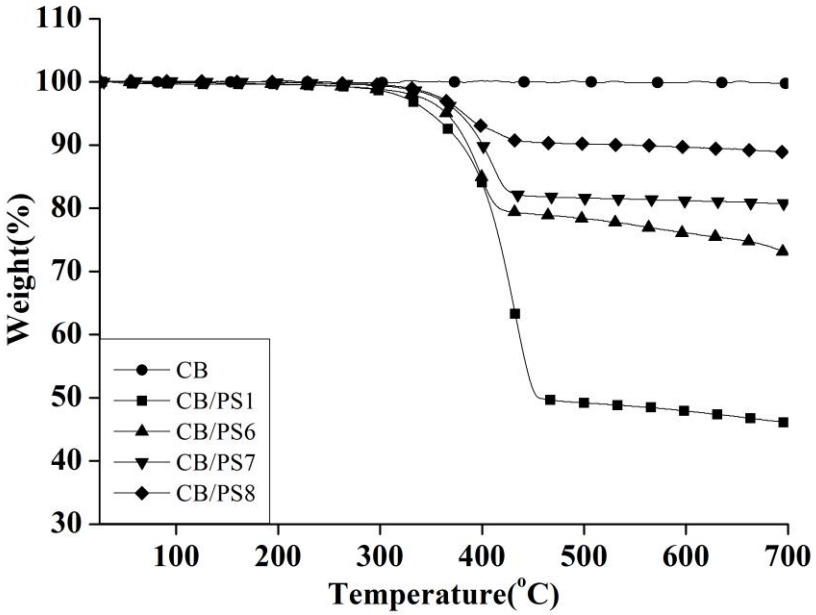

Fig. 3-4 The TGA curves of CB/PS nanocomposites prepared with different amounts of monomer

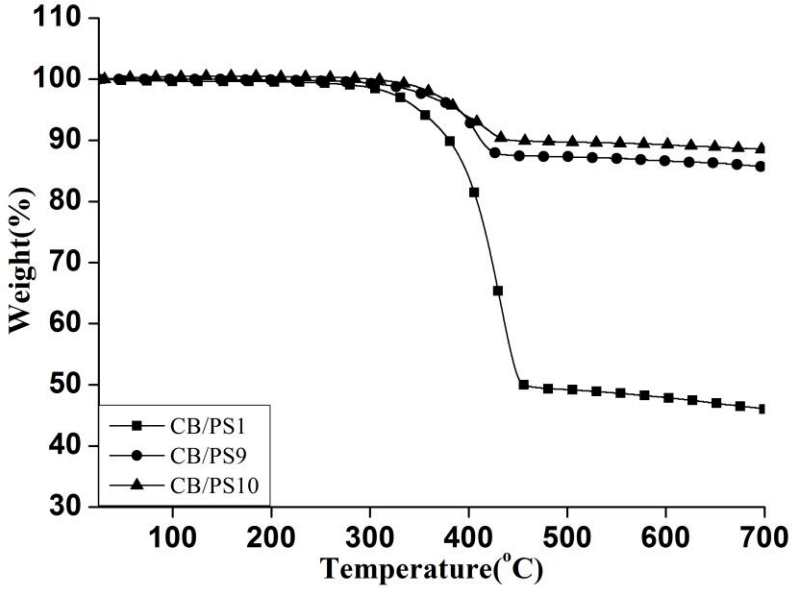

Fig. 3-5 The TGA curves of CB/PS nanocomposites prepared at different temperatures

3.3.5 Percentage grafting (PG) and electrical conductivity

After the polymerization of styrene onto the CB surface, the products were hot-pressed into slices for electrical conductivity measurements. Due to the innate electrical conductivity of CB, the electrical conductivity of CB/PS nanocomposites was much higher than that of pure polystyrene (10^{-16} S/cm). The CB/PS nanocomposites showed semiconductor characteristics. As table 3-1 shows, the PG and electrical conductivity of CB/PS nanocomposites. The PG values were calculated from the TGA weight loss in the temperature range of 260-460 ^{o}C. Both the PG and the conductivity first increased and then decreased with increasing amount of AIBN (CB/PS1-5).

This phenomenon was also seen in Fig. 3-6. It occurred because with the increase of initiator, the polystyrene formed faster, so the probability of the addition reaction of the free radicals onto the CB increased, and the dispersibility improved accordingly. However, with too much initiator added, the coupling of the free radicals with each other to terminate the polymerization might become the dominant reaction [21], which led to the low PG. The increasing of the electrical conductivity is because the dispersibility of CB and PS was improved due to the grafting of PS. However, the electrical conductivity would decrease when the amount of PS became too high.

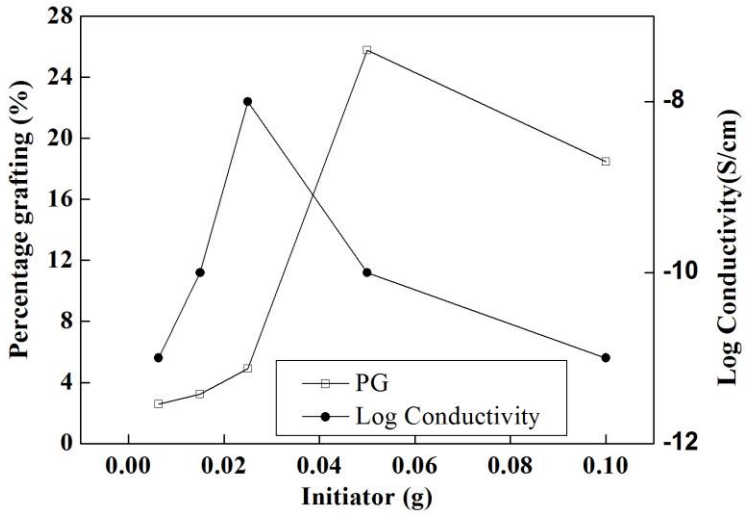

Fig. 3-6 AIBN influence on the PG and electrical conductivity of samples

Furthermore, the PG was the maximum when the AIBN was 0.05 g, but the maximum conductivity occurred when the AIBN was 0.025 g. This might be due to more PS was grafted onto the CB surface, meanwhile more sp2 have been changed to sp3, which can destroy the structure of CB. In order to study the effect of the amount of styrene on conductivity and PG, four specimens (CB/PS1, CB/PS6, CB/PS7 and CB/PS8) were prepared with different amounts of styrene, in which the ratio of AIBN and styrene fixed to 0.5 wt% because the PG has a maximum at this ratio. It was obvious that the conductivity decreased and the PG increased with increasing amount of monomer as shown in Fig. 3-7, because the more monomer was added, more chances of polymer was grafted on the CB surface, and the greater the consumption of CB. The PG decreased and the conductivity increased with the decrease of temperature (specimens CB/PS1, CB/PS9 and CB/PS10) because the optimal temperature of AIBN initiator is around 90 ^{o}C. It was also found that both the PG and the conductivity of nanocomposites which were prepared in IL were better than those values when the specimens were prepared with no IL added (CB/PS1 and CB/PS11). This was because the styrene was well dispersed in IL which contributed to the uniform mixing of CB and styrene.

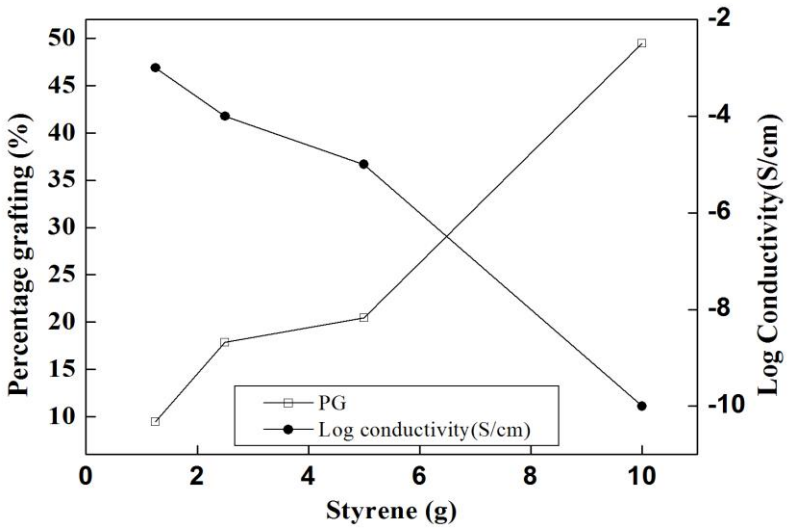

Fig. 3-7 Monomer influence on the PG and electrical conductivity of samples

Fig. 3-8 shows the relationship between PG and conductivity of nanocomposites. The conductivity first increased and then decreased with increasing PG. This was due to the poor dispersibility of CB in PS matrix when the PG was low, and the larger consumption of CB when the PG was high. The dispersibility can also be certified in SEM images as shown in Fig. 3-9.

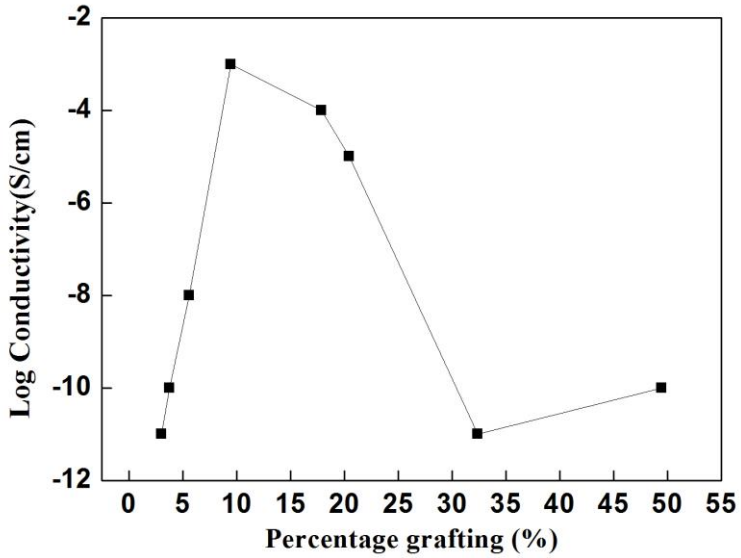

Fig. 3-8 The relationship between PG and electrical conductivity

3.3.6 Morphology images

SEM micrographs are reproduced in Fig. 3-9 to explain the fracture surface of CB/PS composites which were obtained under different conditions. It can be seen there is no phase separation for CB/PS1 (Fig. 3-9 (a)), which indicates the well dispersibility of CB in PS. However, when the amounts of monomer and initiator decreased, clear phase separation could be found on the fracture surface as shown in Fig. 3-9 (b, c). Especially as Fig. 3-9 (c) showed, when the content of initiator was very low, CB aggregates were clearly found. Because of the amount of AIBN was not enough for the polymerization of styrene to polystyrene.

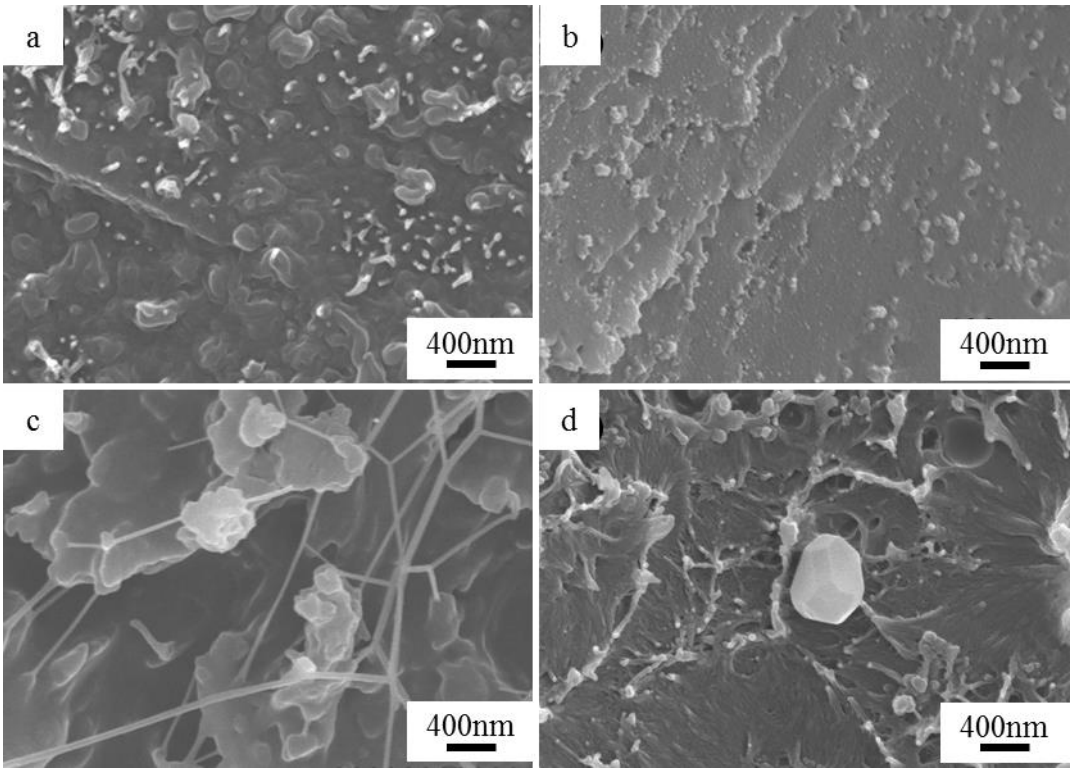

Fig. 3-9 SEM photos of CB/PS composites obtained at different conditions:

(a) CB/PS1, (b) CB/PS2, (c) CB/PS4 and (d) CB/PS6

3.3.7 Microstructure images

The PS grafting enabled the CB to be dispersed in the toluene. When pure CB and CB/PS nanocomposites were sonicated in toluene at the same time, the CB started to settle quickly, while the CB/PS nanocomposites remained homogenous with no sedimentation after two days.

TEM is also widely used to detect morphology of materials. CB and CB/PS were dispersed in toluene in an ultrasonic bath for 30 min, and then deposited on a copper grid covered with a perforated carbon film. As shown in Fig. 3-10, pure CB was easily aggregated with aggregates having average diameters of about 30 nm. However, the CB/PS was well dispersed in toluene and the aggregate diameters increased to about 45 nm after the in situ radical graft polymerization in IL. This indicated that the polystyrene had been successfully grafted onto the CB surface by the proposed method.

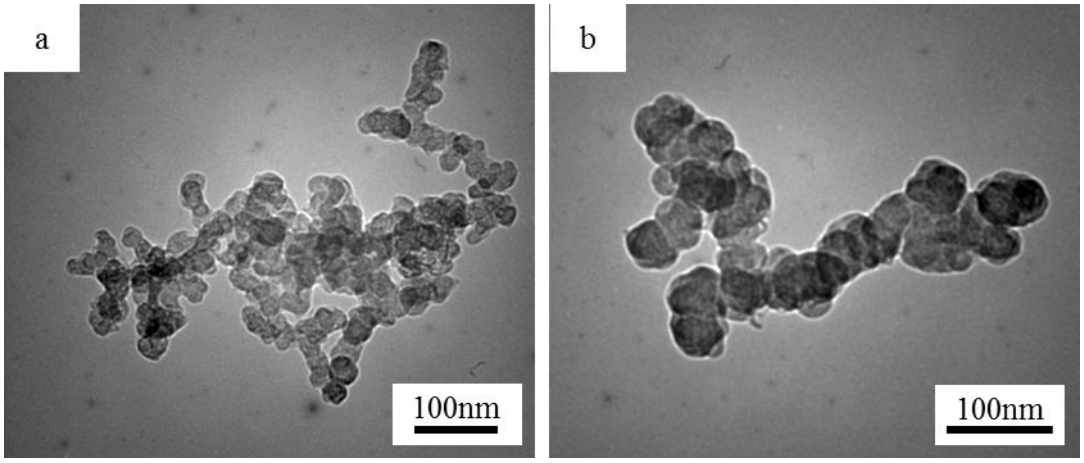

Fig. 3-10 TEM micrographs of (a) CB and (b) CB/PS1

3.3.8 Raman spectroscopy measurements

Historically, Raman spectroscopy has played an important role in characterizing the structure of carbon materials [22]. As shown in Fig. 3-11, the Raman spectrum of the pure CB shows a characteristic D band at 1336 cm^{-1} (defects/disorder-induced modes) and a G band at 1572 cm^{-1} (in-plane stretching tangential modes) with an intensity ratio (ID/IG) of 1.01. As for CB/PS1, the ID/IG intensity ratio increased to 1.12.

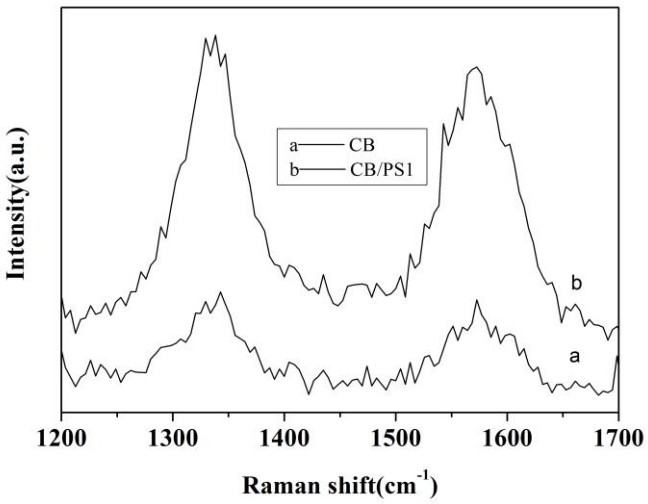

Fig. 3-11 Raman spectra of (a) pure CB and (b) CB/PS1

The change in ID/IG intensity could also be observed from the change of the peak height. For the pure CB, the D band is about the same as the G band. However, for

CB/PS1, the D band has a higher intensity than the G band. The results showed that the in situ solution free radical polymerization had led to an increase in the number of defects in the CB nanoparticles.

3.4 Conclusions

In summary, the preparation of the CB/PS nanocomposites via in situ solution free radical polymerization in IL was carried out. The nanocomposites separated from the IL because of polystyrene's insolubility in the IL. The IL improved the grafting polymerization of styrene on the CB surface. The results of electrical conductivity, FT-IR, SEM and TEM analysis showed that polystyrene grafted and mixed with CB. The electrical conductivity of CB/PS nanocomposites was better than that of pure polystyrene. Both the PG and the conductivity first increased and then decreased with increasing amount of AIBN. And the conductivity decreased and the PG increased with increasing amount of monomer. Furthermore, the conductivity first increased and then decreased with increasing PG. These nanocomposites can be blended with other polymers to get products of improved mechanical properties. The CB/PS was well dispersed in toluene and the aggregate diameters increased from 30 nm to about 45 nm after the in situ radical graft polymerization in IL.

References

[1] Federal Trade Commission (1948): Carbon Black Export I, Et Al. Investigations and Recommendations under the Export Trade Act, 1245-1345.

[2] Y.K. Peng (2007): The Effect of Carbon Black and Silica Fillers on Cure Characteristics and Mechanical Properties of Breaker Compounds, MS Thesis, University Science Malaysia.

[3] J.W. Shen, X.M. Chen, W.Y. Huang, Structure and Electrical Properties of Grafted Polypropylene/Graphite Nanocomposites Prepared by Solution Intercalation, Journal of Applied Polymer Science, 88 (2003) 1864-1869.

[4] A. Yasmin, J.J. Luo, I.M. Daniel, Processing of Expanded Graphite Reinforced Polymer Nanocomposites, Composites Science and Technology, 66 (2006) 1182-1189.

[5] K. Kalaitzidou, H. Fukushima, L.T. Drzala, New Compounding Method for Exfoliated Graphite-Polypropylene Nanocomposites with Enhanced Flexural Properties and Lower Percolation Threshold, Composites Science and Technology, 67 (2007) 2045-2051.

[6] G. Zheng, J. Wu, W. Wang, C. Pan, Characterizations of Expanded Graphite/Polymer Composites Prepared by in Situ Polymerization, Carbon, 42 (2004) 2839-2847.

[7] H. Kim, H.H. Thomas, L.M. Viculis, S. Gilje, R.B. Kaner, Electrical Conductivity of Graphite/Polystyrene Composites Made from Potassium Intercalated Graphite, Carbon, 45 (2007) 1578-1582.

[8] N. Srivastava, R. Mehra, Study of Electrical Properties of Polystyrene/Foliated Graphite Composite, Materials Science-Poland, 27 (2009) 109-122.

[9] D. Azulay, M. Eylon, O. Eshkenazi, D. Toker, M. Balberg, N. Shimoni, Electrical-Thermal Switching in Carbon Black-Polymer Composites as a Local Effect, Physical Review Letters, 90 (2003) 236601.

[10] I. Balberg, A Comprehensive Picture of the Electrical Phenomena in Carbon

Black-Polymer Composites, Carbon, 40 (2002) 139-143.

[11] A. Celzard, E. Mcrae, J. Mareche, G. Furdin, M. Dufort, C. Deleuze, Composites Based on Micron-Sized Exfoliated Graphite Particles: Electrical Conduction, Critical Exponents and Anisotropy, Journal of Physics and Chemistry of Solids, 57 (1996) 715-718.

[12] S. Bouazzaoui, M. Achour, C. Brosseau, Microwave Effective Permittivity of Carbon Black Filled Polymers: Comparison Of Mixing Law and Effective Medium Equation Predictions, Journal of Applied Physics, 110 (2011) 074105-074109.

[13] F. Qin, C. Brosseau, A Review and Analysis of Microwave Absorption in Polymer Composites Filled with Carbonaceous Particles, Journal of Applied Physics, 111 (2012) 061301-061324.

[14] P. Rohatgi, Y. Liu, S. Ray, Friction and Wear of Metal-Matrix Composites, Friction and Wear of Metal-Matrix Composites, ASM Handbook, 18 (1992) 801-811.

[15] N. Radhika, R. Subramanian, S.V. Prasat, Tribological Behaviour of Aluminium/Alumina/Graphite Hybrid Metal Matrix Composite Using Taguchi's Techniques, Journal of Minerals & Materials Characterization & Engineering, 10 (2011) 427-443.

[16] Y. Zhan, G. Zhang, Friction and Wear Behavior of Copper Matrix Composites Reinforced with Sic and Graphite Particles, Tribology Letters, 17 (2004) 91-98.

[17] H.H. Shim, O.K. Kwon, J.R. Youn, Friction and Wear Behavior of Graphite Fiber Reinforced Composites, Polymer Composite, 11 (1990) 337-341.

[18] P. Wasserscheid, T. Welton, Ionic Liquids in Synthesis: Wiley Online Library, (2008).

[19] H. Ma, X. Wan, X. Chen, Q.F. Zhou, Reverse Atom Transfer Radical Polymerization of Methyl Methacrylate in Imidazolium Ionic Liquids, Polymer, 44 (2003) 5311-5316.

[20] J. Ueda, H. Yamaguchi, T. Yamauchi, N. Tsubokawa, Radical Graft Polymerization of Vinyl Monomers onto Nanoparticles in Ionic Liquid Initiated by Azo Groups

Introduced onto the Surface, Journal of Polymer Science Part A: Polymer Chemistry, 45 (2007) 1143-1149.

[21] X.L. Wu, P. Liu, Polymer Grafted Multiwalled Carbon Nanotubes via Facile in situ Solution Radical Polymerization, Journal of Experimental Nanoscience, 5 (2010) 383-389.

[22] V.N. Popov, L. Henrard, P. Lambin, Resonant Raman Spectra of Graphene with Point Defects, Carbon, 47 (2009) 2448-2455.

Chapter 4 The Synergistic Effect of MWCNTs and Carbon Black on the Properties of Polymer Nanocomposites

4.1 Introduction

Carbon nanotube (CNT) has gained substantial attention in various fields since they were discovered in 1991 by Iijima [1], because they have a unique structure and outstanding properties such as high flexibility, low mass density, large aspect ratio, excellent electrical conductivity and mechanical properties [2-5]. The conductive properties of carbon black (CB) allowed their use as a semiconductor substitute in early carbon microphones [6]. However, their ability to aggregate has been found to dramatically hamper the utilization of CNTs and CB in various fields. Recently, immense effort has been made to improve the chemical affinity of CNTs or CB and polymer matrix [7-11]. The modifications of both CNTs and CB include non-covalent attachments and covalent linkages [5, 12]. Non-covalent attachments with polymers involve polymer wrapping and polymer absorption [12]. But a potential disadvantage for the non-covalent attachment approach is the weak forces between CNTs or CB and polymers. Therefore, modifications have been mainly focused on the covalent linkage approach.

The covalent modification involves “grafting to” [13, 14] and “grafting from” strategies [15, 16]. The “grafting to” approach is the reaction of CNTs or CB and pre-formed polymer chains with reactive end groups. In this case, the polymers should be restricted to those with amino or hydroxyl groups and pre-functionalized polymers or copolymers [17-19]. When the polymer is pre-polymerized, it is easy to control the molecular weight. The “grafting from” approach involves the polymerization of monomers from surface-derived initiators on CNTs or CB [20-23]. The polymers can be efficiently grafted on the surface of CNTs or CB without steric hindrance, and the

molecular weight and grafting density cannot be controlled. Also, it is difficult to get strict control of the amounts of initiator and other conditions.

Polystyrene (PS), as a universal polymer, has been used for preparing composites in various fields. It can be polymerized by bulk radical polymerization and solution radical polymerization. It is largely used for manufacturing plastic products because of its high transparency, good electric insulation, rigidity and good resistance to chemical corrosion. PS has been widely used as polymer matrix in carbon nanocomposites. Zhao et al. [15] modified the MWCNTs with PS via nitroxide-mediated radical polymerization, and then copolymerized that with 4-vinylpyridine. Xiao et al. [24] exfoliated graphite/polystyrene composite by polymerization-filling technique. Liu [25] grafted the PS on the MWCNTs thermo-induced bulk radical polymerization of styrene at different polymerizing temperatures. Wu and Liu [26] had successfully grafted the PS on the surface of MWCNTs via the in situ solution radical polymerization. Recently, researchers in several fields have focused on the combination of carbon materials, especially by multiplying the nanotubes graphene sheets [27, 28]. However, there are very few studies works aimed at the co-reinforcement of carbon nano-materials in polymer composites [29]. In this work, the synergistic of MWCNTs and CB was first used to prepare M-C/PS nanocomposites by bulk radical polymerization under different conditions. Comparisons of MWCNTs/PS and CB/PS were made and the comparative evaluations of electrical conductivity and other properties were investigated.

4.2 Experimental

4.2.1 Materials

Styrene was purchased from Nakarai Tesuku Company, Japan. 2, 2'-Azoisobutyronitrile (AIBN) was purchased from Aladdin Reagent in Shanghai, China, and re-crystallized in ethanol.

4.2.2 In situ bulk radical polymerization

A certain amount of carbon nano-materials and 50 mL styrene (St) were mixed in a 100 mL glass bottle with a sealed cover and subjected to ultrasonication for approximately 4 h. The bottle was heated to 90 ^{o}C in an oil bath, and then a certain amount of the initiator AIBN was added. The mixture was magnetically stirred for approximately 6 h. Then, the bottle was placed in an oven heated to 90 ^{o}C complete the polymerization. The entire process required approximately 12 h. Portions of the product were pressed into plates for electrical resistivity measurements, and the remaining product was Soxhlet extracted in toluene. Table 4-1, 4-2 and 4-3 show the polymerization conditions and electrical resistivity for three kinds of nanocomposites.

Table 4-1 The experiment conditions and electrical properties of CB/PS composites

No	CB(g)	St(ml)	AIBN(g)	d(mm)	SR(Ω/□)	VR(Ω•cm)	lg
1	5.0	50	0.25	1.34	2.53×10^{5}	7.20×10^{4}	4.86
2	3.5	50	0.25	1.23	6.17×10^{6}	6.13×10^{5}	5.79
3	2.5	50	0.25	1.29	4.04×10^{6}	3.69×10^{5}	5.57
4	2.0	50	0.25	0.86	3.45×10^{11}	5.82×10^{10}	10.76
5	1.5	50	0.25	1.37	4.53×10^{11}	7.43×10^{10}	10.87
6	1.0	50	0.25	1.12	4.89×10^{11}	7.50×10^{10}	10.90
7	0.5	50	0.25	0.92	5.53×10^{11}	6.52×10^{10}	10.81

Table 4-2 The experiment conditions and electrical properties of MWCNTs/PS composites

No	MWCNTs (g)	St (ml)	AIBN (g)	MWCNTs/PS (g)	d (mm)	SR (Ω/□)	VR (Ω•cm)
1	5.0	50	0.25	39.58	1.10	0.16×10^{3}	0.30×10^{2}
2	3.5	50	0.25	39.819	1.12	3.59×10^{5}	6.27×10^{4}
3	2.5	50	0.25	61.004	2.82	1.04×10^{5}	4.10×10^{4}
4	2.0	50	0.25	44.298	1.14	1.83×10^{6}	5.33×10^{5}
5	1.5	50	0.25	25.835	1.42	3.99×10^{6}	4.25×10^{5}
6	1.0	50	0.25	43.208	1.11	6.01×10^{7}	5.79×10^{6}
7	0.5	50	0.25	42.8716	2.09	6.96×10^{11}	5.61×10^{10}

Table 4-3 The experiment conditions and electrical properties of M-C/PS composites

No	M-C(g)	St(ml)	AIBN(g)	M-C/PS(g)	d(mm)	SR(Ω/□)	VR(Ω•cm)
1	0.5+2.0	50	0.25	45.848	0.546	2.98×10^{6}	4.08×10^{5}
2	1.0+1.5	50	0.25	45.666	0.609	6.15×10^{5}	3.41×10^{4}
3	1.25+1.25	50	0.25	46.200	0.839	7.30×10^{5}	8.67×10^{4}
4	1.5+1.0	50	0.25	46.175	0.843	5.31×10^{5}	4.93×10^{4}
5	2.0+0.5	50	0.25	45.320	0.960	4.31×10^{5}	4.74×10^{4}
6	2.0+3.0	50	0.25	45.772	0.910	1.95×10^{5}	1.80×10^{4}
7	0.6+0.9	50	0.25	44.402	1.038	1.57×10^{9}	5.35×10^{8}
8	0.2+0.3	50	0.25	43.666	0.570	3.57×10^{11}	4.48×10^{10}
9	0.3+1.2	50	0.25	44.875	0.819	3.30×10^{9}	5.99×10^{8}
10	0.6+0.9	50	0.25	45.076	0.880	1.62×10^{8}	9.28×10^{7}
11	0.75+0.75	50	0.25	43.836	0.980	5.34×10^{7}	7.06×10^{7}
12	0.9+0.6	50	0.25	43.873	0.827	2.29×10^{7}	3.62×10^{7}
13	1.2+0.3	50	0.25	44.595	1.098	5.86×10^{8}	1.63×10^{7}
14	0.4+1.6	50	0.25	43.362	1.074	3.84×10^{7}	8.10×10^{6}
15	0.8+1.2	50	0.25	45.134	1.925	2.63×10^{7}	1.87×10^{6}
16	1.0+1.0	50	0.25	45.372	2.015	3.73×10^{8}	1.14×10^{7}
17	1.2+0.8	50	0.25	45.772	1.070	3.46×10^{6}	2.73×10^{6}
18	1.6+0.4	50	0.25	44.505	1.265	4.83×10^{6}	4.21×10^{5}

4.3 Results and discussion

In this work, polystyrene was grafted onto the surfaces of CB, MWCNTs and M-C via in situ bulk radical polymerization. In the polymerization process, the polymer chain radicals that reacted with the C=C bonds of the carbon nano-materials were produced by three approaches: (1) the in situ radical polymerization of the monomers in the presence

of the carbon nano-materials after initiation with an initiator; (2) the thermal radical polymerization of styrene; and (3) polymer chain transfer. Soxhlet extraction was then carried out for some of the polymer nanocomposites to remove unreacted polystyrene coating the polystyrene-grafted carbon nano-materials.

4.3.1 The microstructure of M-C/PS nanocomposites

FT-IR spectroscopy measurements are important in the detection of the structure of M-C/PS nanocomposites. Fig. 4-1 shows the asymmetrical and symmetrical stretching vibrations of $–CH_2$ at 2921 and 2850 cm^{-1}, the flexural vibrations of $–CH_2$ at 1430 cm^{-1}, the characteristic C-C ring stretching vibration at 1649 cm^{-1} and the benzene ring plane stretching vibration of –CH at 756 and 706 cm^{-1} for the M-C/PS nanocomposites [32]. None of these vibrations appeared in the FT-IR spectrum of the pristine M-C with a M/C ratio of 2/3. This finding indicates indicated that the polystyrene chains were grafted onto the M-C surfaces via bulk radical polymerization.

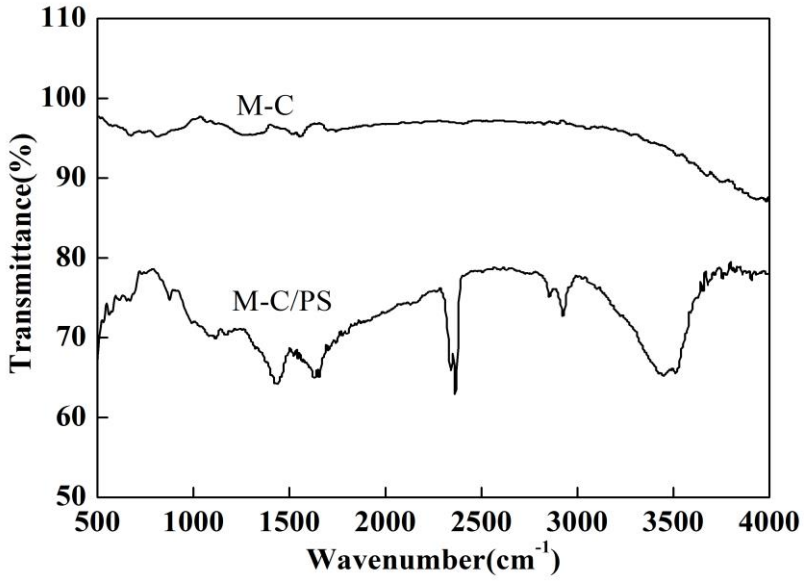

Fig. 4-1 FT-IR spectra of the pristine M-C and M-C/PS composite with the M/C of 2/3 and total content of 5 wt%

4.3.2 The XRD patterns of carbon nano-materials and their nanocomposites

The X-ray patterns of the carbon nano-materials and nanocomposites are shown in Fig. 4-2. The CB and MWCNTs showed two peaks at 25.60° (3.47 Å) and 43.14° (2.12 Å) attributed to the diffraction of the (002) and (100) planes corresponding to the interlayer spacing (0.34 nm) of the nano-materials and reflection of the carbon atoms, respectively; these findings, are in good agreement with the results reported in the literature [30]. Both PS and the nanocomposites showed a broad, amorphous peak centered at 19.61° [31]. All of the nanocomposites showed characteristic diffraction peaks at 25.60° and 43.14º, which clearly indicated that carbon nano-materials were present in the composites with the same crystalline structure as their pristine form.

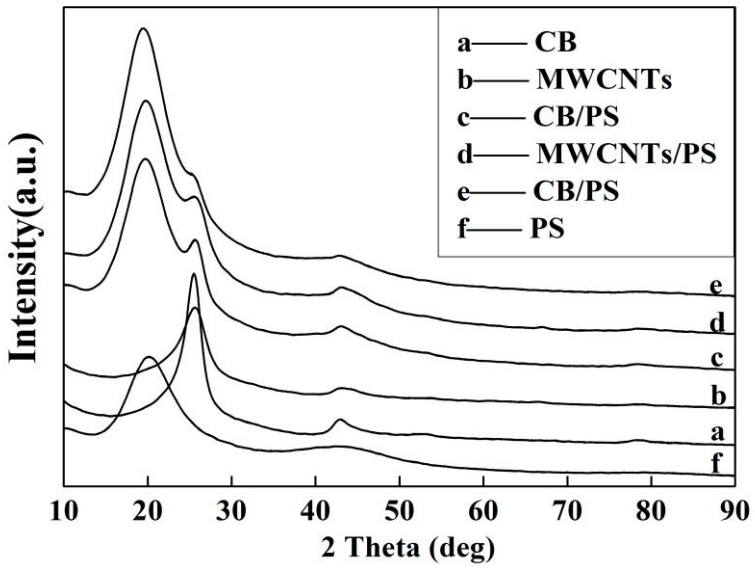

Fig. 4-2 XRD analysis of carbon nano-materials, PS and composites with the content of 5 wt% and the ratio of the MWCNTs to CB is 2/3

4.3.3 Microstructure images of carbon nano-materials and their nanocomposites

TEM imaging is also important in probing the microstructures of materials. All of the pristine materials and composites were dispersed in toluene in an ultrasonic bath for 30 min, and then deposited on a copper grid covered with a perforated carbon film. As shown in Fig. 4-3, pure CB (a) and MWCNTs (b) easily aggregated. However, all of the

nanocomposites were well dispersed in toluene, and the adhesion of polystyrene to the surfaces of the CB, MWCNTs and M-C was clearly observed. This result indicates that the polystyrene was successfully grafted onto the carbon nano-materials surface by the proposed method. In addition, the MWCNTs in the M-C/PS nanocomposites could form bridges between CB particles, which led to an increase in electrical conductivity.

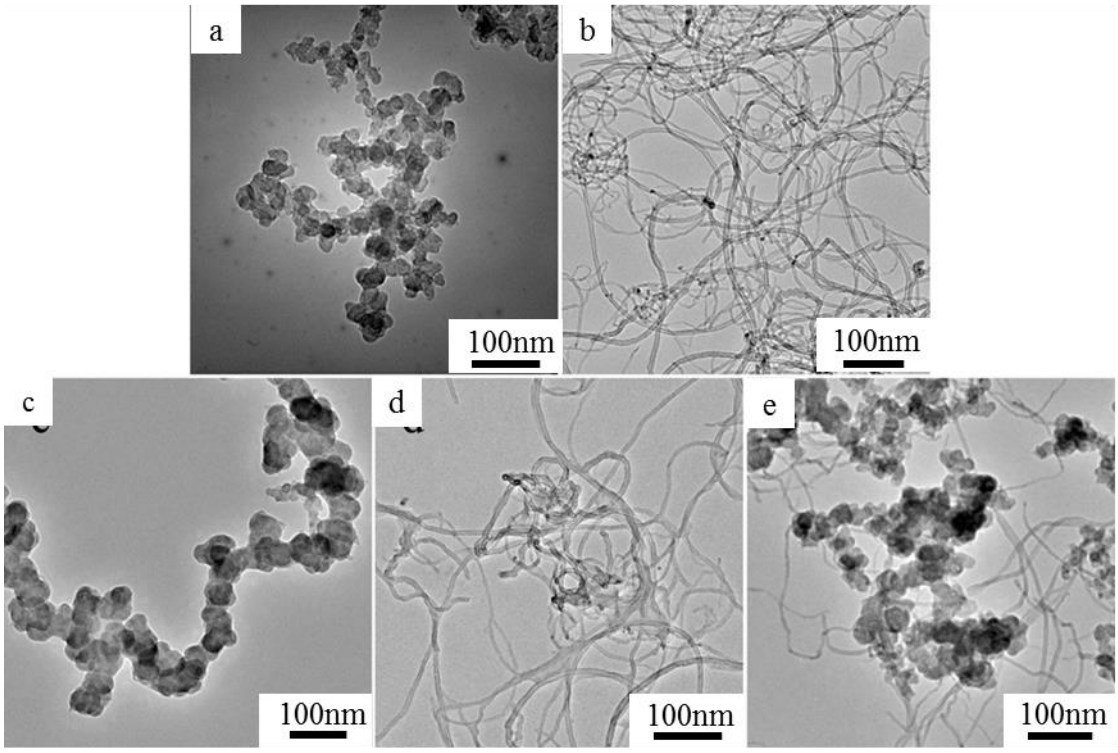

Fig. 4-3 TEM images of (a), CB, (b), MWCNTs, (c), CB/PS,
(d), MWCNTs/PS and (e), M-C/PS

4.3.4 Electrical conductivity

After the polymerization of styrene in the presence of the carbon nano-materials, the products were hot-pressed into slices for electrical conductivity measurements. Fig. 4-4 is demonstrating the change in the electrical resistivities of the CB/PS and MWCNT/PS composites with increasing filler content. The MWCNT/PS nanocomposites exhibited higher electrical conductivity than the CB/PS nanocomposites. For the CB/PS nanocomposites, the electrical resistivity showed a slight change as the CB content reached 4 wt%, decreased sharply when the CB content increased to 5 wt%, and then

gradually decreased with increasing CB content. However, the electrical resistivity of the MWCNT/PS nanocomposites decreased until the MWCNT content reached 5 wt%, remained approximately the same until the content reached 7 wt%, and then decreased with a further increase in the MWCNT content. The electrical resistivities of the CB/PS and MWCNT/PS nanocomposites were similar at filler contents of 5 wt% and 7 wt%, respectively. Pursuant to the concept that low content yields low resistivity, the optimal total content of CB and MWCNTs should be below 5 wt%.

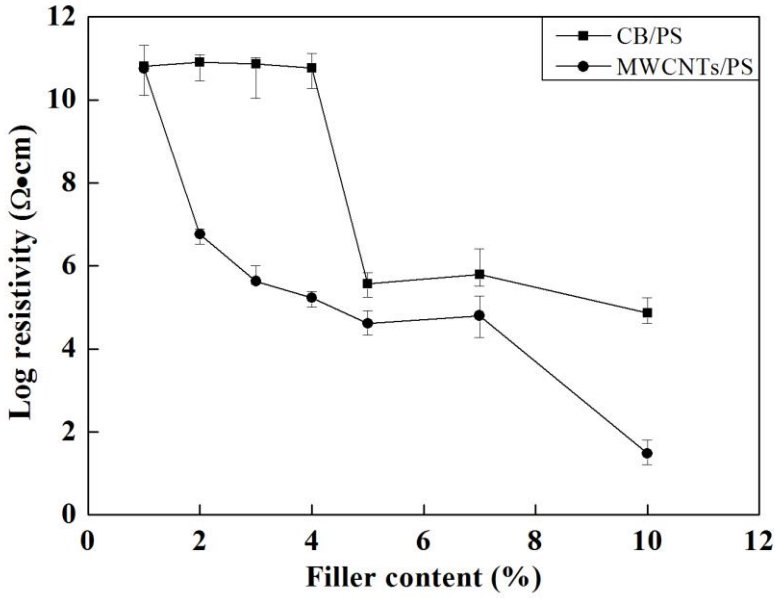

Fig. 4-4 Electrical resistivity of CB/PS and MWCNT/PS composites with different content of CB and MWCNT

4.3.5 The percentage grafting of composites

TGA was used to determine the percentage grafting of PS onto the carbon nano-materials surface. Before the TGA analysis, the CB/PS, MWCNT/PS and M-C/PS nanocomoposites specimens were extracted with the Soxhlet extractor. Fig. 4-5 to Fig. 4-7 show the thermal gravimetric weight of CB, MWCNTs and three kinds nanocomposites with the content is 5 wt%. Compared to CB and MWCNTs, the obviously weight loss can be found in the temperature range of 300-450 °C for the

nanocomposites, which were attributed to the decomposition of the polystyrene grafted onto the carbon nano-materials surface.

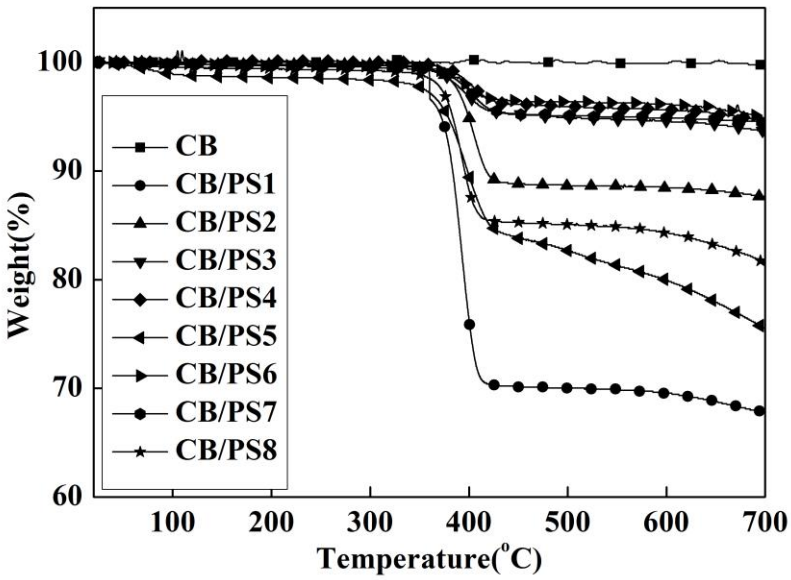

Fig. 4-5 The TGA curves of CB/PS composites in different CB content

For the CB/PS and MWCNTs/PS composites, the weight loss in the temperature range of 300-450 °C is increased first and then irregular changed with the CB and MWCNTs content increasing as shown in Fig. 4-5 and Fig. 4-6. This may be attributed to the error which was operated during the experiment processing. Because of the temperature of the heater is unstable. However, there may be the optical filler content for both CB/PS and MWCNT/PS nanocomposites.

However, the weight loss of M-C/PS nanocomposites is more greatly than both CB/PS and MWCNT/PS nanocomposites as shown in Fig. 4-7, suggesting that more PS was grafted onto the M-C surfaces, because the CB was exfoliated due to the bridging role played by the MWCNTs, which demonstrated that a the good synergistic effect was induced between the particles and nanotubes.

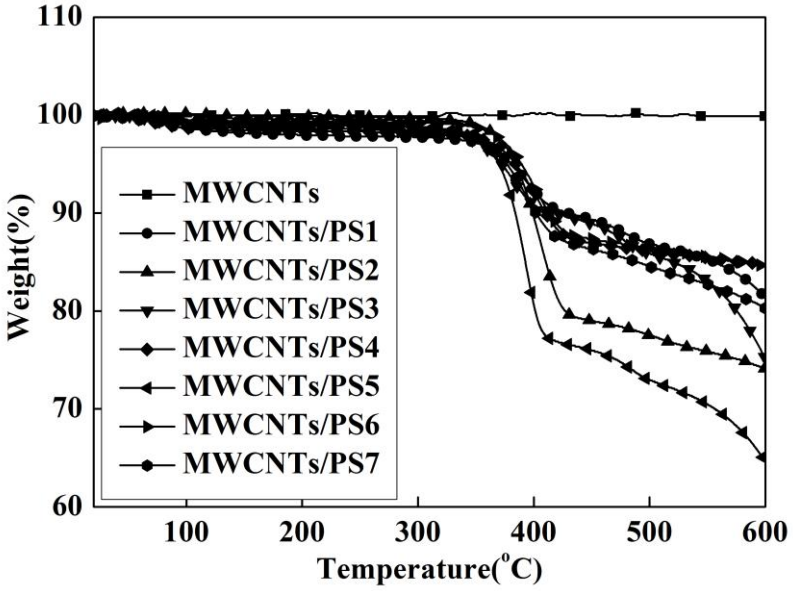

Fig. 4-6 The TGA curves of MWCNT/PS composites in different

MWCNTs content

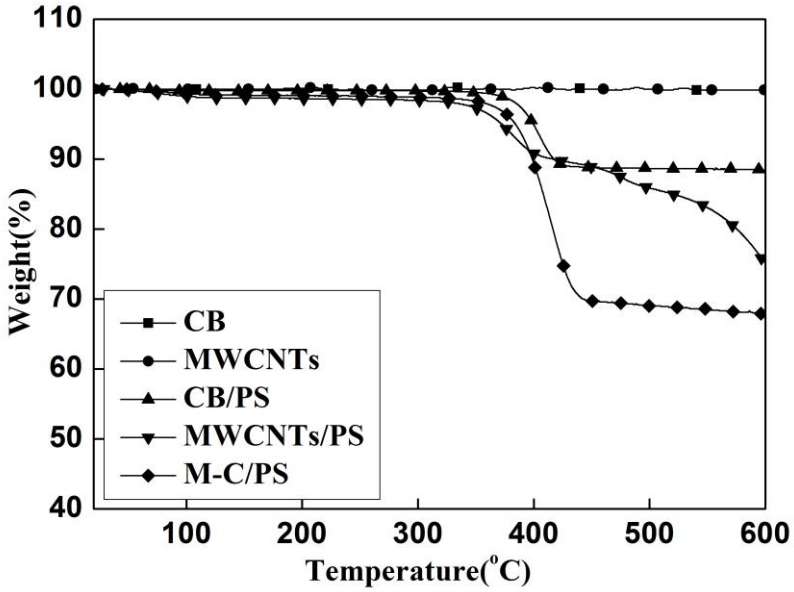

Fig. 4-7 TGA curves of the pristine carbon nano-materials and their composites with the content is 5 wt% and the ratio of the MWCNTs and CB of 2/3

4.3.6 Synergistic effect of MWCNTs and CB on electrical conductivity

Because the electrical resistivity of the CB/PS nanocomposites decreased sharply between 4 wt% and 5wt% and the electrical resistivity of the MWCNT/PS nanocomposites clearly decreased below 5 wt%, M-C/PS nanocomposites with different feeding ratios of CB and MWCNTs with total contents of 3 wt%, 4 wt% and 5 wt% were prepared. The electrical resistivity curves are shown in Fig. 4-8. The electrical resistivity of the M-C/PS nanocomposites with a total M-C content of 3 wt% increased slowly with the M/C ratio. However, the total M-C contents of 4 wt% and 5 wt%, there was an unusual change in the resistivity when the M/C ratio was 1. It can be assumed that MWCNT act as bridges at small concentrations, a role that is enhanced with the increase in the proportion of MWCNTs. However, the MWCNTs can agglomerate when their concentration is continuously increased, degrading the bridge effect. Additionally, the electrical resistivity was observed to remain nearly the same when the ratio was 3/2 or 4/1 for a total M-C content of 5 wt%. Thus, the optimal M/C ratio was confirmed to be 2/3 in view of both the high cost of MWCNTs and the optimal electrical conductivity.

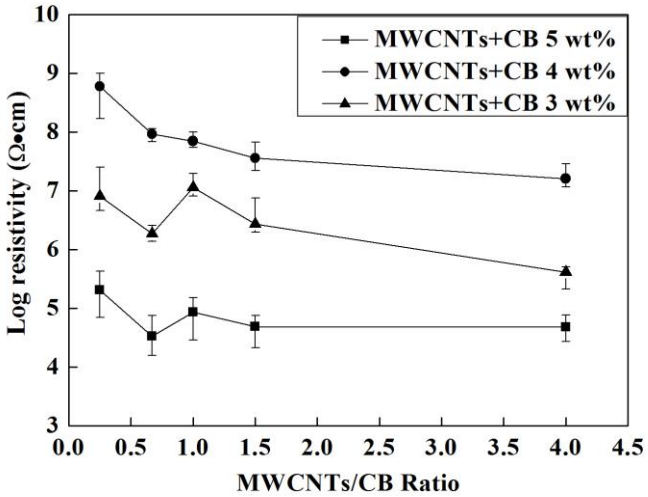

Fig. 4-8 Electrical resistivity of M-C/PS composites in different ratio of CB and MWCNTs (total contents of M-C are 3 wt% and 5 wt%)

To further clarify the synergistic effect between the CB and MWCNTs on the electrical resistivity of the M-C/PS nanocomposites, comparison curves were created as shown in Fig. 4-9. The resistivity of the M-C/PS nanocomposites was observed to be higher than the base line when the proportion of MWCNTs was 80% and the total content of filler was 3 wt% (Fig. 4-9 (a)). This result may be attributed to the fact that a small amount of MWCNTs could not form a network structure with CB and the changes in resistivity were small with the increasing content of MWCNTs. However, for the nanocomposites with total filler contents of 4 wt% and 5 wt% (Fig. 4-9 (b) and (c)), the resistivity curves were below the base line. These results suggest that the synergistic effect between the CB and MWCNTs persisted until the total filler content reached a certain value. Furthermore, the optimum M/C ratio was 2/3, which indicates a lower the content of MWCNTs because of their higher cost.

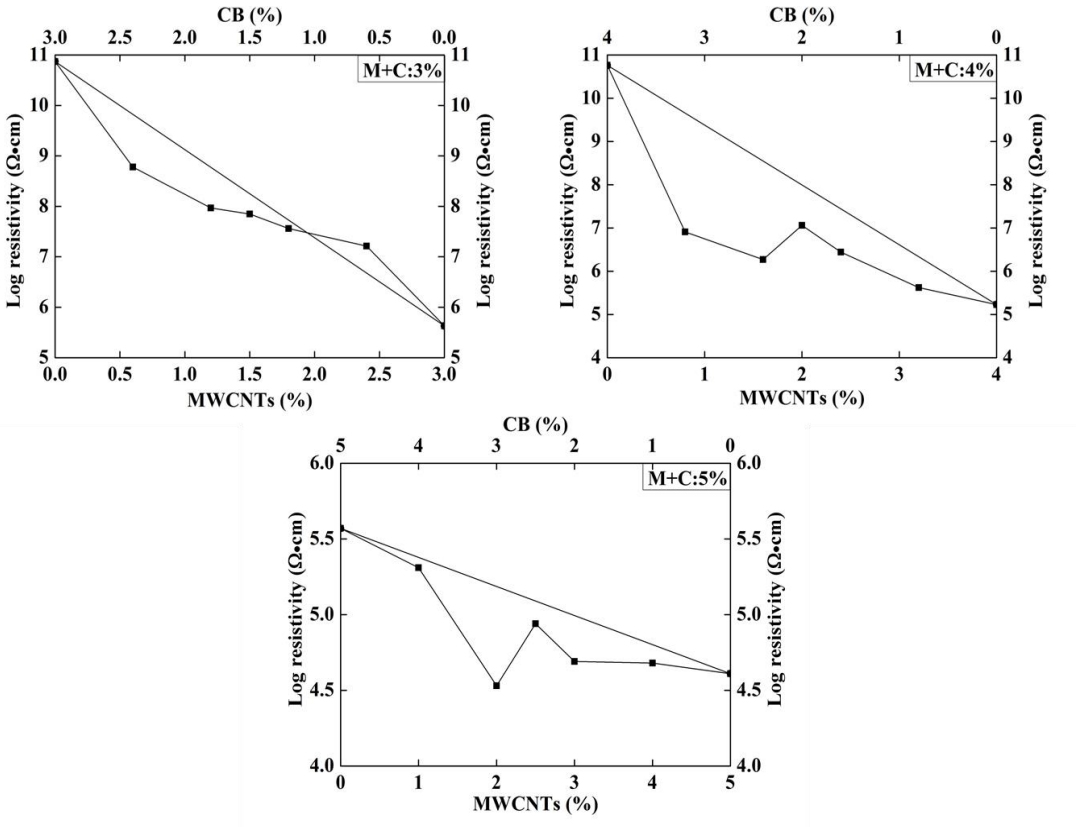

Fig. 4-9 Synergistic effect of the CB and MWCNTs on the electricity of M-C/PS nanocomposites (filler contents are: (a), 3 wt%; (b), 4 wt% and (c), 5 wt%)

Fig. 4-10 shows the effect of the total M-C content on the electrical resistivity of the M-C/PS nanocomposites. The electrical resistivity of the M-C/PS nanocomposites was observed to decrease quickly below an M-C filler content of 5 wt% and then change slightly up to a content of 10 wt%, which confirmed that the optimal total content of CB and MWCNTs was 5 wt%.

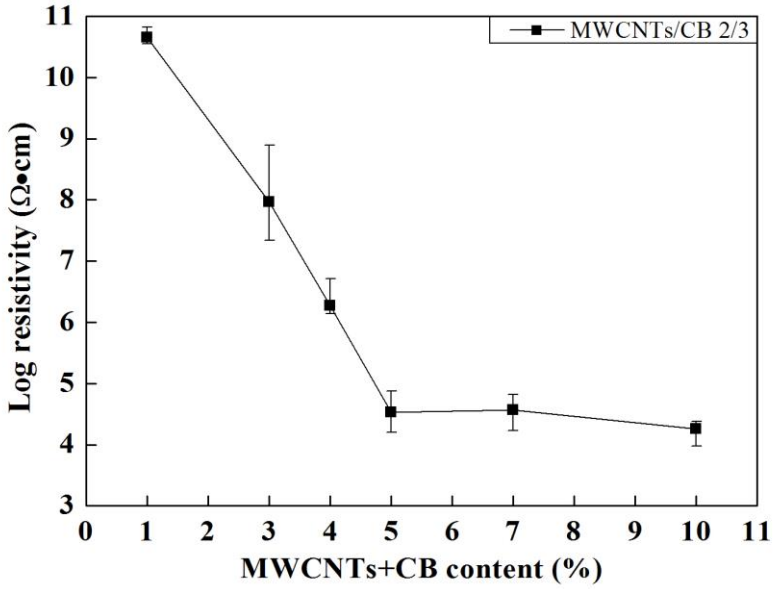

Fig. 4-10 Effect of M-C total content on the electrical resistivity of M-C/PS composites

4.3.7 Mechanical properties of nanocomposites

The bending strength was done to test the mechanical properties of CB/PS, MWCNT/PS and M-C/PS nanocomposites. Fig. 4-11 shows the bending strength change curves of CB/PS and MWCNT/PS nanocomposites with different filler contents. The bending strength decreased with the filler content increasing to 3 wt%. It may be contributed that the defect was occurred during the grafted processing. The bending strength increased a little from 3 wt% to 7 wt% for both CB/PS and MWCNT/PS nanocomposites and then decreased. Because of the carbon materials themselves have well mechanical properties. But when the filler content is too high, the composites will

become brittle.

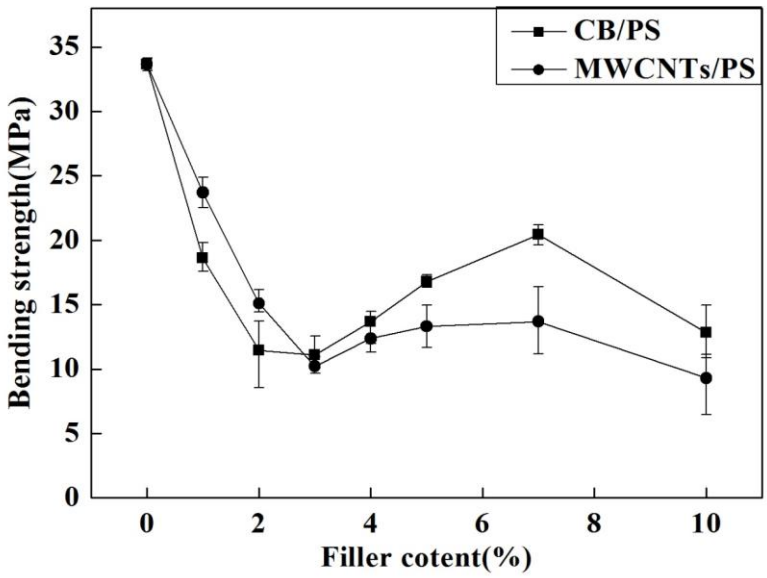

Fig. 4-11 Bending strengths of CB/PS and MWCNT/PS nanocomposites

Fig. 4-12 presents the changes in the bending strengths of the M-C/PS nanocomposites with the M/C ratio for a total content of 5 wt%. It is clear that the bending strength increased with the M/C ratio. However, the bending strength of the M-C/PS nanocomposites decreased with the increase in the total content of MWCNTs and CB, as shown in Fig. 4-13. This behavior can be attributed to the following three effects: First, interfacial defects in the nanocomposites were produced during the nanocomposites fabrication process and the number of defects increased with the filler content [33, 34]. Second, polystyrene is a brittle polymer [35], which makes it more sensitive to these defects. Finally, the three-point bending test is also sensitive to interfacial defects. The decrease in the bending strength with the increase in the total content of MWCNTs and CB was observed to be small, which suggests that the compatibility between the nano-materials and polystyrene was improved.

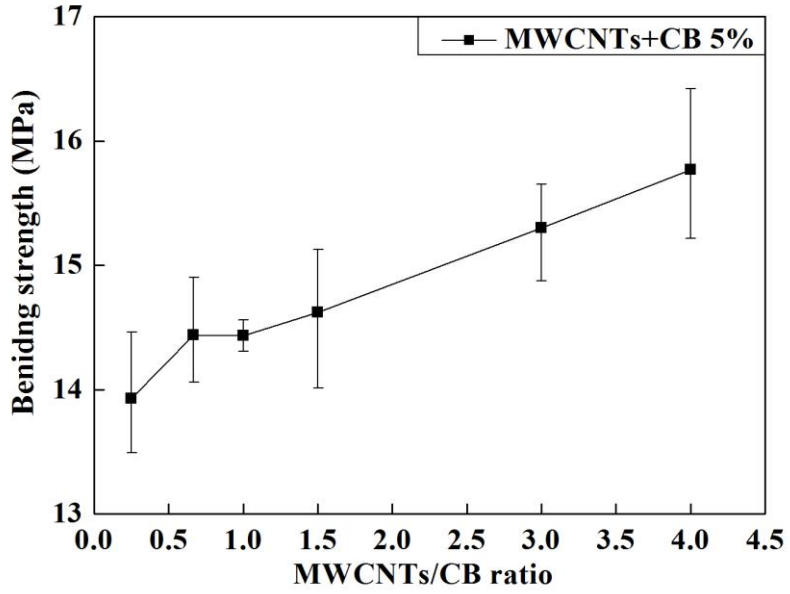

Fig. 4-12 The bending strength of the M-C/PS composites in different ratios of CB and MWCNTs (the total contents of CB and MWCNTs is 5 wt%)

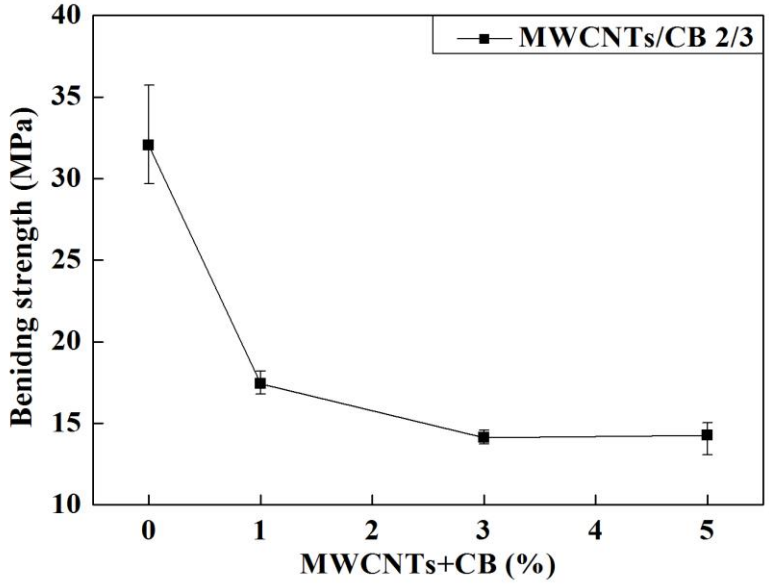

Fig. 4-13 The bending strength of M-C/PS composites in different total contents of CB and MWCNTs

4.4 Conclusions

CB/PS and MWCNT/PS nanocomposites were prepared by bulk radical polymerization. The synergistic effect between MWCNTs and CB on the properties of the nanocomposites was investigated by comparing the properties of the CB/PS and MWCNT/PS nanocomposites. The results showed that the MWCNTs and CB exerted a favorable synergistic effect on the M-C/PS nanocomposites with respect to their electrical and mechanical properties. The long MWCNTs could crosslink the CB and thereby form a network structure. In addition, TEM and TGA results suggest that the percentage of PS grafted onto the M-C mixture was higher than that on either the MWCNTs or CB alone. Furthermore, the bending strength increased with the M/C ratio. However, the bending strength of the M-C/PS nanocomposites decreased with the increase in the total content of MWCNTs and CB. The results of this study demonstrated that M-C/PS nanocomposites can be blended with other polymers to yield products with improved mechanical properties.

References

[1] I. Sumino, Helical Microtubules of Graphitic Carbon, Nature, 354 (1991) 56-58.

[2] D. Tasis, N. Tagmatarchis, A. Bianco, M. Prato, Chemistry of Carbon Nanotubes, Chemical Reviews, 106 (2006) 1105-1136.

[3] T. Durkop, B.M. Kim, A.M.S. Fuhrer, Properties and Applications of High-Mobility Semiconducting Nanotubes, Journal of Physics: Condensed Matter, 16 (2004) R553-R580.

[4] A.B. Sulong, N. Muhamad, J. Sahari, R. Ramli, B.M. Deros, Electrical Conductivity Behaviour of Chemical Functionalized Mwcnts Epoxy Nanocomposites, European Journal of Scientific Research, 29 (2009) 13-21.

[5] Z. Spitalskya, D. Tasisb, K. Papagelisb, C. Galiotis, Carbon Nanotube-Polymer Composites: Chemistry, Processing, Mechanical and Electrical Properties, Progress in Polymer Science, 35 (2010) 357-401.

[6] N. Deprez, D.S. Mclachlan, The Analysis of the Electrical Conductivity of Graphite Conductivity of Graphite Powders During Compaction, Journal of Physics D: Applied Physics, 21 (1988) 101-107.

[7] Y.P. Sun, K. Fu, Y. Lin, W. Huang, Functionalized Carbon Nanotubes: Properties and Applications, Accounts of Chemical Research, 35 (2002) 1096-1104.

[8] H. Kuzmany, A. Kukovecz, F. Simon, M. Holzweber, Ch. Kramberger, T. Pichle, Functionalization of Carbon Nanotubes, Synthetic Metals, 141 (2004) 113-122.

[9] H. Kong, C. Gao, D.Y. Yan, Controlled Functionalization of Multi-walled Carbon Nanotubes by in Situ Atom Transfer Radical Polymerization, Journal of the American Chemical Society, 126 (2004) 412-413.

[10] N.I. Kovtyukhova, T.E. Mallouk, L. Pan, E.C. Dickey, Individual Single Walled Nanotubes and Hydrogels Made by Oxidative Exfoliation of Carbon Nanotube Ropes, Journal of the American Chemical Society, 125 (2003) 9761-9769.

[11] G.H. Zheng, J.S. Wu, W.P. Wang, C.Y. Pan, Characterization of Expanded

Graphite/Polymer Composites Prepared by in situ Polymerization, Carbon, 42 (2004) 2839-2847.

[12] P. Liu, Modifications of Carbon Nanotubes with Polymers, European Polymer Journal, 41 (2005) 2693-2703.

[13] G.J. Wang, Z.H. Qu, L. Liu, Q. Shi, J.L. Guo, Study of SMA Graft Modified MWNT/PVC Composite Materials, Materials Science and Engineering A, 472 (2008) 136-139.

[14] G. Mountrichas, S. Pispas, N. Tagmatarchis, Grafting-to Approach for The Functionalization of Carbon Nanotubes with Polystyrene, Materials Science and Engineering: B, 152 (2008) 40-43.

[15] X.D. Zhao, X.H. Fan, X.F. Chen, C.P. Chai, And Q.F. Zhou, Surface Modification of Multiwalled Carbon Nanotubes via Nitroxide-Mediated Radical Polymerization, Journal of Polymer Science Part A: Polymer Chemistry, 44 (2006) 4656-4667.

[16] B.X. Yang, J.H. Shi, K.P. Pramoda, S.H. Goh, Enhancement of the Mechanical Properties of Polypropylene Using Polypropylene-Grafted Multi-walled Carbon Nanotubes, Composites Science and Technology, 68 (2008) 2490-2497.

[17] Y. Lin, B. Zhou, K.A.S. Fernando, P. Liu, L.F. Allard, Y.P. Sun, Polymeric Carbon Nanocomposites from Carbon Nanotubes Functionalized with Matrix Polymer, Macromolecules, 36 (2003) 7199-7204.

[18] B. Zhao, H. Hu, A. Yu, D. Perea, R.C. Haddon, Synthesis and Characterization of Water Soluble Single-Walled Carbon Nanotube Graft Copolymers, Journal of the American Chemical Society, 127 (2005) 8197-8203.

[19] Y.X. Liu, Z.J. Du, Y. Li, C. Zhang, C.J. Li, X.P. Yang, H.Q. Li, Surface Covalent Encapsulation of Multi-walled Carbon Nanotubes with Poly(Acryloyl Chloride) Grafted Poly(Ethylene Glycol), Journal of Polymer Science Part A: Polymer Chemistry, 44 (2006) 6880-6887.

[20] Z. Yao, N. Braidy, G.A. Botton, A. Adronov, Polymerization from the Surface of Single-Walled Carbon Nanotubes-Preparation and Characterization of Nanocomposites,

Journal of the American Chemical Society, 125 (2003) 16015-16024.

[21] H. Kong, C. Gao, D.Y. Yan, Functionalization of Multi-walled Carbon Nanotubes by Atom Transfer Radical Polymerization and Defunctionalization of the Products, Macromolecules, 37 (2004) 4022-4030.

[22] X.F. Li, W.C. Guan, H.B. Yan, L. Huang, Fabrication and Atomic Force Microscopy/Friction Force Microscopy (Afm/Ffm) Studies of Polyacrylamide-Carbon Nanotubes (PAM-CNTs) Copolymer Thin Films, Materials Chemistry and Physics, 88 (2004) 53-58.

[23] C.Y. Hong, Y.Z. You, C.Y. Pan, A New Approach to Functionalize Multi-Walled Carbon Nanotubes by the Use of Functional Polymers, Polymer, 47 (2006) 4300-4309.

[24] P. Xiao, M. Xiao, K.C. Gong, Preparation of Exfoliated Graphite/Polystyrene Composite by Polymerization-Filling Technique, Polymer, 42 (2001) 4813-4816.

[25] P. Liu, Facile Graft Polystyrene Onto Multi-Walled Carbon Nanotubes via in situ Thermo-Induced Radical Polymerization, Journal of Nanoparticle Research, 11 (2009) 1011-1016.

[26] X.L. Wu, P. Liu, Polymer Grafted Multi-walled Carbon Nanotubes via Facile in Situsolution Radical Polymerization, Journal of Experimental Nanoscience, 5 (2010) 383-389.

[27] C.S. Rout, A. Kumar, T.S. Fisher, U.K. Gautam, Y. Bando, D. Golberg, Synthesis of Chemically Bonded CNT-Graphene Heterostructure Arrays, RSC Advances, 2 (2012) 8250-8253.

[28] D.Y. Cai, M. Song, C.X. Xu, Highly Conductive Carbon-Nanotube/Graphite-Oxide Hybrid Films, Advanced Materials, 20 (2008) 1706-1709.

[29] B.J. Kim, J.H. Byun, S.J. Park, Effects of Graphenes/CNTs Co-Reinforcement on Electrical and Mechanical Properties of HDPE Matrix Nanocomposites, Bulletin of the Korean Chemical Society, 31 (2010) 2261-2264.

[30] B. Zhang, Y.T. Xu, Y.F. Zheng, L.Z. Dai, M.Q. Zhang, J. Yang, Y.J. Chen, X.D. Chen, J.Y. Zhou, A Facile Synthesis of Polypyrrole/Carbon Nanotube Composites with

Ultrathin, Uniform and Thickness-Tunable Polypyrrole Shells, Nanoscale Research Letters, 6 (2011) 431-439.

[31] M. Erol1, E. Çelik, Graphite-Flake Carbon-Black-Reinforced Polystyrene-Matrix Composite Films Deposited on Glass-Fiber Woven Fabrics as Plane Heaters, Materials Technology, 47 (2013) 25-28.

[32] X.L. Wu, J.H. Qiu, P. Liu, E. Sakai, L. Lei, Polystyrene Grafted Carbon Black Synthesis via in Situ Solution Radical Polymerization in Ionic Liquid, Journal of Polymer Research, 20 (2013) 167-173.

[33] Y.K. Choi, K.I. Sugimoto, S.M. Song, Y. Gotoh, Y. Ohkoshi, M. Endo, Mechanical and Physical Properties of Epoxy Composites Reinforced by Vapor Grown Carbon Nanofibers, Carbon, 43 (2005) 2199-2208.

[34] T. Takeda, Y. Shindo, F. Narita, Y. Mito, Tensile Characterization of Carbon Nanotube-Reinforced Polymer Composites at Cryogenic Temperatures: Experimens and Multiscale Simulations, Materials Transactions, 50 (2009) 436-445.

[35] M.B. Kasen, Cryogenic Properties of Filamentary-Reinforced Composites: an Update, Cryogenics, 21 (1981) 323-340.

Chapter 5 Poly (Lactic Acid) Based MWCNT/PMMA Composites Prepared by Pickering Emulsions Polymerization

5.1 Introduction

Using colloid particles to prepare and stabilize emulsions was called “Pickering” emulsions, has attracted increasing interest in recent years [1-3]. In contrast to conventional emulsions, which are usually thermodynamically unstable and stabilized by surfactants or amphiphilic linear copolymers, Pickering emulsions are often super-stable due to the nearly irreversible adsorption of the colloid particles at the oil/water interface [4]. These particles can be prepared in different ways. The most common way is surface modification of natural or commercial inorganic nanoparticles [5, 6]. Pickering emulsions technique has been applied in the foods, agrochemicals, cosmetics and medications. Different types of colloid particles acted as surfactants have been employed for Pickering emulsifiers such as clays, metal oxides and silica [7-9]. Self-assembly of the colloid particles at the oil/water interface in Pickering emulsions is thermodynamically favorable due to the reduction of the interfacial energy of the system upon the creation of a new interface between colloid particles and liquid phases instead of the oil/water interface.

Carbon nanotubes (CNTs) have been applied in various fields such as conductive composites, mechanical fillers because of their unique structure, mechanical and electrical properties [10-12]. However, their poor solubility or dispersibility in solvent and polymer matrix has imposed many barriers for their widespread use in many of these applications. Surface modification of CNTs has become an efficient approach to promote the solubility of CNTs in common solvents and increase their affinity with organic polymeric matrices [13, 14], as a result to improve the interfacial properties of the nanocomposites [15]. By far, there were many excellent works reported on the covalent surface functionalization of MWCNTs with various strategies [16-22]. Among the

strategies for surface grafting polymers onto CNTs, including “grafting to” [23-25], “grafting from” [26-28], “free radical addition” and so on. Jia et al. prepared PMMA/CNT composites by an in situ process [29]. CNTs can be initiated by AIBN to open their π-bonds, which imply that CNTs may participate in PMMA polymerization and form a strong combining interface between the CNTs and the PMMA matrix. Poly (methyl methacrylate) (PMMA)/carbon nanotubes composites had been prepared by in situ microemulsion polymerization for gas sensor. The uniform film of composites was obtained and the electrical properties were enhanced compared with the composites from solution mixing of PMMA and carbon nanotubes [30]. However, most of these methods are conducted in the organic solvent, which is bad to environment and healthy.

In chapter 3 and 4, the carbon powder and nanotubes were modified with in situ radical polymerization and bulk polymerization, which were solvent consumption and bad to environment. In the present work, MWCNT/PMMA composites were prepared by Pickering emulsion polymerization. MWCNTs displayed the functional surfactant activity during the process of Pickering emulsions polymerization was examined by SEM and TEM. The MWCNT/PMMA exhibited high electric conductivity. The poly (lactic acid) (PLA) based conductive composites were prepared and characterized by mixing the MWCNT/PMMA and PLA.

5.2 Experimental

5.2.1 Preparation of MWCNT/PMMA composites by Pickering emulsions polymerization

A certain amount of MWCNTs were dispersed in the corresponding amount of DI water and homogenized 30 min by means of ultrasonic vibration in a 250 mL round-bottom flask that was water-bathed. Methyl methacrylate monomer (MMA) was added into the flask and then dispersed evenly with ultrasonic for 30 min. Then the flask was placed in a water bath at 80 ^{o}C, mechanically stirred at 400 rpm in environment full

of nitrogen. Afterwards, AIBN was added into the mixture and the mixture was refluxed at 80 ^{o}C for 12 h. Then, the MWCNT/PMMA was washed with distilled water and finally dried in a vacuum oven at 50 ^{o}C. The conditions of preparing progress are listed in table 5-1. PMMA was prepared under the same condition of MWCNT/PMMA2 without the MWCNTs adding.

Table 5-1 The conditions and electrical resistivity of MWCNT/PMMA preparation

NO	MWCNTs (g)	MMA (ml)	MWCNT/PMMA (g)	SR/Ω/□	VR/Ω·cm
1	1	2	2.754	0.68	0.068
2	1	4	4.389	9	0.9
3	1	6	5.850	13	1.2
4	1	8	5.756	17	1.7
5	1	10	9.641	3.2×10^{3}	3.2×10^{2}

5.2.2 Preparation of PLA based conductive composites

A twin-screw extruder was used for prior mixing of MWCNTs or MWCNT/PMMA and PA6. The extruding temperatures were: C1, 180 ^{o}C; C2, 180 ^{o}C; C3 and C4, 170 ^{o}C. The injection molding machine was used to form the mixture plates into dumbbell (30 mm × 5 mm × 2 mm). The injection temperature was 180 ^{o}C, molding temperature was 50 ^{o}C, and the injection rate was 17.6 mm/s.

5.3 Results and discussions

5.3.1 MWCNTs as a surfactant

Fig. 5-1 shows the synthetic process of Pickering emulsion polymerization of methyl methacrylate monomer using the MWCNTs as the stabilizer. While the oil phase of methyl methacrylate monomer was emulsified by the homogenizer, the splitting oil droplets with size ranging from nanometer to submicron would exhibit high surface free energy owing to their relatively large surface area. At the same time, MWCNTs

possessing both hydrophobic part (a largely hydrophobic basal plane) and hydrophilic part (hydrophilic edges like edge-OH groups) in the water medium, tended to adsorbed onto the surfaces of emulsified oil droplets. This adsorbing process could effectively raise the surface free energy of small droplets, not only preventing further coagulation among the droplets but also forming oil droplets covered with the MWCNTs [31]. The MWCNTs therefore could serve as a kind of stabilizer to maintain the stability of monomer droplets. Upon polymerization of the methyl methacrylate monomer droplets, the MWCNT/PMMA composite particles with a structure similar to the core-shell were then obtained.

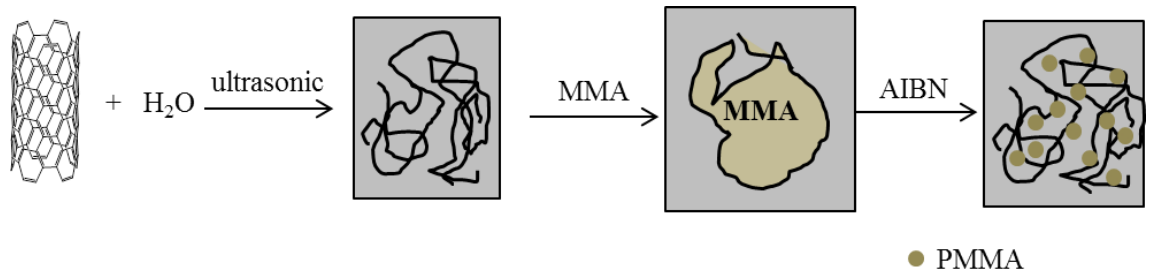

Fig. 5-1 Scheme of MWCNT/PMMA composites obtained by Pickering emulsion polymerization

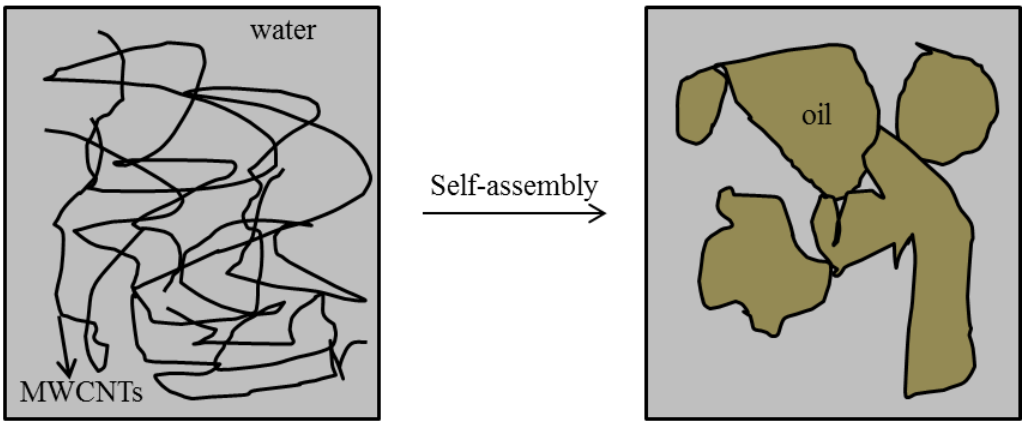

Fig. 5-2 The self-assembly of MWCNTs at the interface in W/O system

Using MWCNTs as surfactant in Pickering emulsion polymerization requires sufficient presence of nanolayers at the liquid-liquid interface. Adsorption of particles at liquid-liquid interface is originated from reduction of free energy of the system [32].

MWCNTs can serve as an emulsifier in Pickering emulsions as long as it has a moderate affinity to both immiscible phases. As shown in Fig. 5-2, the MWCNTs sheets with hydrophilic functional groups are able to stay at the oil/water interface and form stable oil dispersions in the aqueous phase.

5.3.2 FT-IR spectrum of MWCNT/PMMA composites

The FT-IR spectrum is very important to investigate the molecular structure and material composition of composites. Fig. 5-3 presents the FT-IR spectrum curves of MWCNTs, MWCNT/PMMA composites and PMMA. Compared the curve of MWCNTs, both PMMA (Fig. 5-3 (c)) and MWCNT/PMMA composites (Fig. 5-3 (b)) show the symmetric stretching vibration peak and antisymmetric stretching vibration of $–CH_2$ at 2996 and 2943 cm^{-1} and the stretching vibration peak of –C=O at 1725 cm^{-1}. The absorption at 1445 cm^{-1} can characterize the flexural vibrations of $–CH_2$. In addition, 1244 cm^{-1} is the stretching vibration of C–O–C in acetyl compound, and 1152 cm^{-1} is the stretching vibration of C–O. All of these peaks appear in the curves of PMMA and MWCNT/PMMA composites rather than in the curves of MWCNTs, which suggests the existing of PMMA in composites.

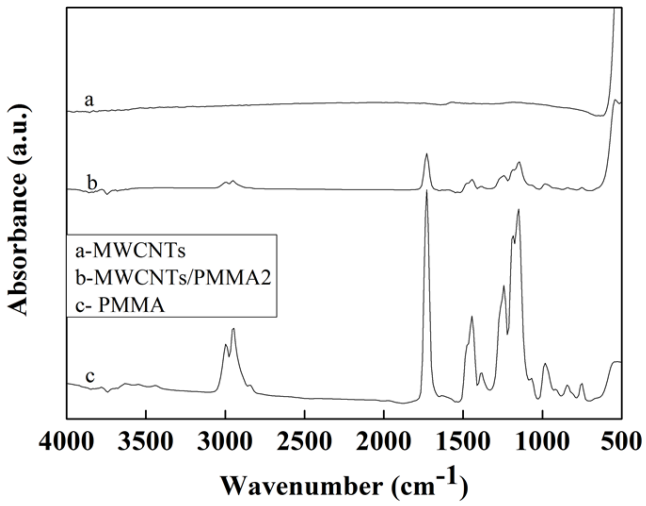

Fig. 5-3 FT-IR spectrum of MWCNTs (a), MWCNT/PMMA composites (b) and PMMA (c)

5.3.3 Thermal properties of MWCNT/PMMA composites

The thermal degradation and flammability of polymers is largely affected by the incorporation of MWCNTs. In this work, thermal gravimetric analysis was carried out to evaluate MWCNTs as a thermal stabilizer for PMMA. Fig. 5-4 shows the thermal gravimetric analysis of MWCNTs, PMMA and MWCNT/PMMA composites. We can find that there is no weight loss for the MWCNTs till 700 ^{o}C. The PMMA decomposed completely from about 200 ^{o}C to 400 ^{o}C.

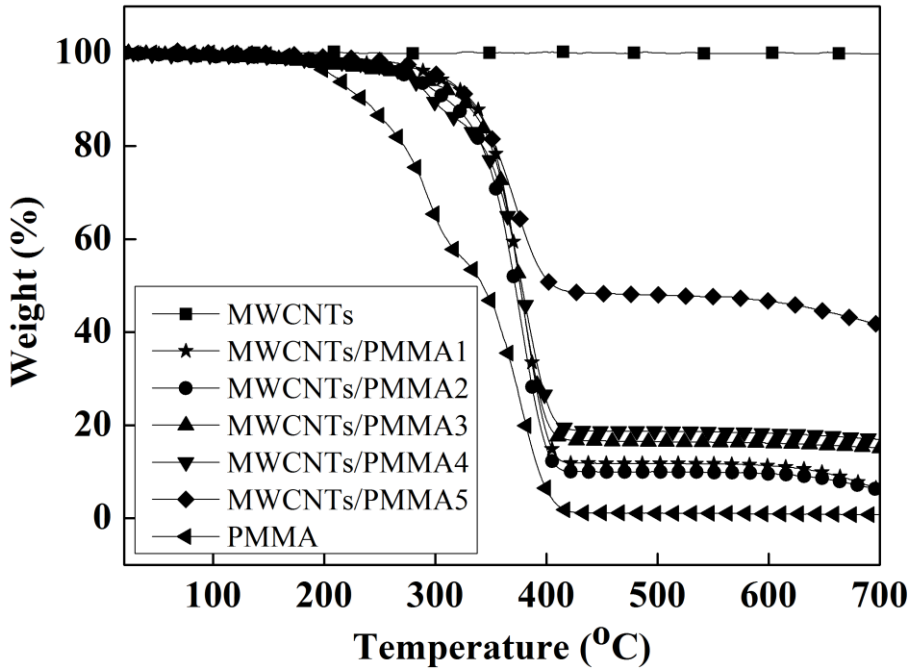

Fig. 5-4 TGA curves of MWCNTs, PMMA and MWCNT/PMMA composites

However, for the MWCNT/PMMA composites, the weight loss began from about 300 ^{o}C, which suggests that the MWCNTs can improve the thermal stability of PMMA by Pickering emulsion polymerization. It can be observed that the temperature of decomposition decreased as the MWCNTs was correspondingly increased. It could be attributed that the high monomer concentration resulted in high molecular weight and degree of polymerization. Furthermore, the weight loss increased with the MMA content

increasing, the complete weight loss of PMMA suggests the weight loss from 300 ^{o}C to 420 ^{o}C is the decomposition of PMMA.

5.3.4 Electronic properties of MWCNT/PMMA composites

The conductivities of the samples after Pickering emulsion polymerization were determined and listed in Table 5-1. The electrical resistivity changes are shown in Fig. 5-5. As it can be seen, the volume resistivity was ranging from 0.068 Ω·cm to 3.2×10^{2} Ω·cm as the amounts of methyl methacrylate monomer increased from 2 ml to 10 ml, lead open the possibility for practical applications of the composite either as a conductive material or directly to the sensor design. However, in the present work the composite microstructure was similar to Pickering emulsions phenomenon, which indicated that increased conductivity of the composite compared to neat PMMA was caused by percolation (direct contact of MWCNTs) since the conductive material is located at the surface of the particles of PMMA. The similar discovers have been reported by others [33]. The changing curve of electrical resistivity with the MMA content shows that the electrical resistivity of composites decreased slowly. It suggests that the ratio of MWCNTs and MMA can be changed from 1/8 to 1/4 for different purposes.

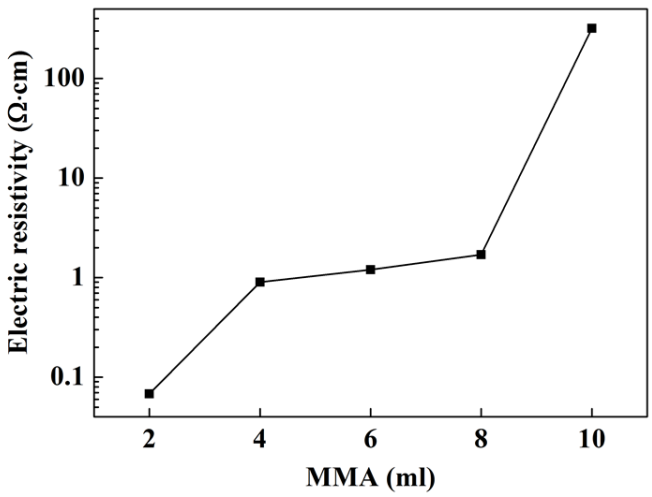

Fig. 5-5 The electrical resistivity of MWCNT/PMMA composites

5.3.5 Morphology of MWCNT/PMMA composites

Fig. 5-6 shows SEM images of PMMA and MWCNT/PMMA composites obtained by Pickering emulsion polymerization. It is clearly the polymer particles were sphere with the sizes of variety distribution, ranging from 100 nm to 500 nm which referred the MWCNTs was a successful stabilizer. The PMMA spheres reduce as the amount of MMA monomer decrease. The PMMA sphere gradually reduced owing to the monomer concentration decrease. Even though there was only number of spheres can be observed when the ratio of MWCNTs and MMA was 5 g and 1 ml. It is obviously seen that the spherical PMMA were embedded in MWCNTs with the low content of MMA as given in Fig. 5-6 (a). However, with the content of MMA increased, the MWCNTs gradually cannot be seen and it cannot be seen absolutely when the content of MMA is 10 mL as shown in Fig. 5-6 (e). PMMA prepared without the MWCNTs under the same condition of sample 2 is shown in Fig. 5-6 (f). It shows uniform microspheres with the average diameter about 1 μm.

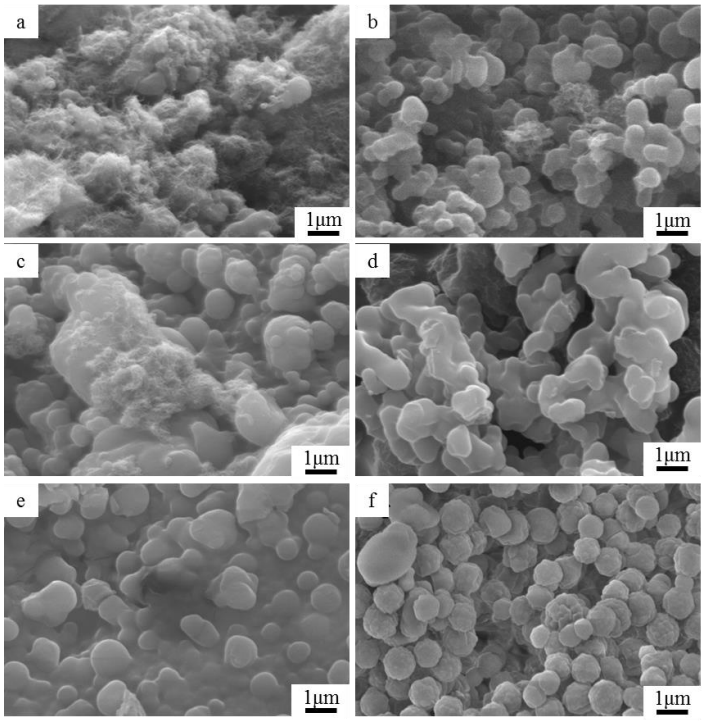

Fig. 5-6 SEM images of MWCNT/PMMA composites (a-e) and PMMA (f)

5.3.6 Microstructure images of MWCNT/PMMA composites

Transmission electron microscopy (TEM) is usually used to investigate the internal structure of materials in micron or nanoscale size. In the present work, all the samples were dispersed in ethanol in ultrasonic bath for 30 min, and then deposited on a copper grid covered with a perforated carbon film. Fig. 5-7 shows the TEM images of MWCNT/PMMA composites which were prepared with the MMA content changed and PMMA which were prepared in the same conditions of MWCNT/PMMA2 without the MWCNTs. It can be seen that the PMMA dispersed as microspheres with the diameter is about 500 nm (Fig. 5-7 (f)), which are smaller than the spheres from SEM images. Because a small amount of PMMA can dissolve in ethanol. MWCNTs as stabilizer can stabilize the PMMA microspheres as shown in Fig. 5-7 (a, b, c, d, e). When the content of MMA was small, the PMMA spheres were embedded in the net of MWCNTs (Fig. 5-7 (a, b, c)). With the increasing of MMA amount, the PMMA is out of MWCNTs (Fig. 5-7 (d, e)). It is because when the amount of MMA increased, the extra parts of PMMA will wrap the MWCNTs with the PMMA sphere inside. In addition, the MWCNTs were cut into short nanotubes during the preparing progress, especially in Fig. 5-7 (e).

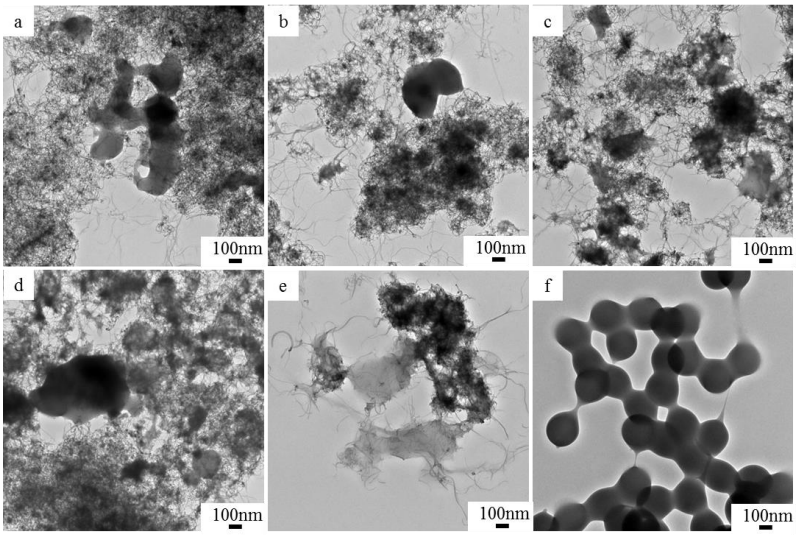

Fig. 5-7 Microstructure images of MWCNT/PMMA composites ((a), MWCNT/PMMA1, (b), MWCNT/PMMA2, (c), MWCNT/PMMA3, (d), MWCNT/PMMA4, (e), MWCNT/PMMA5) and PMMA (f)

5.3.7 Mechanical properties of PLA based conductive composites

Two series of PLA based conductive composites with MWCNT/PMMA were prepared by twin-screw extruding and injection molding. For one, the percentage content of MWCNTs was determined to be 1 wt% by adding a certain content of MWCNT/PMMA sample 1 to 5. Tensile strength and fracture strain was tested and shown in Fig. 5-8. It is obvious that both tensile strength and fracture strain of PLA based MWCNT/PMMA composites are lower than MWCNT/PLA composites and decreased with the MMA content as 4 mL. It may be attributed that the MWCNTs were damaged and cut off during the process of MWCNT/PMMA preparing. The MWCNTs become shorter when the content of MMA increasing. Furthermore, as shown in Fig. 5-10, the MWCNTs were coated onto the surface of the PMMA microspheres, which led to the poor intersolubility between PLA and PMMA. The same variation trend has been studied in the TEM images of Fig. 5-7. Especially for MWCNT/PMMA2 (Fig. 5-10 (b)), the MWCNTs coated PMMA microspheres were stripped from PLA and the interface gap can be seen clearly, which is the point for the decrease of the mechanical properties.

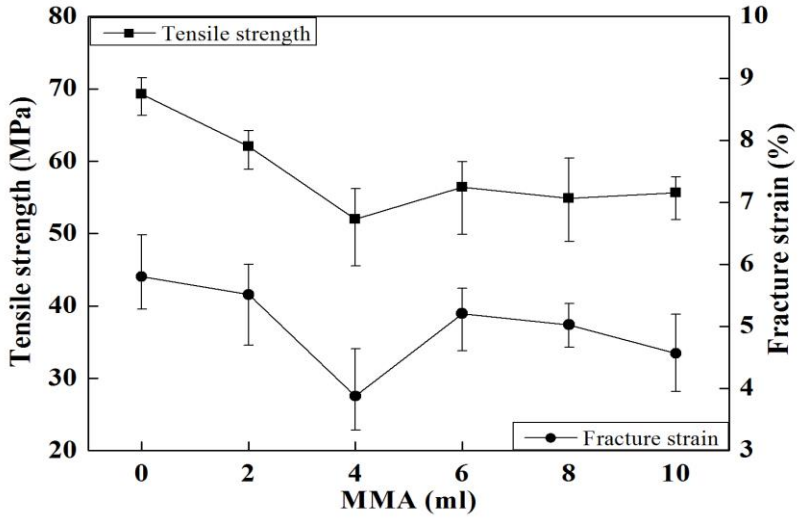

Fig. 5-8 Tensile strength and fracture strain of PLA based MWCNT/PMMA composites with different additions of MMA

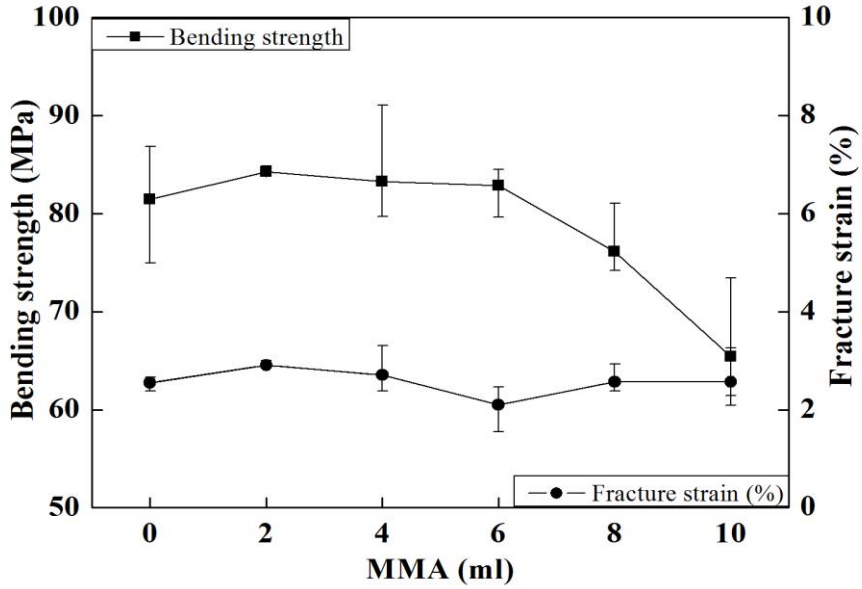

Fig. 5-9 Bending strength and fracture strain of PLA based MWCNT/PMMA composites with different additions of MMA

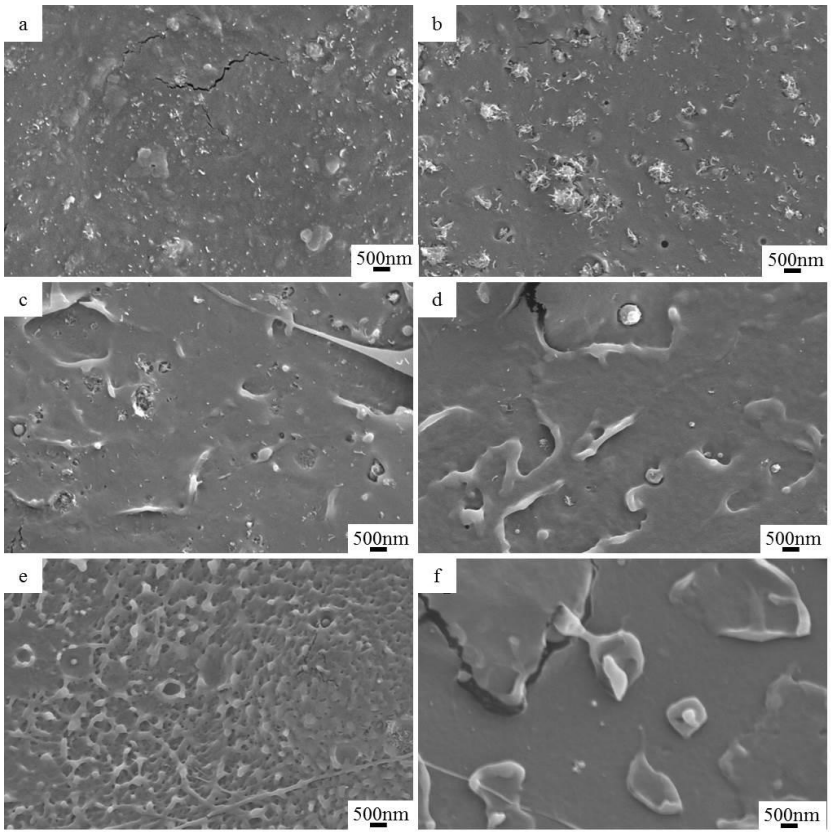

Fig. 5-10 SEM images of MWCNT/PMMA and PLA based MWCNT/PMMA

Bending strength and fracture strain of MWCNT/PMMA composites and PLA based composites were also tested and shown in Fig. 5-9. Bending strength changed a little with the increasing MMA content before 6 mL, and then changed a little. It suggests that the structure damage of MWCNTs decreased the mechanical properties greatly as described above.

For the other one, considering the high MMA content and electrical conductivity and well compatibility with PLA, the percentage content of MWCNT/PMMA4 was confirmed to be 10 wt%, 20 wt%, 30 wt%, 40 wt% and 50 wt%. The comparison was the PLA/PMMA composite with their ratio of 1/1, and the PMMA was prepared under the same condition with MWCNT/PMMA4. Fig. 5-11 and Fig. 5-12 present the tensile and bending tests for the PLA based composites. It is clear that the tensile strength, bending strength and fracture strain decreased just a little with the increase of MWCNT/PMMA content.

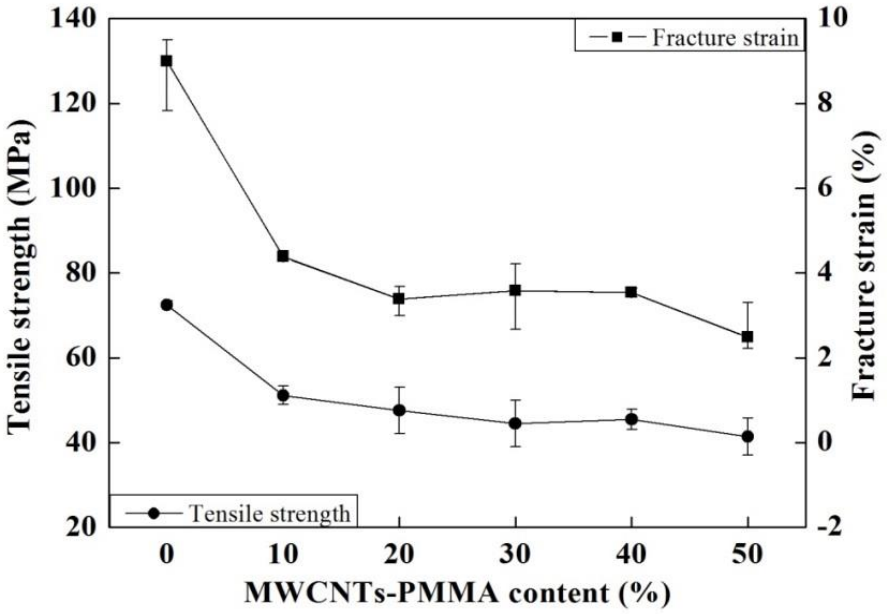

Fig. 5-11 Tensile strength and fracture strain of PLA based MWCNT/PMMA composites with different additions of MWCNT/PMMA4

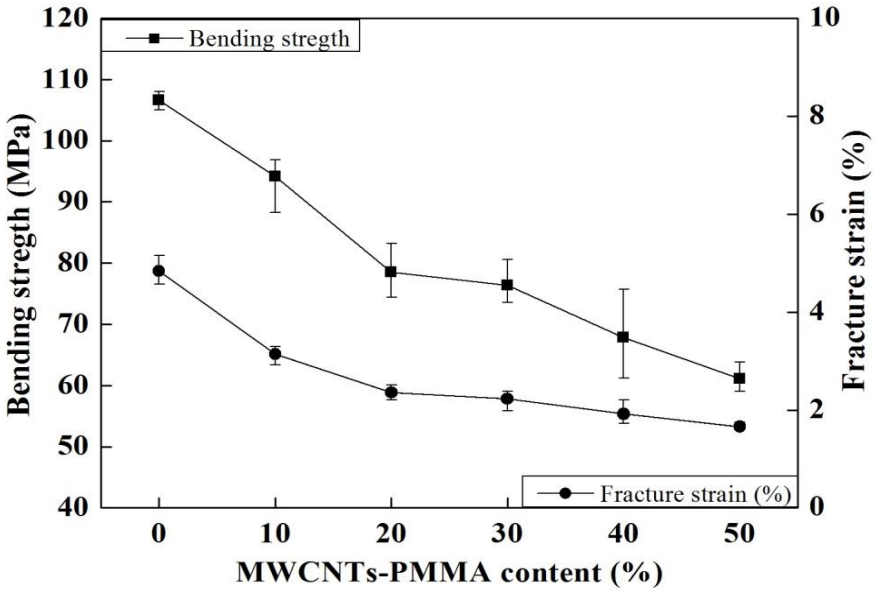

Fig. 5-12 Bending strength and fracture strain of PLA based MWCNT/PMMA composites with different additions of MWCNT/PMMA4

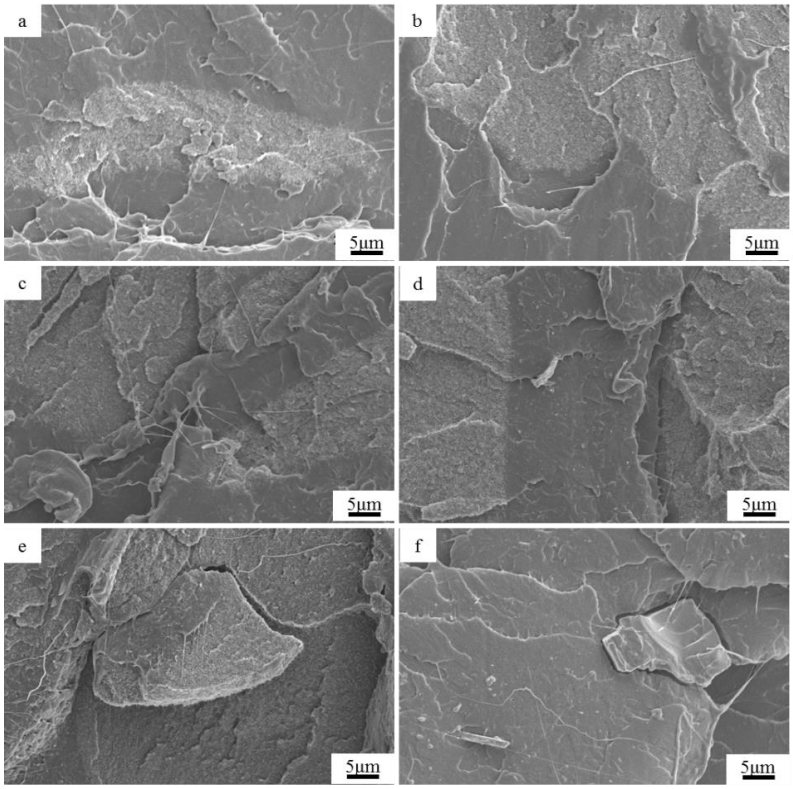

Fig. 5-13 SEM images of PLA based MWCNT/PMMA composites with different additions of MWCNT/PMMA4 ((a), 10 wt%, (b), 20 wt%, (c), 30 wt%, (d), 40 wt%, (e), 50 wt%) and PLA/PMMA ((f), PLA/PMMA=1/1)

Fig. 5-13 demonstrates the morphology images of PLA based MWCNT/PMMA composites with different additions of MWCNT/PMMA4 and PLA/PMMA. The section of PLA and MWCNT/PMMA composites can be seen easily, while there is no interface gap between them. It is the main reason for the small changes of mechanical properties of PLA based composites.

5.4 Conclusions

The MWCNT/PMMA composites were prepared by Pickering emulsion polymerization of methyl methacrylate monomer using the multi-walled carbon nanotubes (MWCNTs) as a surfactant. The morphology of obtained composites was investigated by SEM. It suggested the MWCNTs were successful stabilizer and the resulted size of the composites were heterogeneous, ranging from 100 nm to 500 nm. The structure of composites was also confirmed by the FT-IR spectrum. Moreover, MWCNT/PMMA composites exhibited good electrical conductivities and could be applied as conductive materials. The TGA results illustrated the thermal stability of MWCNT/PMMA composites was decreased as the concentration of monomer reduced.

Furthermore, two series PLA based conductive composites were prepared by the mixture of MWCNT/PMMA and PLA plates with twin-screw extruding and injection molding process. For one, the MWCNTs content was confirmed as 1.022 wt%. For another, the percentage content in PLA based conductive composites of MWCNT/PMMA4 was confirmed to be 10 wt%, 20 wt%, 30 wt%, 40 wt% and 50 wt%. The mechanical properties decreased with MMA content increasing, which suggested the structure damage of MWCNTs during the Pickering emulsion polymerization.

References

[1] B.P. Binks, Particles as Surfactants-Similarities and Differences, Current Opinion in Colloid & Interface Science, 7 (2002) 21-41.

[2] M. Klapper, S. Nenov, R. Haschick, K. Muller, K. Mullen, Oil-in-Oil Emulsions: A Unique Tool for the Formation of Polymer Nanoparticles, Accounts of Chemical Research, 41 (2008) 1190-1201.

[3] R. Aveyard, B.P. Binks, J.H. Clint, Emulsions Stabilised Solely by Colloidal Particles, Advances in Colloid and Interface Science, 100-102 (2003) 503-546.

[4] X.Y. Liu, C.L. Yi, Y. Zhu, Y.Q. Yang, J.Q. Jiang, Z.G. Cui, M. Jiang, Pickering Emulsions Stabilized by Self-Assembled Colloidal Particles of Copolymers of P(St-Alt-Man)-Co-P(VM-Alt-Man), Journal of Colloid and Interface Science, 351 (2010) 315-322.

[5] M. Klapper, S. Nenov, R. Haschick, K. MÜLler, K. MÜLlen, Oil-In-Oil Emulsions: a Unique Tool for the Formation of Polymer Nanoparticles, Accounts of Chemical Research, 41 (9) (2008) 1190-1201.

[6] D.E. Tambe, M.M. Sharma, Factors Controlling the Stability of Colloid- Stabilized Emulsions, Journal of Colloid and Interface Science, 157 (1993) 244-253.

[7] J.A. Balmer, A. Schmid, S.P. Armes, Colloidal Nanocomposite Particles: *Quo Vadis*? Journal of Materials Chemistry, 18 (2008) 5722-5730.

[8] S. Sacanna, A.P. Philipse, A Generic Single Step Synthesis of Monodisperse Core/Shell Colloids Based on Spontaneous Pickering Emulsification, Advanced Materials, 19 (2007) 3824-3826.

[9] J. Chen, C. Cheng, W. Chiu, C. Lee, N. Liang, Synthesis of Zno/Polystyrene Composites Particles by Pickering Emulsion Polymerizatio, European Polymer Journal, 44 (2008) 3271-3279.

[10] S.B. Sinnott, R. Andrews, Carbon Nanotubes: Synthesis, Properties, and Applications, Critical Reviews in Solid State and Materials Sciences, 26 (2001)

145-249.

[11] M. Terrones, Science and Technology of the Twenty-First Century: Synthesis, Properties, And Applications of Carbon Nanotubes, Annual Review of Materials Research, 33 (2003) 419-501.

[12] D. Tasis, N. Tagmatarchis, A. Bianco, M. Prato, Chemistry of Carbon Nanotubes. Chemical Reviews, 106 (2006) 1105-1136.

[13] Y.P. Sun, K. Fu, Y. Lin, W. Huang, Functionalized Carbon Nanotubes: Properties and Applications, Accounts of Chemical Research, 35 (2002) 1096-1104.

[14] P. Liu, Modifications of Carbon Nanotubes with Polymers, European Polymer Journal, 41 (2005) 2693-2703.

[15] M. Raja, A.M. Shanmugharaj, S.H. Ryu, Influence of Surface Functionalized Carbon Nanotube on the Properties of Polyurethane Nanocomposites, Soft Matter, 6 (2008) 65-74.

[16] F. Liang, J. Beach, K. Kobashi, A. Sadana, Y. Vega-Cantu, J. Tour, W.E. Billups, In Situ Polymerization Initiated by Single-Walled Carbon Nanotube Salts, Chemistry of Materials, 18 (2006) 4764-4767.

[17] H.X. Wu, X.Q. Qiu, R.F. Cai, S.X. Qian, Poly (N-Vinyl Carbazole)-Grafted Multiwalled Carbon Nanotubes: Synthesis via Direct Free Radical Reaction and Optical Limiting Properties, Applied Surface Science, 253 (2007) 5122-5128.

[18] J. Ge, D. Zhang, Q. Li, H.Q. Hou, M. Graham, L.M. Dai, F. Harris, S. Cheng, Multiwalled Carbon Nanotubes with Chemically Grafted Polyetherimides, Journal of the American Chemical Society, 127 (2005) 9984-9985.

[19] G. Mountrichas, S. Pispas, N. Tagmatarchis, Grafting-to Approach for the Functionalization of Carbon Nanotubes with Polystyrene, Materials Science and Engineering: B, 152 (2008) 40-43.

[20] P. Liu, Facile Graft Polystyrene onto Multi-Walled Carbon Nanotubes via in Situ Thermo-Induced Radical Polymerization, Journal of Nanoparticle Research, 11 (2009) 1011-1016.

[21] X.L. Wu, P. Liu, Polymer Grafted Multi-walled Carbon Nanotubes via Facile in situ Solution Radical Polymerization, Journal of Experimental Nanoscience, 5 (2010) 383-389.

[22] Y.M. Ying, R. Saini, F. Liang, A. Sadana, W. E. Billups, Functionalization of Carbon Nanotubes by Free Radicals, Organic Letters, 5 (2003) 1471-1473.

[23] D. Baskaran, J.R. Dunlap, J.W. Mays, M.S. Bratcher, Grafting Efficiency of Hydroxy-Terminated Poly (Methyl Methacrylate) with Multiwalled Carbon Nanotubes, Macromol, Rapid Commun, 26 (2005) 481-486.

[24] G. Mountrichas, S. Pispa, N. Tagmatarchis, Grafting-to Approach for the Functionalization of Carbon Nanotubes with Polystyrene, Materials Science and Engineering: B, 152 (2005) 40-43.

[25] H.M. Li, F.O. Cheng, A.M. Duft, A. Adronov, Functionalization of Single-Walled Carbon Nanotubes with Well-Defined Polystyrene by ‘‘Click’’ Coupling, Journal of the American Chemical Society, 127 (2005) 14518-14524.

[26] Z. Yao, N. Braidy, G.A. Botton, A. Adronov, Polymerization from the Surface of Single-Walled Carbon Nanotubes - Preparation and Characterization of Nanocomposites, Journal of the American Chemical Society, 125 (2003) 16015-16024.

[27] S. Qin, D. Qin, W.T. Ford, D.E. Resasco, J.E. Herrera, Polymer Brushes on Single-Walled Carbon Nanotubes by Atom Transfer Radical Polymerization of N-Butyl Methacrylate, Journal of the American Chemical Society, 126 (2004) 170-176.

[28] J.H. Chang, B.G. Kim, H.-K. Kim, I.S. Choi, H. Paik, Covalent Attachment of Polystyrene on Multi-Walled Carbon Nanotubes via Nitroxide Mediated Polymerization, Composite Interfaces, 14 (2007) 5-6.

[29] Z.J. Jia, Z.Y. Wang, C.L. Xu, J. Liang, B.G. Wei, D.H. Wu, S.W. Zhu, Study on Poly (Methyl Methacrylate):Carbon Nanotube Composites, Materials Science and Engineering A, 271 (1999) 395-400.

[30] S.M. Shang, L. Li, X.M. Yang, Y.Y. Wei, Polymethylmethacrylate-Carbon Nanotubes Composites Prepared by Microemulsion Polymerization for Gas Sensor,

Composites Science and Technology, 69 (2009) 1156-1159.

[31] C.H. Wu, W.Y. Chiu, T.M. Don, Conductive Composite Particles Synthesized via Pickering Emulsion Polymerization Using Conductive Latex of Poly (3,4-Ethylenedioxythiophene) (PEDOT) as Stabilizer. Polymer, 53 (2012) 1086-1092.

[32] M.M. Gudarzi, F. Sharif, Self Assembly of Graphene Oxide at the Liquid-Liquid Interface: a New Route to the Fabrication of Graphene Based Composites, Soft Matter, 7 (2011) 3432-3440.

[33] E.A.Z. Contreras, C.A.H. Escobar, A.N. Fontes, S.G. F. Gallardo, Synthesis of Carbon Black/Polystyrene Conductive Nanocomposite, Pickering Emulsion Effect Characterized by TEM, Micron, 42 (2011) 263-270.

Chapter 6 Preparation and Characterization of Polyamide Composites with Modified Graphite Powder

6.1 Introduction

The use of graphite powder GP as filler in order to enhance the electrical conductivity and mechanical properties of composites has been increased greatly [1, 2]. GP consist of several layers of honeycomb lattices of carbon atoms with sp2 hybridization which tightly bonded the atoms in hexagonal rings [3-5]. In GP, elemental carbon has the lowest energy state at ambient temperature and pressure [3]. It may be naturally occurred or synthetically produced. GP have been used in machinery, space navigation and the nuclear industry because of their self-lubrication property [6, 7]. Especially, GP have been widely applied for parts subject friction and wear products as reinforced filler [8-11]. Suresha et al. [12] reported that graphite can not only reduce the friction coefficient and wear rate, but also enhance the thermal conductivity and the mechanical properties of the polymer matrix. Kalaitzidou et al. [13] have demonstrated the use of exfoliated graphite platelets to enhance the thermal and mechanical properties of polymeric resins. GP also have highly electrical conductivity (with an electrical conductivity of 10^4 S/cm at ambient temperature), as a result, they have been used as electrical conductive enhancement material [14].

However, GP easily aggregate and have a poor dispersibility in the polymer matrix due to the strong Van der Waals attraction [15]. Most recent research studies focused on the functionalization of GP to increase their affinity with polymers and allow wider applications [16-21]. Ganguli et al. [22] have chemically treated the graphite flakes to make their well compatibility with the epoxy system and they studied the thermal, electrical and flow properties of the resultant composites. GP have been modified with polystyrene via in situ solution radical polymerization in ionic liquid in our previous

work [23]. Because of polyamide (PA) has been widely used as engineering tribo-polymers due to their good combination of properties, such as superior thermal, mechanical and tribological properties [24-27]. Furthermore they can be easily molded and are low cost [28]. And there are many studies on graphite-filled PA to form composites. Graphite-based PA composites have potential applications in electrochemical displays, sensors, and as anti-static and corrosion-resistance coatings [29-31]. Uhl et al. [32] have used a variety of graphite-based polyamide 6 ((PA6)/graphite) composites prepared by melt blending. They found an enhancement of the thermal stability without any significant deterioration of the mechanical properties for PA6.

In chapter 3, 4 and 5, the carbon powders and nanotubes were modified with in situ radical polymerization and bulk polymerization, which belong to "grafting from" method. This method just applied to vinyl monomer like styrene and methyl methacrylate. In this chapter, the GP were first oxidized with hydrogen peroxide to generate a hydroxyl group. The GP with the hydroxyl group (GP-OH) can be well dispersed in water. Then these hydroxyl-functionalized GP were reacted with hexamethylene diisocryanate to introduce an amino group; this was designated as GP-NH_2. The GP-NH_2 has excellent affinity with PA6. The structure and morphological properties of the modified products were determined by testing them in several ways. GP-NH_2/PA composites were prepared via injection molding to discuss their mechanical properties. Comparisons of GP/PA, and GP-OH/PA composites prepared under the same conditions were made.

6.2 Experimental

6.2.1 Materials

GP (highly purified graphite powders, HOP) with a size of about 4 μm were dried at 100 ^{o}C for 2 d before use. Polyamide 6 (PA6, CM1017) was obtained from Toray

Industries Inc., Japan. Hydrogen peroxide aqueous solution (30%) was purchased from Santoku Chemical Industries Co., Ltd., Japan. Hexamethylene diisocryanate and toluene were purchased from Nakalai Tesque, Inc. in Japan, and were used without any other purification.

6.2.2 Instruments and measurements

Twin-screw extruder was used for prior mixing of GP and modified GP with PA6. The extruding temperatures were: C1, 210 ^{o}C; C2, 220 ^{o}C; C3 and C4, 230 ^{o}C. The injection molding machine was used to form the mixture plates into dumbbell (30 mm × 5 mm × 2 mm) and rectangular (60 mm × 10 mm × 4 mm) shape. The injection temperature was 230 ^{o}C, molding temperature was 80 ^{o}C, and the injection rate was 17.6 mm/s. Microstructure was observed in the specimens with a polarized optical microscope (Eclipse ME600D, Nikon, Japan). Elemental analysis was done by putting about 2 mg samples, wrapped in foil into an element analyzer (2400 Series Ⅱ CHNS/O Analyzer, Perkin-Elmer Corp., USA). X-ray photoelectron spectroscopy (Perkin-Elmer Corp., USA) measurements were done by sticking a sample on an electrically conductive adhesive.

6.2.3 Modification of GP and preparation of composites

First, modification of GP was carried out; 10 g GP was mixed with 120 mL 10 wt% H_2O_2 in a three-neck 250 mL round-bottom flask equipped with a condenser and a mechanical stirrer. The flask was placed in a heated oil bath and kept at 100 ^{o}C with stirring for 3 h. The product was washed with deionized water several times and dried in vacuum oven at 50 ^{o}C for 24 h to get GP-OH.

Next, composites were prepared; 5 g GP-OH was suspended in 40 mL toluene, then 5 mL hexamethylene diisocryanate was dropped into the toluene suspension. This mixture was stirred at room temperature for 24 h. The obtained product was washed with toluene and dried in vacuum for 24 h to get GP-NH_2. The modification process is

summarized as scheme 6-1.

Finally, GP, GP-OH and GP-NH_2 were mixed and twin-screw extruded with PA in different contents, respectively, before being formed into the desirable shapes by the injection molding process.

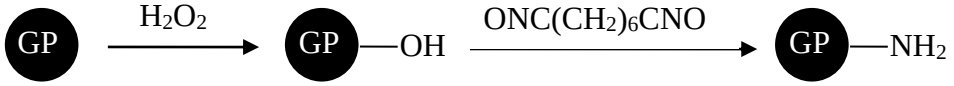

Scheme 6-1 The modification process of GP

6.3 Results and discussion

6.3.1 Elemental analysis of GP before and after modification

Table 6-1 lists the elemental analysis results of GP, GP-OH and GP-NH_2 samples. After was modified with hydrogen peroxide, the content of carbon (C) decreases and the content of hydrogen (H) increases. With the further modification using hexamethylene diisocryanate, the content of C was decreased more and the contents of H and nitrogen (N) were increased. These changes indicate that the GP are successfully modified by the proposed chemical method.

Table 6-1 Elemental analysis results of GP, GP-OH and GP-NH_2 samples

Samples	C(%)	H(%)	N(%)
GPs	99.545	0.010	0.060
GPs-OH	98.830	0.100	0.040
GPs-NH_2	89.865	1.505	3.925

6.3.2 XPS analysis of unmodified and modified GP

The XPS curves of GP, GP-OH and GP-NH_2 samples are shown in Fig. 6-1. In the curve of GP, only the C1s peak is clearly seen at 284.5 eV, along with a slight O1s at 531.0 eV. After the GP were oxidized with H_2O_2, the O1s peak becomes stronger. However, for the GP-NH_2, the peaks of both O and N increase compared to GP and GP-OH. This is because after the GP-OH was modified with hexamethylene diisocryanate, the -OH of the GP-OH reacted with -CNO to form -O-CO-NH-.

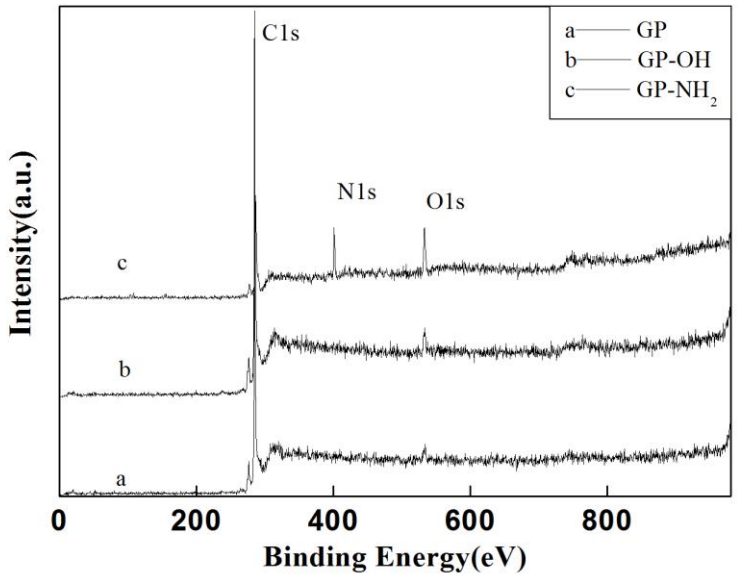

Fig. 6-1 XPS curves of GP, GP-OH and GP-NH_2 samples

6.3.3 TGA curves of unmodified and modified GP

TGA can detect the stability of the GP before and after modification. Fig. 6-2 shows the TGA curves of GP, GP-OH and GP-NH_2 samples. The GP have hardly any weight loss until 800 ^oC, which indicates that they have high thermal stability [31, 32]. The weight loss of GP-OH that begins from about 600 ^oC may be attributed to breaking of the stable π=π double bonds of GP to form C-C single bond. However, there is a big weight loss for GP-NH_2 from about 260 ^oC to 340 ^oC. That is because the -OH functional groups was successfully removed by the modifying process.

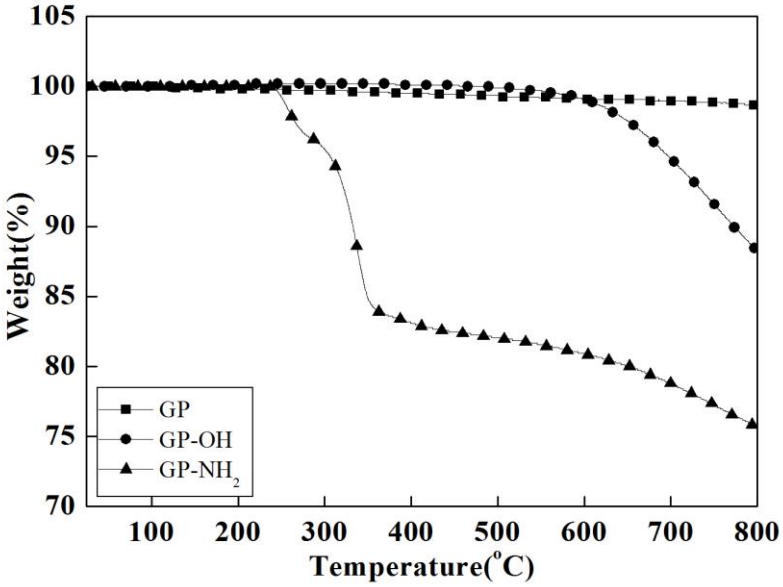

Fig. 6-2 TGA curves of GP, GP-OH and GP-NH_2 samples

6.3.4 Electrical properties of unmodified and modified GP

The electrical resistivity was measured with four-probe device and the conductivity was calculated and shown in Fig. 6-3. It is obviously to see that the electrical conductivity is decreased from the 1.1×10^2 S/cm for GP to 90.9 for GP-OH and 2.6 for GP-NH_2 respectively. It is due to the internal structure of GP was damaged during the modified progress, in which parts of π=π double bonds of GP have been changed to C-C single bond. Moreover, the GP relative amount decreased because the grafted of hexamethylene diisocryanate. The result shows the efficient modification has been successfully conducted. Because the GP were used in this work is HOP with the size of about 4 μm, which is used to improve the fraction and mechanical of the composites. So the electric conductivity of composites is just about 10^{-10} S/cm, has a good effect on preventing static electricity because of the friction.

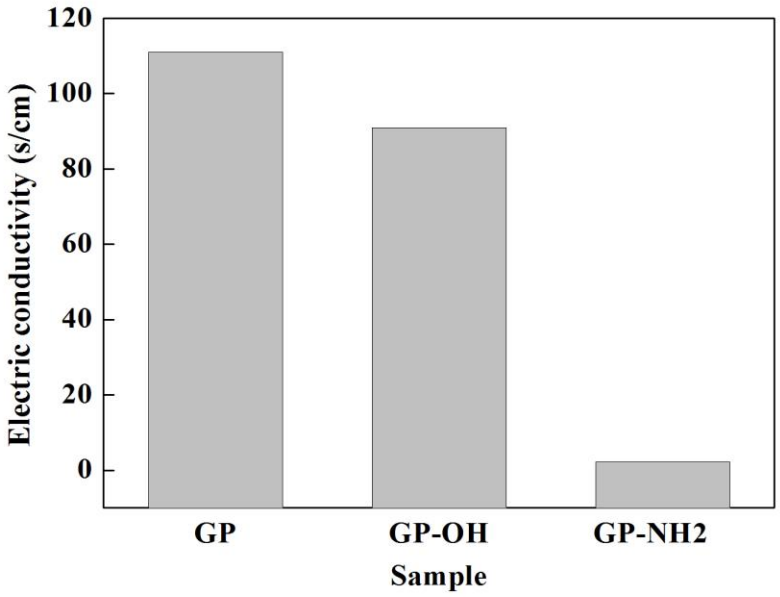

Fig. 6-3 Electrical conductivity of GP, GP-OH and GP-NH_2 samples

6.3.5 Mechanical properties

Fig. 6-4 shows the effect of filler content on the tensile strength of composites. The tensile strength of the GP/PA composites increases first and then decreases with the increasing content of GP; the maximum tensile strength is 78.735 MPa when the GP content is 3 wt%. This behavior is attributed to the high strength of GP and the poor affinity between GP and PA that led to brittle failure of composite, as seen in SEM images when the GP content increased. For the GP-OH/PA composite, the tensile strength increases greatly to 77.06 MPa when the GP-OH content is 1 wt%, but tensile strength is its minimum value when the GP-OH content is 3 wt%. However, the tensile strength of GP-NH_2/PA composite is generally lower than the tensile strength values of GP/PA and GP-OH/PA composites. GP-NH_2/PA composites has an obvious maximum of 71.44 MPa when the GP-NH_2 content is 1 wt% and a minimum of 63.93 MPa with the GP-NH_2 content is 3 wt%, which is even less than the tensile strength of PA6 (64.78 MPa). This phenomenon can be explained by the SEM obsercations of the microstructure, which indicate the larger GP-NH_2 content hinders the plastic

deformation of PA6.

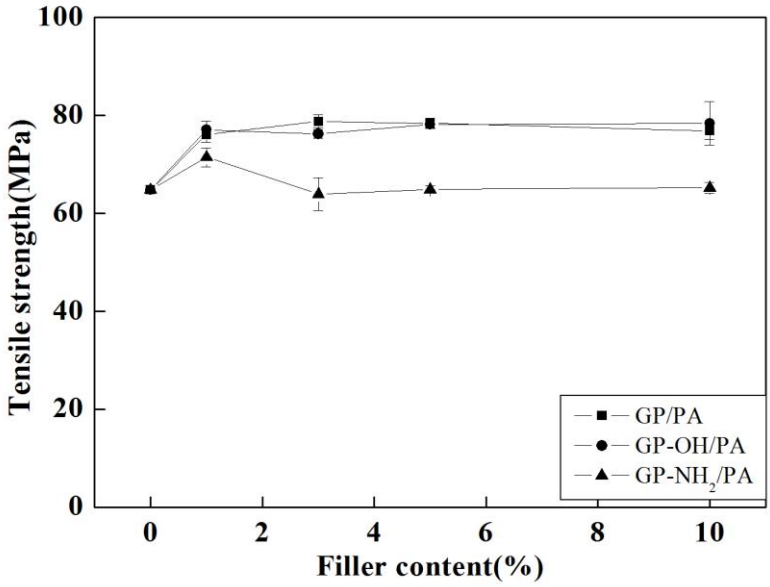

Fig. 6-4 The effect of filler content on tensile strength of composites

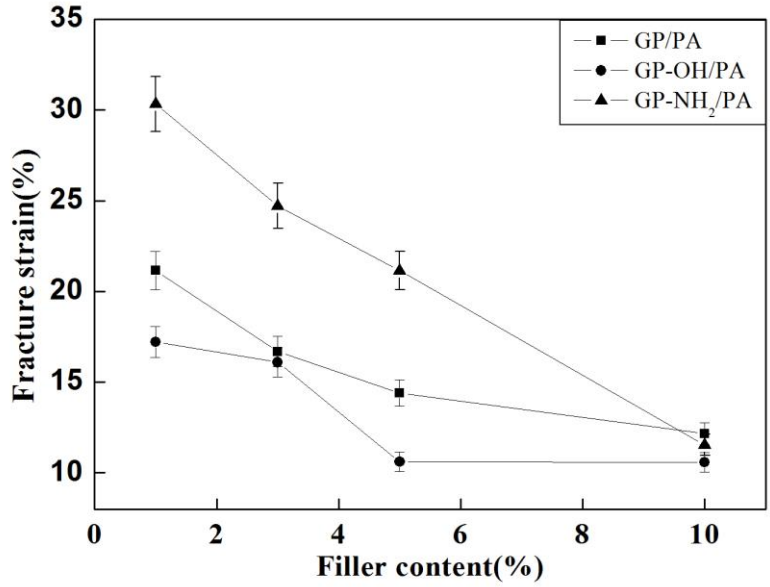

Fig. 6-5 The effect of filler content on fracture strain of composites

The tensile strength changes can also be explained by the curves of strain to failure (Fig. 6-5) and Young's modulus (Fig. 6-6). The strain to failure of all the composites

decreases with the increasing filler content. The GP-NH_2/PA composite has better extensibility compare to GP/PA and GP-OH/PA composites. This suggests that GP-NH_2 has good affinity with PA6, which proved the successful modification of GP. But the GP-OH/PA composite has brittle properties, the same as GP/PA composite. This suggests that GP-NH_2 has good affinity with PA, which proves the successful modification of GP.

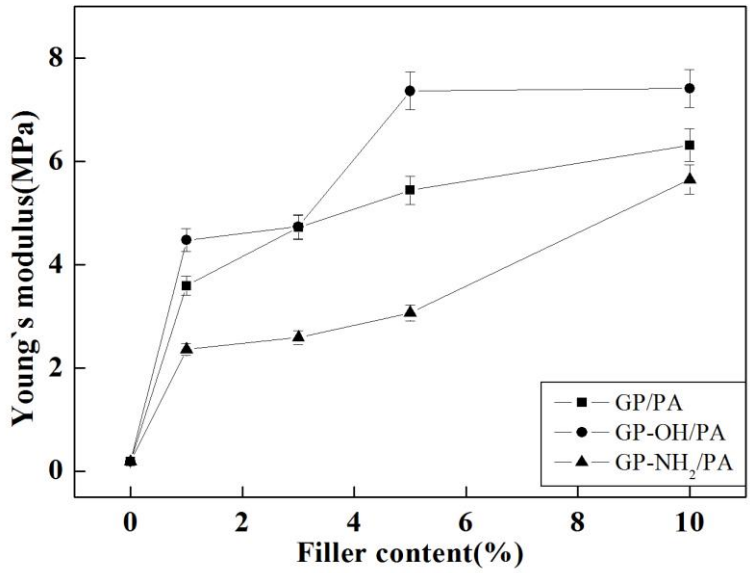

Fig. 6-6 The effect of filler content on Young's modulus of composites

Fig. 6-7 shows the dynamic mechanical analysis (DMA) curves of composites with the filler content is 5 wt%. It can be found that the storage modulus decreased first and then nearly stable over 60 ºC. Furthermore, the storage modulus of the composites is higher than the PA6 and consistent with the Young's modulus in Fig. 6-6, which suggests the GP improved the thermal stability of composites. But the loss tangent was affect a little.

Fig. 6-8 shows the changes of bending strength for the three kinds of composites. The bending strength of GP/PA increases with the increasing content of GP until 5 wt%. The bending strength of GP-OH/PA increases greatly for the GP-OH content 1 wt%, and

then increases slowly. But the bending strength of GP-NH_2/PA composite has a minimum when the GP-NH_2 content is 3 wt%, which is consistent with the changes of tensile strength.

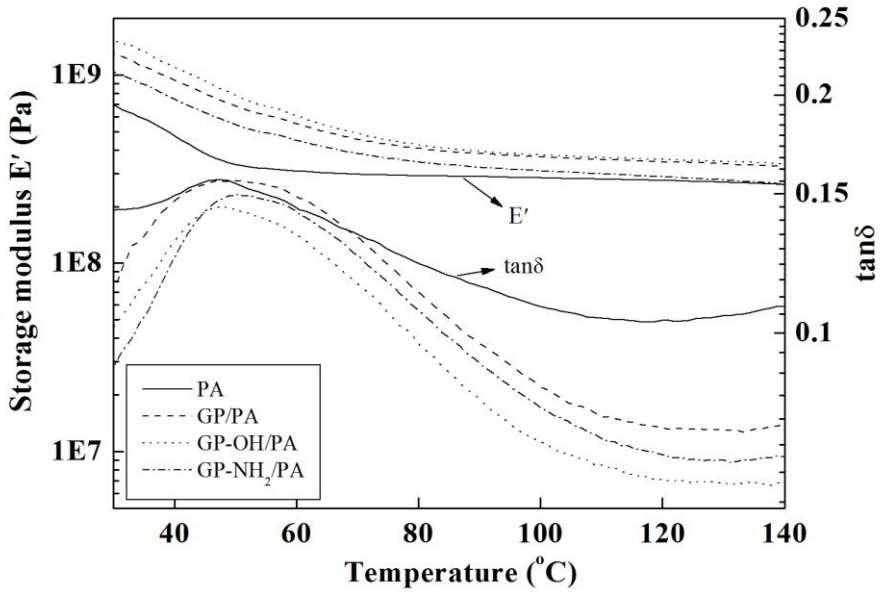

Fig. 6-7 DMA curves of composites with the filler content is 5 wt%

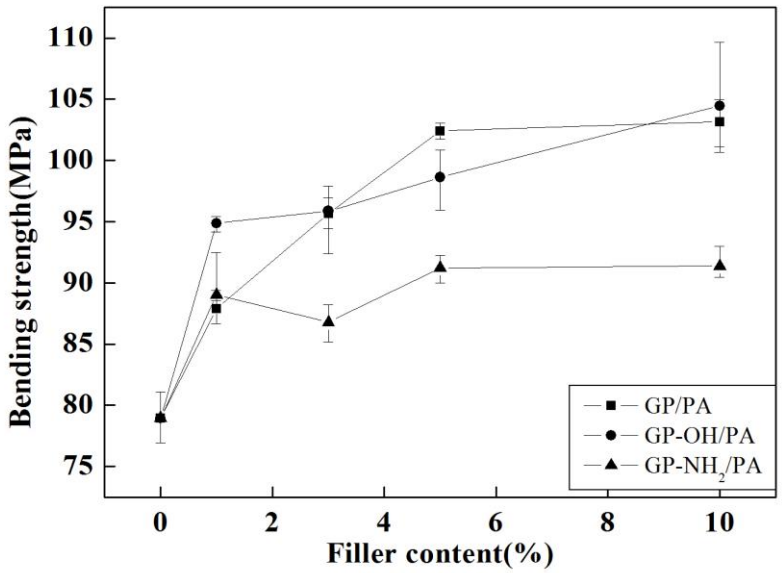

Fig. 6-8 The effect of filler content on bending strength of composites

6.3.6 Optical microscope and morphology observations of fracture surface

Fig. 6-9 shows the optical microscope images and tensile fracture surface SEM images of the GP/PA and GP-NH_2/PA composites (filler content 10 wt%). Because optical microscope and SEM images of GP-OH/PA and GP/PA composites are similar, the GP-OH/PA composites images are not showed. There are no obvious bulk aggregates of GP and GP-NH_2 in GP/PA and GP-NH_2/PA composites (Fig. 6-9 (a) and (b)), which shows good dispersion of fillers in PA6 because the twin-screw extrusion process before the injection molding process improves the dispersibility of filler in PA. Therefore, the mechanical properties of tensile strength, Young's modulus and bending strength of all the composites increase. Fig. 6-9 (c) shows a smooth surface after tensile failure, which is typical for brittle fracture. But the fracture surface of GP-NH_2/PA composite as shown in Fig. 6-9 (d) has a stretched fibrous resin which indicates ductile fracture.

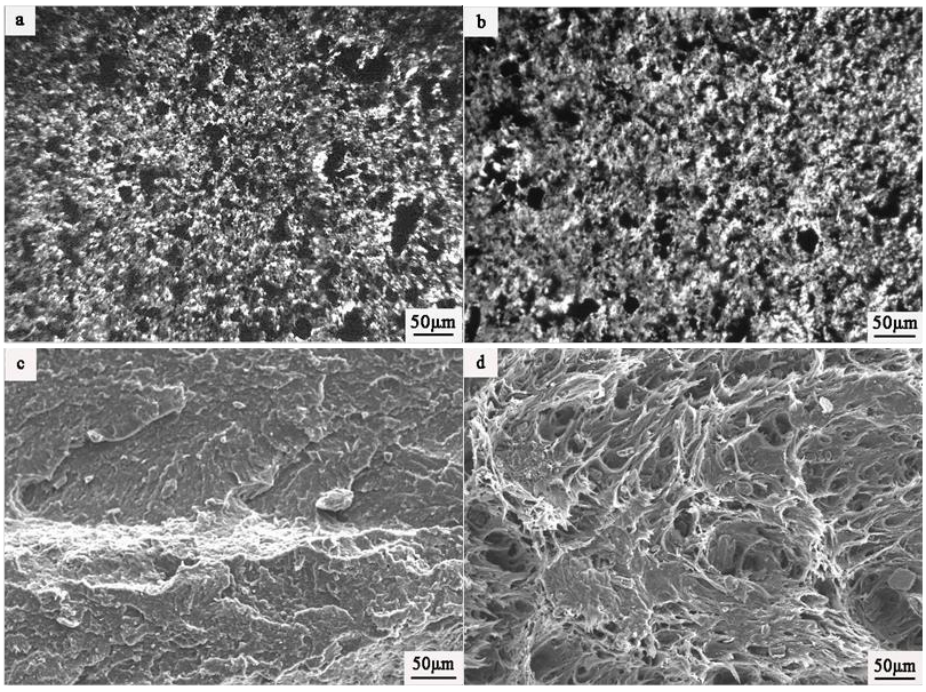

Fig. 6-9 The optical microscope images for GP/PA (a) and GP-NH_2/PA (b) composites and tensile fracture surface SEM images for GP/PA (c) and GP-NH_2/PA (d) composites; GP filler content was 10 wt% in all 4 composites

On the other hand, from the fracture surface shown in Fig. 6-10 (a), the interface of GP and PA can be clearly observed, and lots of PA6 molecules are just sticking onto the surface of GP (Fig. 6-10 (b)) because of their poor chemical combination. With the increasing GP content, defects in the interface between GP and PA6 increase, which also increases the stress concentration around the defects. This phenomenon has less effect on the tensile strength of composites, but the fracture strain can be decreased greatly as shown in Fig. 6-5. Furthermore, as shown in Fig. 6-11 (a), the surface texture of GP has been changed a little after it was modified and the size of the GP aggregates is smaller, which leads to the decrease of the tensile and bending strength of GP-NH_2/PA. The jagged surface of the hole after the tensile failure (Fig. 6-11 (b)) shows some remaining GP aggregates which caused the failure. This suggests the good affinity of GP-NH_2 and PA6 leads to the stronger fracture strain of GP-NH_2/PA composite than the GP/PA and GP-OH/PA composites.

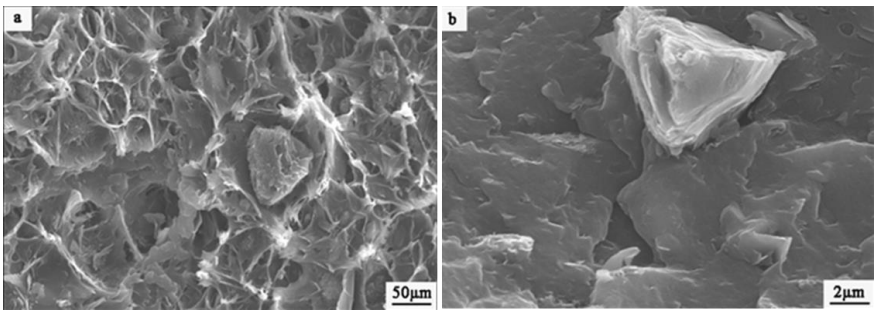

Fig. 6-10 The tensile fracture surface (a) and liquid nitrogen quenched surface (b) of GP/PA (GP filler content 10 wt%) composites

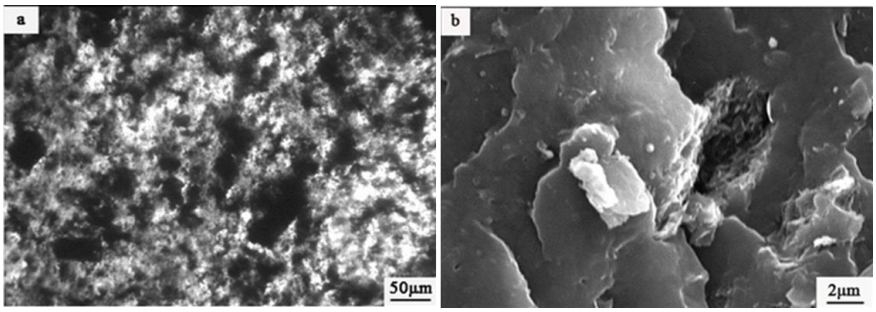

Fig. 6-11 The optical microscope image (a) and liquid nitrogen quenched surface (b) of GP-NH_2/PA (GP filler content 10 wt%) composites

6.3.7 XRD patterns

PA6 is known to crystallize predominantly in α- and γ- phases, depending on the polymer processing conditions and the presence of nucleating agents [33]. Crystallites of α- phase are comprised of folded chains whereas those of the γ- phase contain unfolded chains [34, 35]. Particularly, α- crystalline phase is known to be thermodynamically more stable, whereas the γ- crystalline phase is kinetically favored [36]. PA6 contains two sharp peaks, the peak at 2θ=26^o is the (200) crystallinity and that at 44^o is the (002) crystallinity planes as shown in Fig. 6-12 (b, c, d), indicating a somewhat strictly ordered arrangement of the molecules with a partly crystalline structure [37].

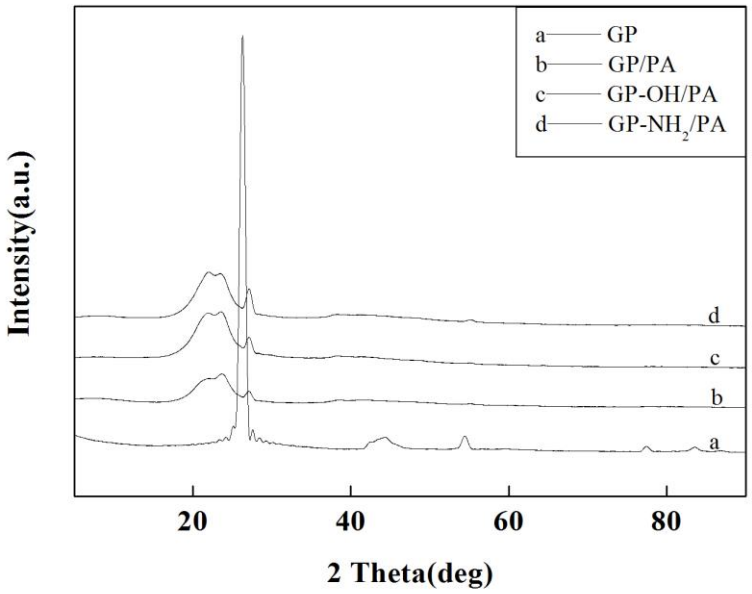

Fig. 6-12 X-ray diffraction patterns of GP sample (a), GP/PA (b), GP-OH/PA (c) and GP-NH_2/PA (d) composites

As shown in Fig. 6-12 (a), the GP pattern exhibits distinct peaks at 2θ=26^o, 44^o, 54^o and 77^o, which are respectively the (002), (100), (004) and (110) crystallinity planes [38]. For the composites, the diffraction peak at 27^o ((002) plane) corresponds to a wide d-spacing, larger than that of GP. This may be due to the attachment of PA microspheres

along the edges of the stacked GP which disrupts the Van der Waals interactions and therefore enlarges the d-spacing of the GP.

6.4 Conclusions

GP have been modified with hydrogen peroxide and hexamethylene diisocryanate to improve their affinity with PA6 matrix. Elemental analysis, XPS and TGA results all verified the successful modification of GP by the proposed chemical method. The electrical properties investigated that the structure of GP was damaged during the modification progress. The GP/PA, GP-OH/PA and GP-NH_2/PA composites were prepared by twin-screw extrusion and injection molding process. XRD patterns showed the crystallinity planes for the composites. The mechanical properties, especially the extensibility of GP-NH_2/PA were clearly improved after the modification because of the good affinity of between the modified GP and PA. Optical microscope images indicated the dispersion of unmodified and modified GP in PA6. SEM images of composites were obtained showing the interface morphology of cross sections after liquid nitrogen quenching and tensile fracture.

References

[1] P.J. Mather, M. Thomask, Carbon Black/High Density Polyethylene Conducting Composite Materials, Journal of Materials Science, 32 (1997) 401-407.

[2] M.D. Wakeman, L. Zingraff, P.-E. Bourban, J.-A.E. Manson, P. Blanchard, Stamp Forming of Carbon Fiber/PA12 Composites-A Comparison of a Reactive Impregnation Process and a Commingled Yarn System, Composites Science and Technology, 66 (2006) 19-35.

[3] B.T. Kelly, Physics of Graphite, Applied Science Publishers, London, (1981) Pp 1-33.

[4] R. Sengupta, M. Bhattacharya, S. Bandyopadhyay, A.K. Bhowmick, A Review on the Mechanical and Electrical Properties of Graphite and Modified Graphite Reinforced Polymer Composites, Progress in Polymer Science, 36 (2011) 638-670.

[5] K.S. Novoselov, A.K. Geim, S.V. Morozov, S.V. Dubonos, Y. Zhang, D. Jiang, Electric Field Effect in Atomically Thin Carbon Films, Science, 306 (2004) 666-669.

[6] N. Priyantha, P. Jayaweera, A. Sanjurjo, K. Lau, F. Lu, K. Krist, Corrosion-Resistant Metallic Coatings for Applications in Highly Aggressive Environments, Surface and Coatings Technology, 163-164 (2003) 31-36.

[7] Q.L. Wang, Y.F. Hu, M. He, Effect of Filler on the Self-Lubrication Performance of Graphite Antimony Composites, Journal of China University of Mining and Technology, 18 (2008) 0441-0443.

[8] Y.Z. Cai, S.W. Fan, H.Y. Liu, L.T. Zhang, L.F Cheng, B.X. Dong, J. Jiang, Microstructures and Improved Wear Resistance of 3D Needled C/Sic Composites with Graphite Filler, Composites Science and Technology, 69 (2009) 2447-2453.

[9] P. Rupnowski, M. Gentz, M. Kumosa, Mechanical Response of a Unidirectional Graphite Fiber/Polyimide Composite as a Function of Temperature, Composites Science and Technology, 66 (2006)1045-1055.

[10] S.Z. Wang, S. Adanur, B.Z. Jang, Mechanical and Thermo-Mechanical Failure

Mechanism Analysis of Fiber/Filler Reinforced Phenolic Matrix Composites, Composites Part B, 28B (1997) 215-231.

[11] M. Gentz, B. Benedikt, J.K. Sutter, M. Kumosa, Residual Stresses in Unidirectional Graphite Fiber/Polyimide Composites as a Function of Aging, Composites Science and Technology, 64 (2004) 1671-1677.

[12] B. Suresha, Siddaramaiah, Kishore, S. Seetharamu, P. Sampath Kumaran, Investigations on the Influence of Graphite Filler on Dry Sliding Wear and Abrasive Wear Behaviour of Carbon Fabric Reinforced Epoxy Composites, Wear, 267 (2009) 1405-1414.

[13] K. Kalaitzidou, H. Fukushima, L.T. Drzal, A New Compounding Method for Exfoliated Graphite-Polypropylene Nanocomposites with Enhanced Flexural Properties and Lower Percolation Threshold, Composites Science and Technology, 67 (2007) 2045-2051.

[14] D. Bryan, L. Khalid, Use of Exfoliated Graphite Filler to Enhance Polymer Physical Properties, Carbon, 45 (2007) 1727-1734.

[15] G. Zheng, J. Wu, W. Wang, C. Pan, Characterizations of Expanded Graphite/Polymer Composites Prepared BBY in situ Polymerization, Carbon, 42 (2004) 2839-2847.

[16] E.K. Sichel, Carbon Black Polymer Composites, Marcel Dekker, New York, (1982).

[17] H. Buqa, C. Grogger, M.V. Santis Alvarez, J.O. Besenhard, M. Winter, Surface Modification of Graphite Anodes by Combination of High Temperature Gas Treatment and Silylation in Nonaqueous Solution, Journal of Power Sources, 97-98 (2001) 126-128.

[18] H.W. Hu, G.H. Chen, M. Fang, W.F. Zhao, Modification of Graphite Oxide Nanoparticles Prepared via Electrochemically Oxidizing Method, Synthetic Metals, 159 (2009)1505-1507.

[19] E.T. Saraswati, T. Matsuda, A. Ogino, M. Nagatsu, Surface Modification of

Graphite Encapsulated Iron Nanoparticles by Plasma Processing, Diamond and Related Materials, 20 (2011) 359-363.

[20] E. Horozova, T. Dodevska, N. Dimcheva, Modified Graphites: Application to the Development of Enzyme-Based Amperometric Biosensors, Bioelectrochemistry, 74 (2009) 260-264.

[21] A. Kaşgöz, D. Akın, A. Durmus, N. Ercan, F. ÖksÜZömer, A. Kaşgöz, Effects of Various Polyolefin Copolymers on the Interfacial Interaction, Microstructure and Physical Properties of Cyclic Olefin Copolymer(COC)/Graphite Composites, Journal of Polymer Research, 20 (2013) 194-205.

[22] S. Ganguli, A.K. Roy, D.P. Anderson, Improved Thermal Conductivity for Chemically Functionalized Exfoliated Graphite/Epoxy Composites, Carbon, 46 (2008) 806-817.

[23] X.L. Wu, J.H. Qiu, P. Liu, E. Sakai, L. Lei, Polystyrene Grafted Carbon Black Synthesis via in situ Solution Radical Polymerization in Ionic Liquid, Journal of Polymer Research, 20 (2013) 167-173.

[24] B. Suresha, B.N. Ravi Kumar, M. Venkataramareddy, T. Jayaraju, Role of Micro/Nano Fillers on Mechanical and Tribological Properties of Polyamide66/Polypropylene Composites, Materials & Design, 31 (2010)1993-2000.

[25] J.R. Araujo, C.B. Adamo, M.-A. Paoli, Conductive Composites of Polyamide-6 with Polyaniline Coated Vegetal fiber, Chemical Engineering Journal, 174 (2011) 425-431.

[26] J.J. Rajesh, J. Bijwe, B. Venkataraman, U.S. Tewari, Effect of Impinging Velocity on the Erosive Wear Behaviour of Polyamides, Tribology International, 37 (2004) 219-226.

[27] J.J. Rajesh, J. Bijwe, U.S. Tewari, B. Venkataraman, Erosive Wear Behavior of Various Polyamides, Wear, 249 (2001) 702-714.

[28] J.J. Rajesh, J. Bijwe, U.S. Tewari, Abrasive Wear Performance of Various Polyamides, Wear, 252 (2002) 769-776.

[29] G. Pinto, A. Jimmenez-Martin, Conducting Aluminum-Filled Nylon 6 Composites. Polymer Composites, 22 (2001) 65-70.

[30] Y.X. Pan, Z.Z. Yu, Y.C. Ou, G.H. Hu, A New Process of Fabricating Electrically Conducting Nylon 6/Graphite Nanocomposites via Intercalation Polymerization, Journal of Polymer Science Part B: Polymer Physics, 38 (2000)1626-1633.

[31] Y. Liu, G.S. Yang, Non-Isothermal Crystallization Kinetics of Polyamide-6/Graphite Oxide Nanocomposites, Thermochimica Acta, 500 (2010) 13-20.

[32] F.M. Uhl, Q. Yao, H. Nakajima, E. Manias, A.C. Wilkie, Expandable Graphite/Polyamide-6 Nanocomposites, Polymer Degradation and Stability, 89 (2005)70-84.

[33] F.M. Zhang, C. Mihoc, F. Ahmed, C. Lathe, E. Burkel, Thermal Stability of Carbon Nanotubes, Fullerene and Graphite Under Spark Plasma Sintering, Polymer Degradation and Stability, 510 (2011) 109-114.

[34] X.L. Wu, P. Liu, Facile Preparation and Characterization of Graphene Nanosheets/Polystyrene Composites, Macromolecular Research, 18 (2010) 1008-1012.

[35] N.A. Isitman, M. Aykol, C. Kaynak, Nanoclay Assisted Strengthening of the Fiber/Matrix Interface in Functionally Filled Polyamide 6 Composites, Composite Structures, 92 (2010) 2181-2186.

[36] D.M. Lincoln, R.A. Vaia, Z.G. Wang, B.S. Hsiao, Temperature Dependence of Polymer Crystalline Morphology in Nylon 6/Montmorillonite Nanocomposites, Polymer, 42 (2001) 9975-9985.

[37] C. Ramesh, E.B. Gowd, High-Temperature X-Ray Diffraction Studies on the Crystalline Transitions in the α- and γ-Forms of Nylon-6, Macromolecules, 34 (2001)3308-3313.

[38] N.S. Murthy, Hydrogen Bonding, Mobility, and Structural Transitions in Aliphatic Polyamides, Journal of Polymer Science Part B: Polymer Physics, 44 (2006) 1763-1782.

[39] J. Kosanetzky, B. Knoerr, G. Harding, U. Neitzel, X Ray Diffraction Measurements

of Some Plastic Materials and Body Tissues, Medical Physics, 14 (1987) 526-532.

[40] Z.Q. Li, C.J. Lu, Z.P. Xia, Y. Zhou, Z. Luo, X-Ray Diffraction Patterns of Graphite and Turbostratic Carbon, Carbon, 45 (2007)1686-1695.

Chapter 7 Conclusions

7.1 General conclusions and remarks

Carbon materials touch every aspect of our daily lives. Activated carbons are used for water and air purification, carbon black is used to reinforce tires, carbon fiber composites are used to manufacture ultra-light graphite sporting goods and aircraft brakes, and carbon foams are used to make fire retardant insulation. Carbon nanotubes can be used for numerous applications ranging from sensors and actuators to composites. Graphene has been used as field effect transistors, sensors, and electromechanical resonators. However, carbon materials are all aggregate easily, and the poor interfacial adhesion between carbon materials and other matrix limits their widely use. In the present study, the composites of several kinds of carbon materials are investigated. Different types of surface treatment of carbon materials are available to improve the interfacial adhesion between carbon materials and polymer matrix and the influences on the composite properties are well studied. The significantly improved electrical conductivity, mechanical properties and other properties of composites are attributed to the interfacial adhesion improvement by carbon materials surface treatment is investigated by properties test.

In chapter 1, the research backgrounds, research significance, summary of the research and the construction of this thesis are described. The objectives of the research are to study the influence of different natural fiber treatment on the properties of natural fiber composites.

In chapter 2, the properties of polymer matrix and rice straw fiber are presented. The experimental methods and characteristics are also presented in this chapter.

In chapter 3, the preparation of the CB/PS nanocomposites via in situ solution free radical polymerization in IL was carried out. The nanocomposites separated from the IL because of polystyrene’s insolubility in the IL. The IL improved the grafting

polymerization of styrene on the CB surface. The results of electrical conductivity, FT-IR, SEM and TEM analysis showed that polystyrene grafted and mixed with CB. The CB/PS can be well dispersed in toluene and the aggregate diameters increased after the in situ radical graft polymerization in IL. The electrical conductivity of CB/PS nanocomposites was better than that of pure polystyrene. Both the PG and the conductivity first increased and then decreased with increasing amount of AIBN. And the conductivity decreased and the PG increased with increasing amount of monomer. Furthermore, the conductivity first increased and then decreased with increasing PG. These nanocomposites can be blended with other polymers to get products of improved mechanical properties.

In chapter 4, The CB/PS and MWCNT/PS nanocomposites were prepared by bulk radical polymerization. The synergistic effect of MWCNTs and CB on the properties of nanocomposites was investigated based on the comparison of the properties between CB/PS and MWCNT/PS nanocomposites. The results showed well multiply effect of MWCNTs and CB on the M-C/PS nanocomposites in electrical and mechanical properties. MWCNTs, as long nanotube, can crosslink the CB and formed network structure. In addition, the structure test and thermal stability suggested that the grafting percentage of PS on M-C was higher than both MWCNTs and CB. The M-C/PS nanocomposite can be blended with other polymers to get products of improved mechanical properties. The bending strength increased with the M/G ratio increasing. However, the bending strength of M-C/PS nanocomposites decreased with total content of MWCNTs and CB increasing.

In chapter 5, the MWCNT/PMMA composites were prepared by Pickering emulsion polymerization of methyl methacrylate monomer using the multi-walled carbon nanotube (MWCNT) as a surfactant. The morphology of obtained composites was investigated by SEM. It suggested the MWCNTs were successful stabilizer and the resulted size of the composites were heterogeneous, ranging from 100 nm to 500 nm. The structure of composites was also confirmed by the FT-IR spectrum. Moreover,

MWCNT/PMMA composites exhibited good electrical conductivities and could be applied as conductive materials. The TGA results illustrated the thermal stability of MWCNT/PMMA composites was decreased as the concentration of monomer reduced. Furthermore, poly (lactic acid) (PLA) based conductive composites were prepared by the mixture of MWCNT/PMMA and PLA plates with twin-screw extruding and injection molding process. The MWCNTs content was confirmed as 1.022%. The mechanical properties decreased with MMA content increasing, which suggested the structure damage of MWCNTs during the Pickering emulsion polymerization.

In chapter 6, in order to improve the affinity between polyamide 6 (PA6) and graphite powders (GP), the GP were modified by a proposed chemical method. First, the GP were oxidized with hydrogen peroxide to form GP-OH. Then GP-OH was modified with hexamethylene diisocryanate formed GP-NH_2. Elemental analysis, XPS and TGA results verified the successful modification of GP by the proposed chemical method. The electrical properties investigated that the structure of GP was damaged during the modification progress. The GP/PA, GP-OH/PA and GP-NH_2/PA composites were prepared by twin-screw extrusion and injection molding process. XRD patterns showed the crystallinity planes for the composites. The mechanical properties, especially the extensibility of GP-NH_2/PA were clearly improved after the modification because of the good affinity of between the modified GP and PA. Optical microscope images indicated the dispersion of unmodified and modified GP in PA6. SEM images of composites were obtained showing the interface morphology of cross sections after liquid nitrogen quenching and tensile fracture.

In chapter 7, general conclusions of the study are made. The next works to be carried out are also prospected.

7.2 Future work

Nanocomposites and conductive composites have been studied for several decades, lots of technologies have been practical applied. However, there are still plenty of

shortages such as low electrical conductivity, poor mechanical properties, inadequately thermal stability and so on. A lot of work should be conducted to solve these problems.

(1) Design the new modification method for the filler (multi-walled carbon nanotubes, graphite, graphene and so on) to improve their interfacial adhesion with plastics. The effect of modification on the structure of filler will be studied to make sure the electrical conductivity, mechanical properties, thermal properties of composites can be improved.

(2) Prepare the degradable conductive composites by treating the conductive fillers with chemical method. The most important point is the affinity improvement of treated fillers and degradable plastics without the sharply conductivity decreasing.

(3) Synthesis the novel conductive composites with the multiply of two or more fillers which can form conductive net or bridge. The conductive net or bridge may improve the electrical conductivity of composites greatly.

Publications

Ⅰ. Periodical papers

[1] **Xueli Wu**, Jianhui Qiu, Peng Liu, Eiichi Sakai. The Synergistic Effect of MWCNTs and Graphite Powders on the Properties of Polymer Nanocomposites. Chemical Engineering Journal, 246 (2014), pp. 211-216, (IF=3.473).

[2] **Xueli Wu**, Jianhui Qiu, Peng Liu, Eiichi Sakai. Preparation and Characterization of Polyamide Composites with Modified Graphite Powders. Journal of Polymer Research, 20 (2013), pp. 284-291, (IF=2.019).

[3] **Xueli Wu**, Jianhui Qiu, Peng Liu, Eiichi Sakai, Lin Lei. Polystyrene Grafted Carbon Black Synthesis via in Situ Solution Radical Polymerization in Ionic Liquid. Journal of Polymer Research, 20 (2013), pp. 167-173, (IF=2.019).

[4] **Xueli Wu**, Jianhui Qiu, Lin Lei, Yang Zhao, Eiichi Sakai. The Mechanical Characteristics of Straw/poly (Lactic Acid) Composite Materials, Advanced Materials Research, 335-336 (2011), pp. 153-156, (EI).

[5] **Xueli Wu**, Jianhui Qiu, Eiichi Sakai, Wenjuan Zhang, Peng Liu. Poly (Lactic Acid) Based Conductive Composites with the PMMA Treated MWCNTs via Pickering Emulsions Polymerization, European Polymer Journal, (Under Reviewing), (IF=2.562).

[6] Lin Lei, Jianhui Qiu, Yang Zhao, **Xueli Wu**, Eiichi Sakai. Synthesizing Electrically Conductive Graphene-Poly (Methyl Methacrylate) (GNS-PMMA) Composites and Poly (lactic Acid) (PLA)-Based Conductive Films. Science of Advanced Materials, 4 (2012), pp. 912-919, (IF=2.509).

[7] Lin Lei, Jianhui Qiu, **Xueli Wu**, Yang Zhao, Eiichi Sakai. Graphene-Poly (Methyl Methacrylate) Composites Prepared by Two Methods, Advanced Materials Research, 335-336 (2011), pp. 49-53, (EI).

[8] Jianhui Qiu, Kengo Uchiya, Lin Lei, **Xueli Wu**, Yang Zhao. Surface Electrical Resistances Properties of CNF/PC Nano-Composite Processing by Injection Molding. Advanced Materials Research, 339(2011), pp. 367-370, (EI).

[9] Peng Liu, Pengcheng Du, Longxiang Zhu, Zhihui Wu, Hongmei Wang, Ming Chen, **Xueli Wu**, Jianhui Qiu. Attapulgite/Polylactide Nanocomposites: Effect of Polymer Brush Length. Materials Letters, 117 (2014), PP. 214-216.

[10] Peng Liu, Jianhui Qiu, **Xueli Wu**. Synthesis of Polyaniline Nanorods/Polystyrene

Composite via Facile in Situ Radical Bulk Polymerization. Journal of the Taiwan Institute of Chemical Engineers, 44 (2013), pp. 686-690, (IF=2.084).

[11] Takuya Murata, Jianhui Qiu, **Xueli Wu**. Effect of Rolling Temperature on Microstructure and Tensile Properties of Polypropylene. Polymer Engineering & Science, (2013), pp. 1-9, (IF=1.243).

[12] Jianhui Qiu, Takuya Murata, **Xueli Wu**, Masayoshi Kitagawa, Makoto Kudo. Plastic Deformation Mechanism of Crystalline Polymer Materials in the Equal Channel Angular Extrusion Process. Journal of Materials Processing Technology, 212 (2012), pp. 1528-1536, (IF=1.953).

[13] Peng Liu, Jianhui Qiu, **Xueli Wu**. Well-defined Polyaniline Nanotubes and Nanofibers Surface-modified with Poly (methyl methacrylate) via In-situ Radical Polymerization. Materials Letters, 77 (2012), pp. 4-6, (IF=2.224).

[14] Jianhui Qiu, Takuya Murata, **Xueli Wu**, Makoto Kudo, Eiichi Sakai. Plastic Deformation Mechanism of Crystalline Polymer Materials During the Rolling Process. Journal of Materials Science, 48 (2012), pp. 1920-1931, (IF=2.163).

[15] Takuya Murata, Jianhui Qiu, Eiichi Sakai, **Xueli Wu**, Makoto Kudo. Morphology Change of Extrusion Molded Crystalline Polymer by Rolling Process. Advanced Materials Research, 391-392 (2012), pp. 595-599, (EI).

[16] Peng Liu, Jianhui Qiu, Xue Wang, **Xueli Wu.** Facile Preparation of Polyaniline Nanosheets via Chemical Oxidative Polymerization in Saturated NaCl Aqueous Solution for Supercapacitors. International Journal of Electrochemical Science, 7 (2012), pp. 6134-6141, (IF=3.729).

[17] Wu Zhong, Peng Liu, Zhaobin Tang, **Xueli Wu**, Jianhui Qiu. Facile Approach for Superparamagnetic CNT-Fe3O4/Polystyrene Tricomponent Nanocomposite via Synergetic Dispersion. Industrial & Engineering Chemistry Research, 51 (2012), pp. 12017-12024, (IF=2.206).

[18] Liang Shao, Jianhui Qiu, Lin Lei, **Xueli Wu**. Properties and Structural Investigation of One-dimensional SAM-ATP/PANI Nanofibers and Nanotubes. Synthetic Metals, 162 (2012), pp. 2322-2328, (IF=2.109).

[19] Peng Liu, Wu Zhong, **Xueli Wu**, Jianhui Qiu. Facile Synergetic Dispersion Approach for Magnetic Fe_3O_4@Graphene Oxide/Polystyrene Tri-component Nanocomposite via Radical Bulk Polymerization. Chemical Engineering Journal, 219 (2012), pp. 10-18, (IF=3.473).

[20] Yang Zhao, Jianhui Qiu, Huixia Feng, Min Zhang, Lin Lei, **Xueli Wu**.

Improvement of Tensile and Thermal Properties of Poly (Lactic Acid) Composites with Admicellar-treated Rice Straw Fiber. Chemical Engineering Journal, 173 (2011), PP. 659-666, (IF=3.473).

Ⅱ. Book

Title： The Instruction Manual on IR・Raman analysis, joint authorship

Title ：the surface analysis of straw via admicellar polymerization treatment

Section：Fourth quarter of chapter 19 (Jianhui Qiu、**Xueli Wu**), pp.738-739

Publisher：Technical Information Institute Co., LTD

Publication time：2013-09-21

Ⅲ. International conference paper

[1] **Xueli Wu**, Jianhui Qiu, Eiichi Sakai, Takao Komiyama, Takashi Aoyama, Makoto Kudo. Preparation of Polyamide Composites with Modified Carbon Black. The 10th China-Japan Joint Conference on Composites (CJJCC-10) Chengdu, China, September 7-9, 2012.

[2] **Xueli Wu**, Jianhui Qiu, Eiichi Sakai, Min Zhang, Kazushi Ito, Makoto Kudo, Junichi Kobayashi. Acetic Acid Modification of Straw and Its Composition with Poly (Lactic Acid). The 10th China-Japan Joint Conference on Composites (CJJCC-10) Chengdu, China, September 7-9, 2012.

[3] **Xueli Wu**, Jianhui Qiu, Lin Lei, Yang Zhao, Eiichi Sakai. The Mechanical Characteristics of Straw/poly (Lactic Acid) Composite Materials, 2011 International Conference on Materials and Products Manufacturing Technology, Chengdu, China, October 28-30, 2011.

[4] Lin Lei, Jianhui Qiu, **Xueli Wu**, Yang Zhao, Eiichi Sakai. Graphene-Poly (Methyl Methacrylate) Composites Prepared by Two Methods, 2011 International Conference on Materials and Products Manufacturing Technology, Chengdu, China, October 28-30, 2011.

[5] Jianhui Qiu, **Xueli Wu**, Yang Zhao, Eiichi Sakai, Min Zhang, Kazushi Ito, Junichi Kobayashi. Investigation of the Solubility between Poly (Lactic Acid) and Poly (Methyl Methacrylate) and Morphology of Their Composite. The 10th China-Japan Joint Conference on Composites (CJJCC-10) Chengdu, China, September 7-9, 2012.

[6] Takuya Murata, Jianhui Qiu, Eiichi Sakai, **Xueli Wu**, Makoto Kudo. Deformation

Mechanism of Polypropylene during Rolling Process and Its Tensile Properties. The 10th China-Japan Joint Conference on Composites (CJJCC-10) Chengdu, China, September 7-9, 2012.

[7] Jianhui Qiu, Kengo Uchiya, Lin Lei, **Xueli Wu**, Yang Zhao. Surface Electrical Resistances Properties of CNF/PC Nano-Composite Processing by Injection Molding. 2011 International Conference on Materials and Products Manufacturing Technology, Chengdu, China, October 28-30, 2011.

[8] Jianhui Qiu, Takuya Murata, Kenji Takahashi, **Xueli Wu**. The Plastic Deformation Characteristics of Crystalline Polymer Marerials via Rolling Process. ISCEMP2011 Shenyang, China, November 4-6, 2011.

[9] Takuya Murata, Jianhui Qiu, Eiichi Sakai, **Xueli Wu**, Makoto Kudo. Morphology Change of Extrusion Molded Crystalline Polymer by Rolling Process. ISCEMP2011 Shenyang, China, November 4-6, 2011.

Ⅳ. Domestic conference paper

[1] **Xueli Wu**, Jianhui Qiu, Eiichi Sakai, Teruo Bitoh. Comparison of the Structure and Properties for GPs/PS and MWCNTs/PS Nanocomposites. Proceedings of 49th Autumn Meeting of the Japan Society of Mechanical Engineers Tohoku Branch, No.2013-214, pp.57-58, Iwate University, Morioka, Japan, Sept. 20, 2013.

[2] **Xueli Wu**, Jianhui Qiu, Eiichi Sakai, Takao Komiyama, Takashi Aoyama. The surface treatment of carbon black to improve its dispersity with polyamide. The 69th Tohoku Branch of the Chemical Society of Japan, No. IP110, pp.125, Akita University, Akita, Japan, Sept.15-16, 2012.

[3] **Xueli Wu**, Jianhui Qiu, Lin Lei, Yang Zhao, Eiichi Sakai. Preparation and characterization of CNT/PS conductive composite materials. 19th Autumn Meeting of Japan Society of Polymer Processing, Seikei-Kakou'11, Akita University, Akita, Japan, Oct. 14-15, 2011.

[4] Yuki Iwase, **Xueli Wu**, Jianhui Qiu, Eiichi Sakai, Junichi Kobayashi, Hideaki Mori, Takehiko Takahashi, Kazushi Ito, Makoto Kudo. Preparation of rice straw/biodegradable polymer composites by surface treatment with acetic acid anhydride. Proceedings of 49th Autumn Meeting of the Japan Society of Mechanical

Engineers Tohoku Branch, No.2013-103, pp.5-6, Iwate University, Morioka, Japan, Sept. 20, 2013.

[5] Tomoaki Fujimoto, Xueli Wu, Jianhui Qiu, Tomohiro Konno, Eiichi Sakai, Junichi Kobayashi, Hideaki Mori, Takehiko Takahashi, Kazushi Ito, Makoto Kudo. Preparation of biodegradable composites materials with enzymatic saccharification residues of lignocellulosic biomass. Proceedings of 49th Autumn Meeting of the Japan Society of Mechanical Engineers Tohoku Branch, No.2013-219, pp.67-68, Iwate University, Morioka, Japan, Sept. 20, 2013.

[6] Wenjuan Zhang, Jianhui Qiu, **Xueli Wu,** Eiichi Sakai, Takao Komiyama, Takashi Aoyama. Preparation and characterization of immobilized enzyme. The 69th Tohoku Branch of the Chemical Society of Japan, No. IP124, pp.484, Akita University, Akita, Japan, Sept.15-16, 2012.

[7] Lin Lei, Jianhui Qiu, **Xueli Wu**, Yang Zhao, Eiichi Sakai. Preparation and characterization of GNS/PMMA composites. 19th Autumn Meeting of Japan Society of Polymer Processing, Seikei-Kakou'11, Akita University, Akita, Japan, Oct. 14-15, 2011.

Acknowledgements

I am very glad to express my thanks to a number of people without whom this study could not be possible. First and foremost, I would like to thank my advisor professor Dr. Jianhui Qiu, who is in Department of Machine Intelligence and Systems Engineering, Faculty of Systems Science and Technology, Akita Prefectural University. He imparted the knowledge of material science to me. And his elaborated guidance, considerable encouragement and invaluable discussion during the three years study period make my research of great achievement and my study life unforgettable.

My deepest appreciation would be go to the professors in Department of Machine Intelligence and Systems Engineering, Faculty of Systems Science and Technology at Akita Prefectural University, Dr. Mamoru Mizuno, Dr. Nobuhiro Kanazawa and professor in Department of Mechanical Engineering, Faculty of Textile Science and Technology at Shinshu University, Dr. Qingqing Ni for the comments and suggestions, whose advices have inestimable value for my research.

I greatly appreciate the technical support from Dr. Eiichi Sakai, Dr. Takao Komiyama and Dr. Kazushi Ito in Akita Prefectural University. Thanks for the people who are paying attention to me for my study and life, Mrs. Qiu, who has taken good care of me in the last three years; Professor at Lanzhou University, Dr. Peng Liu; Professor at Chinese Academy of Sciences, Dr. Shaoyun Fu; Professor at Southwest Jiaotong University, Dr. Zuowan Zhou; Dr. Makoto Kudo in Akita. And thanks also go to my peer research group members including Takuya Murata, Guohong Zhang, Yang Zhao, Liang Shao, Lin Lei, Wenjuan Zhang, Liming Zang, Lijun Wang, Yukiko Takeuchi, Yoshie Sugiura, Rie Nobe, Kengo Uchiya, Takafumi Miura, Tomu Hasegawa, Suguru Murakami, Kouya Chida, Taishi Fukuda, Eiki Andou, Takuya Kawai, Katsunori Kondo, Tomohiro Konno, Akira Shimizu, Takashi Watanabe, Yuki Iwase, Tomoaki Fujimoto, Yuya Matsumura, Yuuta Nakamura, Genki Watanabe, Kouhei Kobayashi, as well as my friends Paipai Pan and Jinkui Ma, for assisting with my research and providing

friendship and support.

I sincerely appreciate my Japanese teachers, Eiko Kamada, Kyoko Ikeda, Nobuko Sakamoto, Chika Furukawa and Eiko Fujishima for their support, patience and understanding throughout this endeavor.

I would like to express my sincere gratitude to my family, my father, my mother, my brothers, my sisters and other relevants for their moral support and warm encouragements both on study and life.

Xueli Wu

2014.03 Yurihonjo, Japan